Dynamics of telomeres in a telomerase negative human osteosarcoma cell

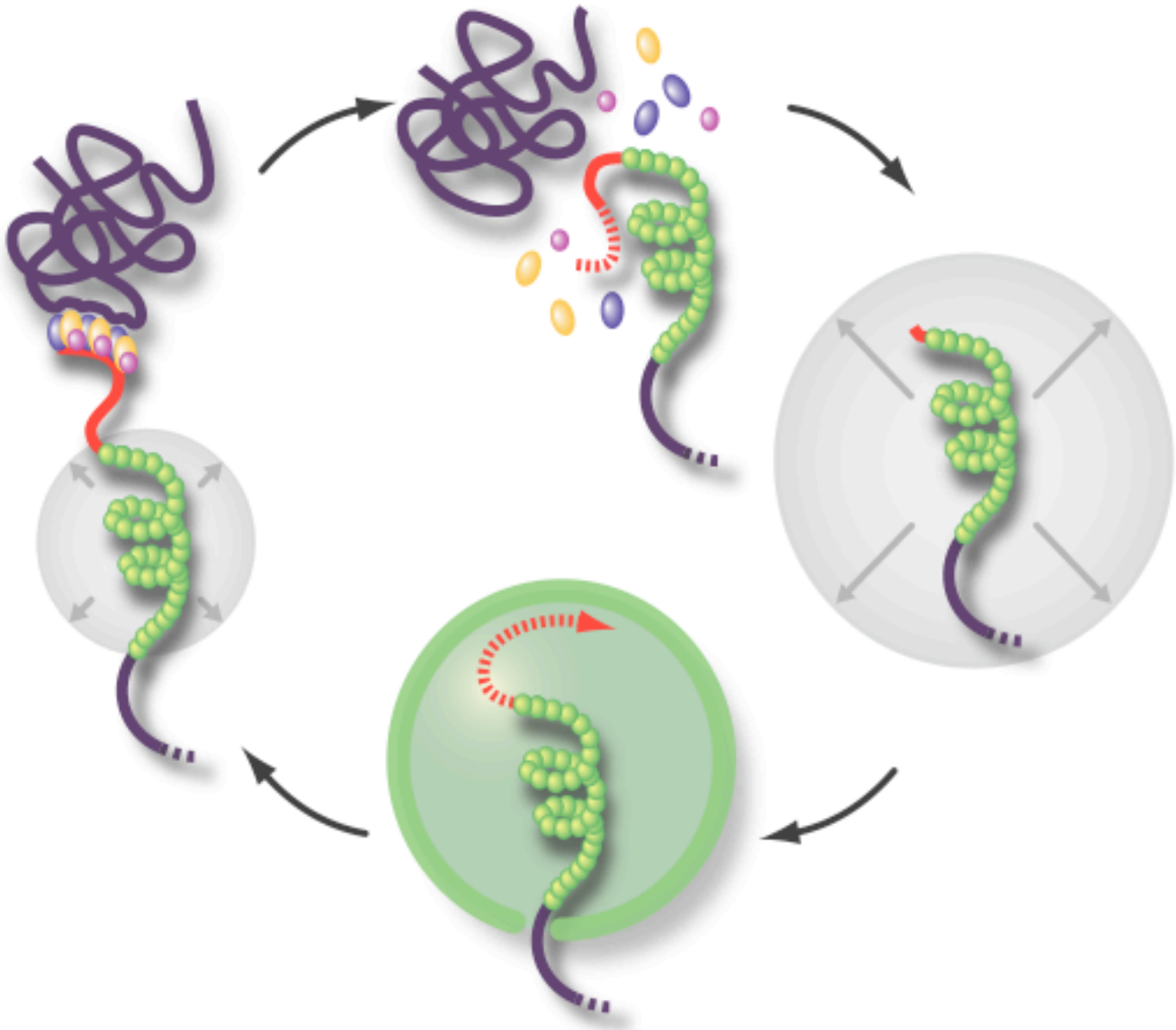

Dissertation submited by Thibaud Jegou

Dissertation
Submitted to the
Combined Faculties for the Natural Sciences an for Mathematics of the
Ruperto-Carola University of Heidelberg, Germany
for the degree of
Doctor of Natural Sciences

Presented by

Diploma Biologist Thibaud Jegou
Born in Quimper, France

Oral examination:

Dynamics of telomeres in a telomerase negative human osteosarcoma cell

Referees: PD Dr. Karsten Rippe
Prof Dr. Harald Herrmann-Lerdon

This work was carried out at the Kirchhofinstitut für Physik, in Heidelberg, in the department “Molecular Biophysics” Between January 2003 and June 2007 under the scientific guidance of PD Dr. Karsten Rippe.

Publications

Thibaud Jegou, Gerrit Heuvelmann, Malte Wachsmuth, Sabine M. Görisch, Karin Greuhlich-Bode, Petra Boukamp, Peter Lichter and Karsten Rippe: Dynamics of telomeres in a telomerase negative human osteosarcoma cell line (in preparation).

Malte Wachsmuth, **Thibaud Jegou**, Ulf Nehrbass and Karsten Rippe: Chromatin dynamics and organization studied by fluorescence fluctuation microscopy of linker histone H1 (in preparation).

Posters

Deutsche Forschungsgemeinschaft (DFG) meeting, program SPP 1128 “Optical analysis of structure and dynamics of supramolecular biological complexes”, 2004:
Thibaud Jegou and Karsten Rippe: Analysis of the interphase chromatin conformation by high resolution fluorescence microscopy: tracing chromatin in vivo

Tagung der Deutschen Gesellschaft für Zellbiologie (DGZ), 2005 Heidelberg:
Thibaud Jegou, Sabine M. Görisch, Peter Lichter and Karsten Rippe: Chromatin organization and dynamics studied by tracing single genomic loci and nuclear bodies in vivo

Workshop on Cell Biology & Microscopy, 2005, Altleiningen:
Thibaud Jegou, Sabine M. Görisch, Peter Lichter and Karsten Rippe: Chromatin organization and dynamics studied by tracing single genomic loci in vivo.

Deutsche Forschungsgemeinschaft (DFG) meeting, program SPP 1128 “Optical analysis of structure and dynamics of supramolecular biological complexes”, 2006:
Thibaud Jegou, Sabine M. Görisch, Peter Lichter and Karsten Rippe: Chromatin organization and dynamics studied by tracing single genomic loci in vivo

International Symposium “Optical Analysis of Biomolecular Machines”, 2006, Max Delbrück Center for Molecular Medicine, Berlin:
Thibaud Jegou, Sabine M. Görisch, Peter Lichter and Karsten Rippe: Chromatin organization and dynamics studied by tracing single genomic loci in vivo.

Acknowledgements

PD Dr. Karsten Rippe möchte ich ganz herzlich danken für die Möglichkeit meine Doktorarbeit in seinem Team machen zu können. Besonders weil diese Stelle eine Art zweite Chance war, nachdem ich eine schlechte Erfahrung mit einer früheren Doktorabeit hatte. Ich möchte mich auch für das spannende Thema sowie die persönliche Betreuung, Ratschläge, “Visionen” und die kompetente mathematische Unterstützung (ich armer Biologe) bedanken. Schließlich bedanke ich mich einfach für den Spass bei der Arbeit während diesen letzten Jahren (gibt es irgendwo auf dieser Welt andere Laborchefs die Computerspiele an ihre Mitarbeiter verschenken?).

Prof. Dr. Herrmann-Lerdon danke ich herzlich für das Interesse an diesem Thema und der Bereitschaft, diese Arbeit vor dem Promotionsausschuss der Naturwissenschaftlich-Mathematischen Gesamtfakultät der Universität Heidelberg zu vertreten.

Gerrit Heuvelman danke ich für die Matlab-Programmierung, ohne die die Berechnung der Telomermobilität ein (noch größerer) Alptraum gewesen wäre.

Dr. Malte Wachsmut danke ich für die Hilfe in der Entwicklung der Berechnung des drei *lac*O loci system im ”moving coral” model.

Prof. Dr. Peter Lichter danke ich für das Interesse an dieser Arbeit, seine Anweisungen und Unterstüzung in den ersten Monaten meiner Doktorarbeit, als wir noch alle Arbeiten im KIP durchführten.

Dr. Ulrike Engel und dem Nikon imaging centre danke ich für die Hilfe bei mikroskopischen Fragen.

Dr. Karin Greulich-Bode danke ich für ihre Hilfe bei PNA FISH, mFISH und für ihre konstant gute Laune.

Dr. Antoaneta Mincheva danke ich für ihre Hilfe bei der chromosome banding-Methode.

Ich bedanke mich herzlich bei allen Chromcon Teamkollegen - alt oder neu - für den Spaß im Labor während dieser letzten viereinhalb Jahre.

I insist to give many thanks to the Worms teams “Holland” (especially Maxima), “Polska Huje” and “Dumkopf” that gave me the possibility to exteriorize my deepest and worst primitive instincts, particularly with the “holly hand grenade” and the “banana”.

Je tiens finalement à remercier ma mère pour son indefectible soutien tout au long de ces années, dans les bons jours comme dans les mauvais.

Mobilis in mobile

"Mobile in a mobile element", Captain Nemo's motto, *20 000 lieux sous les mers*, Jules Vernes.

Table of contents

I. Introduction

1 The mammalian telomere

Telomeres are specialized structures at the ends of linear chromosomes of eukaryotic cells. They are composed of tandem repeats of the TTAGGG DNA sequence, typically 10 to 15 Kbp long in human cells, and specifically bound proteins. During normal DNA replication, telomeric DNA is not completely replicated because synthesis of the lagging strand cannot start from the very end of the DNA. As a result, telomeric DNA is shortened every time a cell divides. A specialized enzyme, the telomerase, is able to synthesize telomere repeats *de novo* but is only expressed at low levels in adult tissues and does not completely compensate this telomere length reduction. Thus, the telomeres can be seen as a biological clock of the cell, as cell division stops when telomeres are too short.

1.1 Structure of the telomere

Telomere repeats binding factors TRF1 and TRF2 and associated proteins are forming a specific nucleoprotein complex with the telomere DNA, known as the "telosome". The function of the telosome is to prevent the end-to-end fusion of chromosomes and to protect telomeres from the DNA double strand breaks repair machinery (Bertuch and Lundblad, 2006).

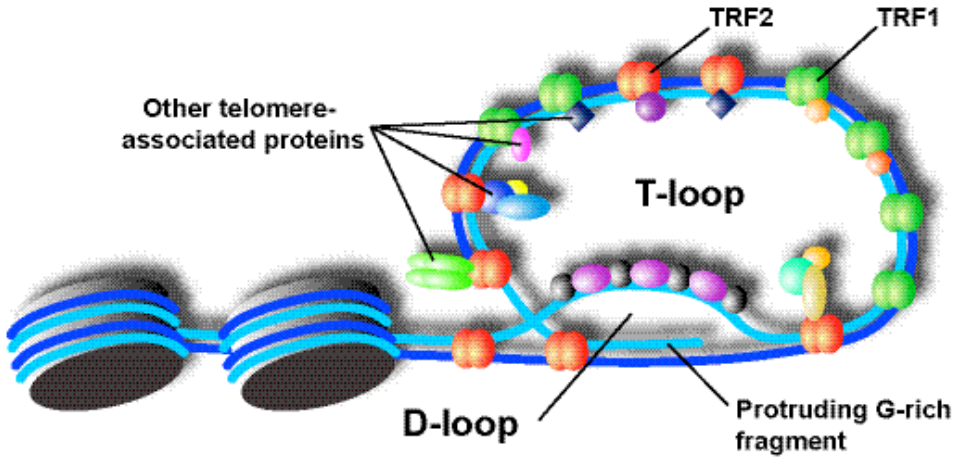

Figure I.1: Schematic representation of the T-loop formation at the telomere end.
The strand invasion of the G-strand is indicated. This particular conformation protects the telomeres from the double strand breaks reparation machinery and prevents the end-to-end fusion of the chromosomes. The components of the telomere repeat binding factor 1 (TRF1) and 2 (TRF2) are shown.

The particularity of eukaryotic telomeres is the protrusion of a single stranded G-rich fragment of 150-200 nucleotides in length. This fragment plays a central role in the telomere structure as it leads to the formation of the T-loop (Fig. I.1). The T-loop is formed by the invasion of the terminal single-stranded DNA into the duplex region of the telomere, thereby creating a solution for the telomere end protection (Griffith et al., 1999). The single stranded overhang also serves as substrate for the telomerase, the enzyme responsible for the elongation of the telomeres.

1.2 Telomeric chromatin

1.2.1 Global chromatin organization

The greatest challenge of the cell nucleus organization is achieving the compaction of a two meter long linear DNA string in a ~10 µm diameter sphere in a manner that preserves its integrity as well as its accessibility to the transcription and replication machinery. This is achieved by the association of DNA with histones and other chromosomal proteins in several levels of compaction (Fig. I.2). At the first level 147 DNA base pairs are wrapped 1.67 times around the core histone, forming the nucleosome, the basic subunit of chromatin (Kornberg, 1974; Olins and Olins, 1974). The histone protein core is a cylinder-shaped structure formed by an octamer made of pairs of the four histones H2A, H2B, H3 and H4. Nucleosomes are connected by a “linker” region of DNA forming a “beads on the string structure”. This first level leads to an approximate six-fold compaction. Core histones have basic terminal tails that are the target of many post-translational modifications such as methylation or acetylation. These modifications, together with the binding of the histone H1 and other chromatin associated factors promotes the formation of the higher orders of chromatin folding and thereby determine the accessibility of DNA to biological processes like transcription, replication repair and recombination. The accessibility of chromatin displays spatial and temporal changes. Regions in the µm length scale at the nuclear periphery, around the nucleolus and at the centromeres display a high degree of compaction. These dense chromatin regions are often referred to as heterochromatin as opposed to the less dense euchromatin (Dillon, 2004; Dillon and Festenstein, 2002). The compaction state and accessibility of these dense chromatin region is affected by histone modifications like histone acetylation (Fejes Tóth et al., 2004; Görisch et al., 2005). DNA accessibility can also be

modulated via the ATP-coupled activity of chromatin remodeling complexes that translocate nucleosomes along the DNA (Becker and Horz, 2002)

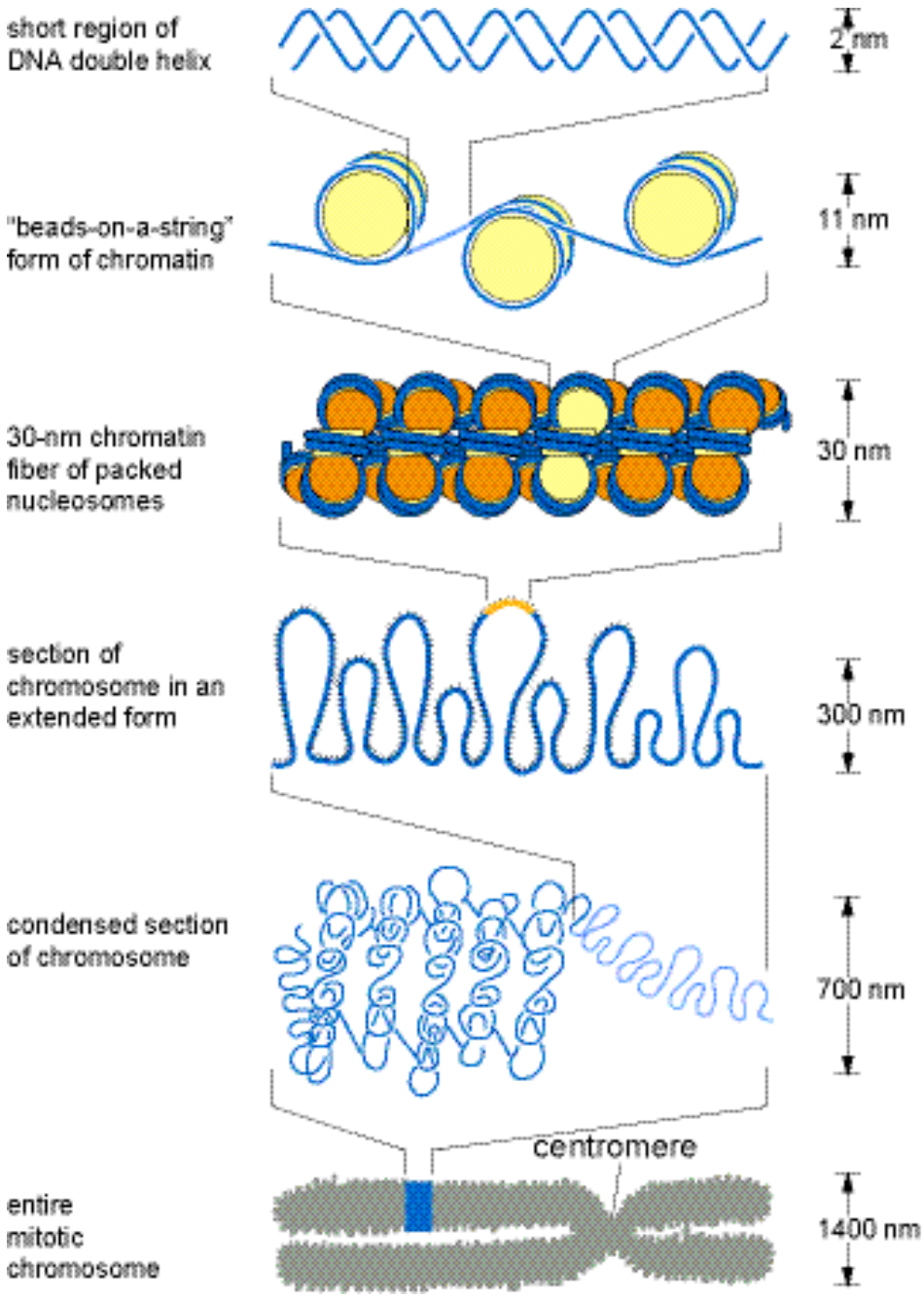

Figure I.2: Different levels of chromatin organization in the mammalian nucleus

This model shows how DNA is packed in the nucleosome and further condensed in the 30 nm chromatin fiber. This fiber associates into loops or rosettes and higher order structures up to the totally condensed state found in mitotic chromosomes. However even the structure of the 30 nm chromatin is not clearly defined and folding into higher order compaction states still needs to be elucidated. Figure adapted from (Alberts et al., 1994).

1.2.2 Telomere constitutive heterochromatin folding

In contrast to yeast, the mammalian telomeres contain histones and telomeres, as well as sub-telomeric regions are displaying epigenetic markers of constitutive heterochromatin (Blasco, 2007). The constitutive heterochromatin is found in inactive regions of repetitive DNA such as pericentric satellites repeats or telomeres and is characterized by an enrichment in heterochromatin protein 1 (HP1) isoforms, histone 3 trimethylation at lysine 9 and histone 4 trimethylation at lysine 20 (Fig. I.3). Quantitative analysis of fluorescence in situ hybridization experiments (Q-FISH) have shown that telomeres are able to cluster in groups of two or three in human fibroblasts (Nagele et al., 2001).

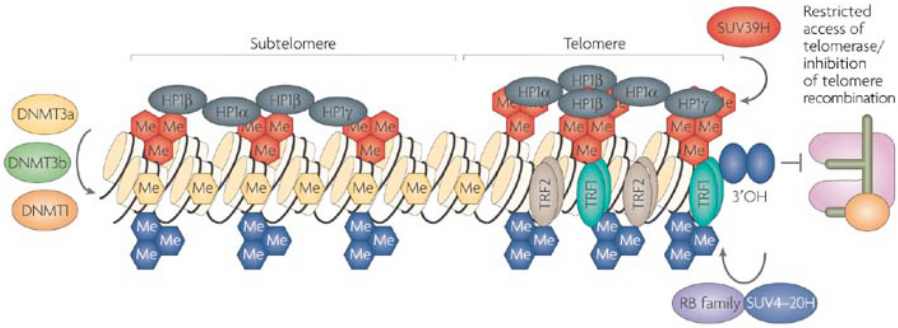

Figure I.3: Telomeres as well as sub-telomeric region are folding in constitutive heterochromatin

Both telomeric and sub-telomeric chromatin regions are enriched in trimethylated H3K9 and H4K20, and HP1 isoforms (see text). In addition subtelomeric DNA is heavily methylated. The constituted telosome shelters the telomere from the telomerase and the recombination machinery. Figure taken from (Blasco, 2007).

1.2.3 Telomere and sub telomeric chromatin relationship are tight

Mammalian telomere repeats, $(TTAGGG)_n$, lack the CpG sequence which is the substrate of DNA methyltransferases (DNMTs) and can therefore not be methylated. On the contrary, the subtelomeric sequences are heavily methylated. Interestingly, the methylation status of the subtelomeric regions seems to play an important role in the regulation of telomere repeat length as DNMT1 deficient mouse embryonic stem cells (ES) show dramatically elongated telomeres as compared to control (Gonzalo et al., 2006). In contrast, in telomerase deficient mice, with short telomeres constitutive heterochromatin markers (Histones H3 and H4 trimetylations) as well as methylation of the subtelomeric regions appear to decrease (Benetti et al., 2007). This suggest that telomere repeats length

influences also the subtelomeric chromatin status (Fig. I.4) (Blasco, 2007). From a functional point of view the telomere displays the ability to silence genes that are located in neighboring subtelomeric regions. This phenomenon known as “telomere positioning effect” (TPE) occurs in mammals as well as in yeast with profound effects on gene expression patterns. It seems that the induction of a more compact chromatin at the telomeres also affects the nearby regions (Baur et al., 2001).

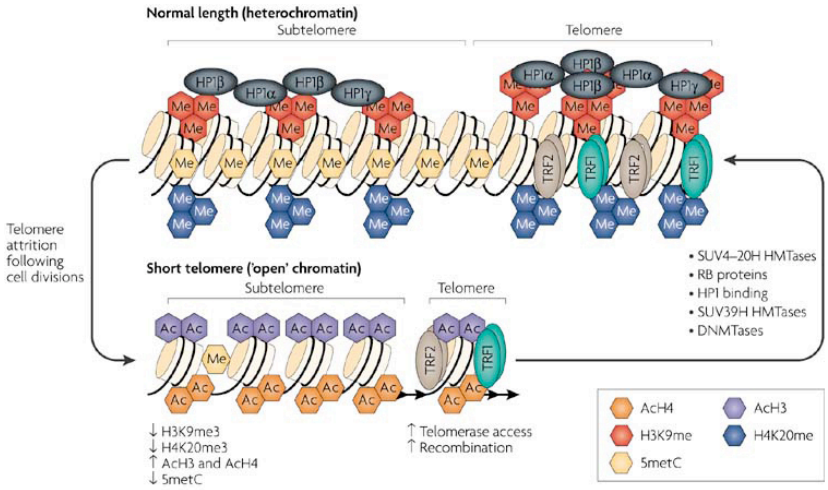

Figure I.4: A model for the role of epigenetic modifications in telomere-length control.

Normal-length telomeres have features of constitutive heterochromatin, such as subtelomeric DNA hypermethylation, hypermethylation of histone H3 at lysine 9 (H3K9) and histone H4 at lysine 20 (H4K20), hypoacetylation of histones H3 and H4, and heterochromatin protein HP1 binding at both telomeres and subtelomeres. This suggests that they have a compacted and 'closed' conformation, which is not accessible to telomerase and represses recombination between telomeric repeats. As telomeres become shorter with increasing cell divisions, these heterochromatic marks are decreased from telomeres and subtelomeres, concomitant with an increased histone acetylation. This leads to a more “open” chromatin state, which allows a greater accessibility of telomere-elongating activities (by telomerase and proteins that are involved in telomere recombination, which can lead to elongation by alternative lengthening of telomeres (ALT)). Once telomeres are sufficiently elongated, they can be assembled into heterochromatin. Figure taken from (Blasco, 2007).

1.3 Telomere lengthening in healthy tissues

In both yeast and mammals, the G-strand overhang is the substrate for telomerase, which consists of a reverse transcriptase (TERT) that is able to synthesize telomeric repeats *de novo* and add them to chromosome ends using an associated RNA molecule (TERC) as a template (Chan and Blackburn, 2002). In

contrast to yeast, humans show telomere attrition with aging. This is thought to result from limiting amounts of telomerase activity in the adult organism, which cannot compensate for the progressive telomere shortening that occurs as cells divide during tissue regeneration (Collins and Mitchell, 2002). During normal DNA replication, telomeric DNA is indeed not completely replicated because synthesis of the lagging strand cannot start from the very end of the DNA. When the telomeric DNA length becomes reduced, the cell enters an irreversible growth arrest referred to as replicative senescence (Bodnar et al., 1998) (Blackburn, 2000). In this regard, telomerase has been found to be crucial for stem-cell function and proliferative potential, providing a possible basis for the known roles of telomerase in cancer and ageing. Whereas short telomeres that arise owing to telomerase deficiency result in impaired stem-cell functionality (Flores et al., 2006), defective tissue regeneration and decreased tumorigenesis (Blasco, 2005), telomerase over expression has the opposite effects.

Tumor cells that undergo a large number of cell divisions need to bypass the telomere mediated limitation of cell proliferation. Most tumor cells achieve this by activating or expressing higher levels of telomerase (Kim et al., 1994) but a subset of about 10 to 15 % of tumor cells bypass the end replication problem in a telomerase-independent manner, the process of which is called alternative lengthening of telomeres (ALT) (Bryan et al., 1995).

2 The alternative telomere lengthening (ALT) pathway

2.1 ALT pathway and cancer

Several unique features are found in ALT cells compared with telomerase-positive tumor cells (Reddel, 2003). It appears that ALT is more often present in cell lines and tumors of mesenchymal origin, such as osteosarcomas and *in vitro* transformed human fibroblasts, than in those of epithelial origin. Telomere lengths of ALT cells are characterized by heterogeneity: some telomeres are extremely long; at the same time, others are very short or even undetectable in a single cell. Asymmetrical telomeres can even be observed at some chromosome ends. ALT cells are moreover characterized by an important chromosomal instability (Henson et al., 2005; Ulaner et al., 2004).

Interestingly, in ALT cells some promyelocytic leukemia (PML) nuclear bodies form specific structures with telomeres that are called APBs for ALT-associated PML bodies (Yeager et al., 1999). The APB structure, composition and putative function are developed in paragraph 4.4.
Although observation in model system suggest that ALT tumor may be relatively benign, they appear to be sometimes lethal in patients (Reddel and Bryan, 2003) but the prognosis significance of ALT seem to vary among tumor type. However, ALT tumors may be less likely to metastasize than telomerase-positive tumors (Henson et al., 2005).

2.2 Putative mechanism of the ALT pathway

When ALT cells are fused with normal cells or telomerase-positive tumor cells, the ALT mechanism is lost in the resulting cell hybrid, suggesting that one or more recessive gene mutations are required for the activation of the ALT pathway (Perrem et al., 1999). Several genes potentially involved in the ALT pathway were recently identified (Jiang et al., 2007). Theses are related to PML body formation (PML), DNA reparation (MRE 11, Rad50) as well as telomere metabolism (TRF1 and TRF2). High rate of telomeric exchanges was demonstrated in ALT cells (Laud et al., 2005; Londono-Vallejo et al., 2004; Muntoni and Reddel, 2005). In budding yeast, telomerase-defective cells maintain telomeres by DNA recombination (see further). Similarly, it was demonstrated that marker DNA cassettes inserted into particular telomeres in ALT cells are duplicated into other telomeres through gene conversion (Dunham et al., 2000). Thus, DNA recombination appears to be involved in the ALT mechanisms but the molecular details are poorly understood.

2.3 DNA recombination, double strand breaks reparation machinery and telomere lengthening.

DNA homologous recombination occurs in all organisms. It was originally thought to be only a system of genetic information exchanges but further studies shown its central role in DNA repair, particularly in case of double strand breaks (DSB), in the rescue of damaged replication forks, the chromosome segregation in meiosis I or the maintenance of telomeres in yeast (McEachern and Haber, 2006; Michel et al., 2004; Symington, 2002).

There are several distinct pathways for DSB repair involving recombination. The two main are referred to as double strand break repair (DSBR) and synthesis-dependant strand annealing (SDSA) (Fig I.5). Both are sharing the first steps: the broken chromosome ends are processed to give single-stranded DNA (ssDNA) tails, which invade an homologous chromosome to copy genetic information into the donor chromosome. Central to the DSBR model is the formation of a DNA joint molecule that harbors two Holliday junctions. Resolution of the exchanged DNA strands can result in crossover, whereby segments of the interacting chromosomes are exchanged (Collins and Newlon, 1994; Schwacha and Kleckner, 1995). On the contrary, in the SDSA model, instead of capturing the second end of the DSB into the recombination intermediate, the invading strand is displaced after repair synthesis and re-anneals with the single-stranded tail on the other DSB end (Allers and Lichten, 2001).

Interestingly yeasts that are lacking the telomerase enzyme are surviving by elongating their telomeres in a replication-dependant manner. This is achieved by using a process named break induced replication (BIR). There are two different of BIR pathways that can be activated by the yeast, one dependant of the recombinase protein Rad51 and one Rad51 independent. The recombination process is triggered either by excessive telomere shortening or by disruption in the function of the telomere binding proteins (reviewed in (Lundblad and Blackburn, 1993; McEachern and Haber, 2006)).

In summary two different aspects of the ALT pathway are identified:

- The involvement of the DNA recombination and the double-strand break reparation machinery.
- The formation of ALT-associated PML bodies complex (see paragraph 4.4) that are shown to associate with telomeres and contain many proteins involved in recombination and reparation machinery.

Thus the dynamic reorganization and reposition of the telomeres as well as the interaction of telomeres with PML bodies appears to be key factors in the study of the ALT mechanism.

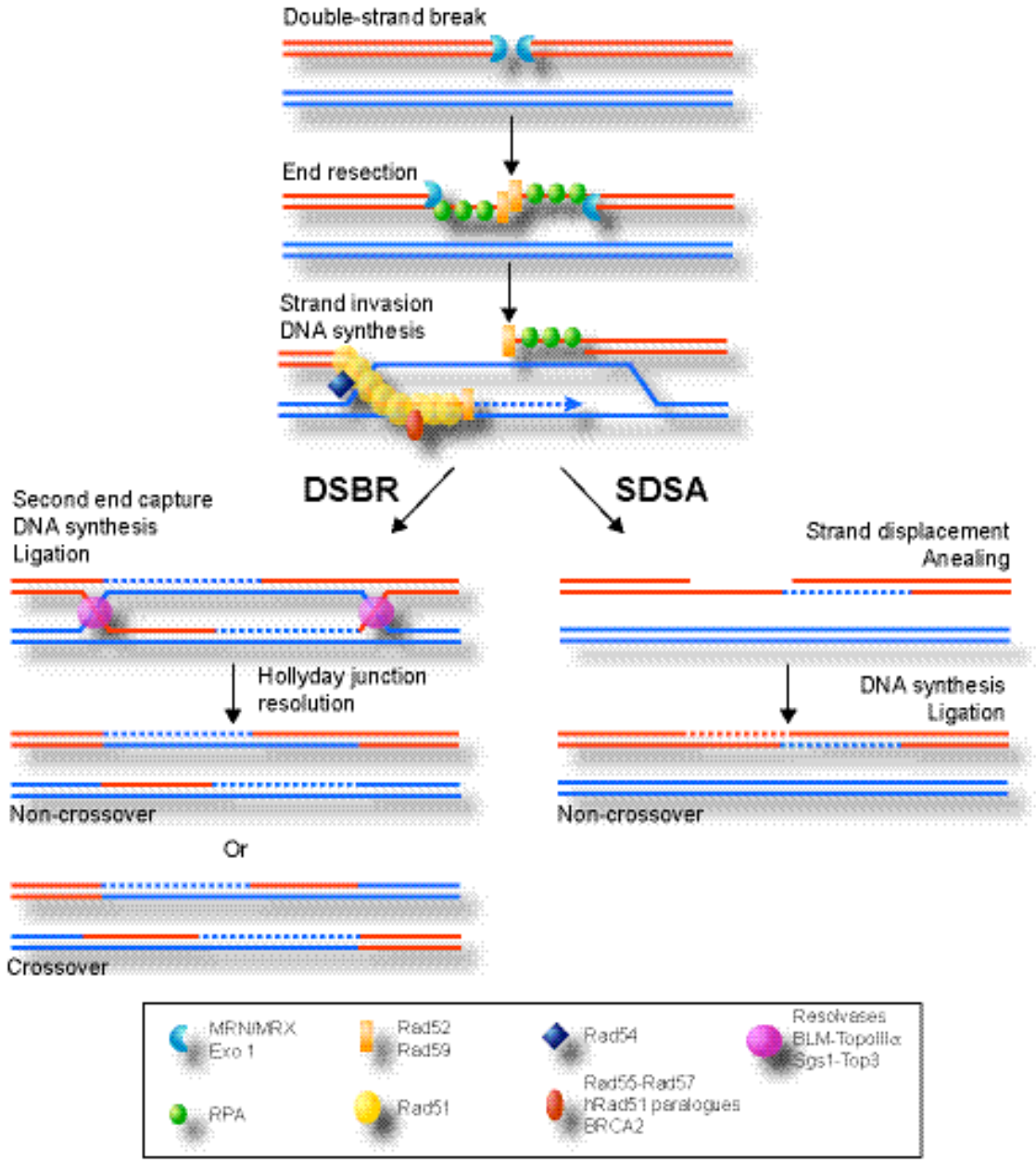

Figure I.5: Repair of DNA double-strand breaks by DSBR and SDSA.

Double-strand breaks (DSBs) can be repaired by several homologous recombination (HR)-mediated pathways, including double-strand break repair (DSBR) and synthesis-dependent strand annealing (SDSA). In both pathways, repair is initiated by resection of a DSB to provide 3′ single-stranded DNA (ssDNA) overhangs that rapidly complex with RPA. Rad51 recruitment displaces RPA leading to the formation of a helical nucleoprotein filament with ssDNA, which can search for an intact homologous template and then catalyze invasion of the ssDNA into a donor sister chromatid or homologous chromosome to form a joint molecule. The resulting joint molecule acts as a primer for DNA synthesis to extend the heteroduplex DNA, which, following further processing and resolution of the joint DNA molecules, leads to repair of the DSB and restoration of DNA integrity. BRCA2, breast cancer 2; BLM–TopoIIIα, Bloom syndrome protein–topoisomerase III alpha; Exo1, exonuclease 1; hRad51, human Rad51; MRN, MRE11–RAD5–NBS1; MRX, Mre11–Rad50–Xrs2; Mre11–Rad50–Xrs2; MRE11, meiotic recombination 11; NBS1, Nijmegen breakage syndrome 1; Rad50, radiation sensitive 50; RPA, replication protein A; Top3, Topoisomerase 3.

3 The dynamic structure of the mammalian nucleus

3.1 General organization: the nuclear compartments

3.1.1 The nucleus

The mammalian cell nucleus is the most prominent compartment of the eukaryotic cell with an average diameter of 10 µm (Fig. I.6). It is confined by a nuclear envelope, a double-membrane structure, of which the outer membrane is contiguous with the rough endoplasmic reticulum and is often studded with ribosomes. The nuclear envelope provides spatial and temporal separation of nuclear and cytoplasmic processes. This separation is however not absolute but selectively regulated: the inner and outer nuclear membranes are fused together at certain sites, forming nuclear pores that serve in the transit of materials between the nucleus and cytoplasm (Stoffler et al., 1999). Electron and light microscope have shown that the nucleus is highly organized and dynamic structure with specialized domains and reaction compartments (Rippe, 2007, in press).

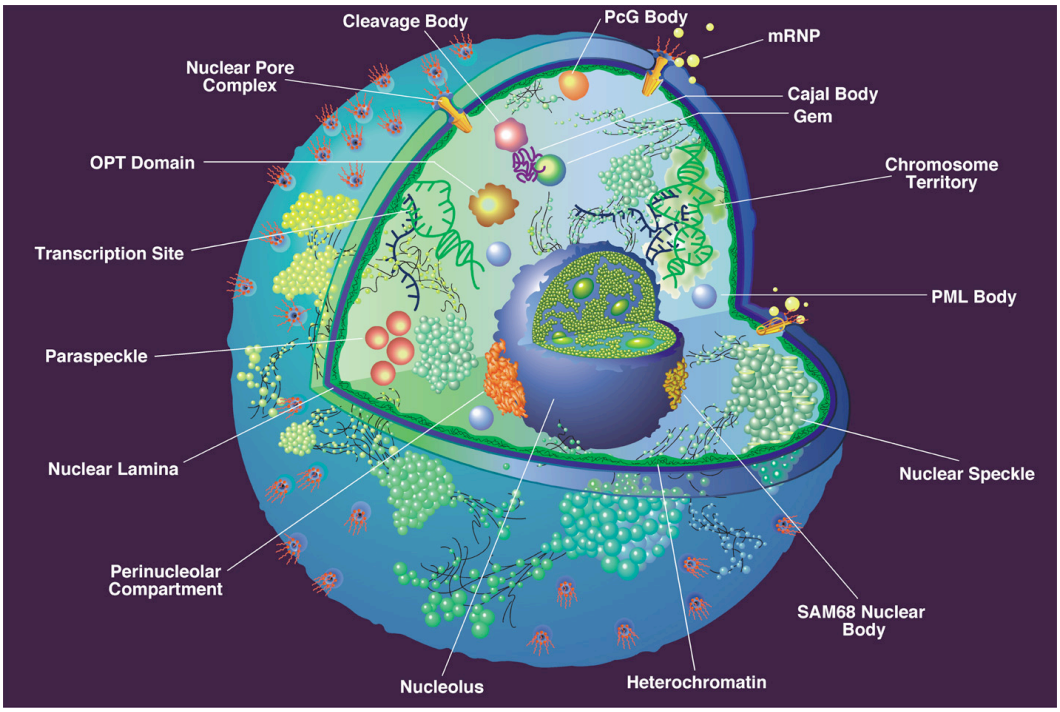

Figure I.6: Model of the mammalian cell nucleus.
The mammalian nucleus is highly compartimentized structure. The nucleus is first bounded by the nuclear envelope and exchanges with the cytoplasm are tightly regulated by nuclear pores. The most prominent structure in the nucleus is the nucleolus, which is the site of the rRNA synthesis. The chromosomes are themselves organized in distinct territories and many nuclear proteins are segregated in multiple mobile clusters: the nuclear bodies. Figure taken from (Spector, 2001).

3.1.2 The chromosomes territories

In the nucleus each chromosome occupies its own distinct region or “territory” as can be observed in fluorescent *in situ* suppression hybridization experiments (Branco and Pombo, 2007; Cremer and Cremer, 2001; Cremer et al., 2006; Cremer et al., 1993; Cremer et al., 1988; Lichter et al., 1988). The boundary of these territories is however not sharp and some interchromosomal interactions via extended chromatin loops can be observed (Branco and Pombo, 2006; Branco and Pombo, 2007). While the position of the chromosome territories in the nucleus seems to be stable over time in the interphase the heritability over cell divisions is subject of controversy (Gerlich and Ellenberg, 2003). A recent study has demonstrated that the global chromatin positioning organizes *de novo* in early S phase (Thomson et al., 2004).

3.1.3 Nuclear bodies

Many activities of the nucleus are concentrated in mobile sub nuclear foci called nuclear bodies, which include nuclear speckles, Cajal bodies PML bodies (Lamond and Sleeman, 2003). Nuclear bodies are mobile structures in the nucleus. Thus, PML and Cajal bodies can combine phases of immobility, where they are apparently associated with chromatin, and phases of fast translocation within the nucleus (Görisch et al., 2004; Muratani et al., 2002; Platani et al., 2002). Nuclear bodies are not surrounded by lipid layer and are usually characterized by specific antigens. Besides of these specific proteins an important variability in the composition of nuclear bodies can be observed over space and time or triggered by specific stimuli.

3.2 Current view of mobility in the nucleus

3.2.1 Dynamics of histones and chromosomal proteins

A number of studies have revealed that the average residence times of chromosomal proteins like for example linker histone H1 (Lever et al., 2000; Misteli et al., 2000) or heterochromatin protein 1 (HP1) (Bornfleth et al., 1999; Cheutin et al., 2003; Festenstein et al., 2003) are surprisingly short and in the order of only a few minutes. Even core histones like H2A and H2B that are usually tightly bound on the hour time scale display a very high mobility in transcriptionally active

regions (Kimura and Cook, 2001) as well as in certain developmental stages (Meshorer et al., 2006).

3.2.2 Mobility of chromatin loci

Chromatin

The translocation of chromatin loci has been studied by monitoring the mobility of a photobleached spot in dye labeled chromatin (Abney et al., 1997) or by tracking fluorescently labeled regions (Bornfleth et al., 1999; Manders et al., 1999; Zink and Cremer, 1998). Average apparent diffusion coefficients of $1\text{-}2\cdot10^{-4}$ μm^2 s^{-1} and an accessible region with a radius of 200 nm were measured (Görisch et al., 2005). Using the *lac*O/LacI-GFP system in mammalian cells as well as in yeast and Drosophila, rapid but locally restricted movements were found on a length scale of 300 to 500 nm (Chubb et al., 2002; Heun et al., 2001; Marshall et al., 1997; Vazquez et al., 2001). The movements of different sites in human living cells revealed that *lac*O inserts located at nucleoli or the nuclear periphery are significantly less mobile than more nucleoplasmic loci. For the latter sites, a mean diffusion coefficient in human cells of $1.3\cdot10^{-4}$ μm^2 s^{-1} was reported (Chubb et al., 2002).

Telomeres

The mobility of telomeres in yeast was extensively studied by *in vivo lac*O array labeling (Bystricky et al., 2005; Hediger et al., 2002; Rosa et al., 2006). On the contrary to mammalians, yeast telomeres are known to cluster together and to anchor at the nuclear envelope. Nevertheless yeast telomeres are able to display fast movements over a radius of 300 nm in average with significant differences between the chromosomes.

As an alternative approach to the *lac*O/LacI system, peptide nucleic acid probes (PNAs) directed against telomeres were also used to analyze the diffusion properties of telomeres in the human U2OS ALT cell line (Molenaar et al., 2003). It was shown that the telomeres are divided in two populations. The vast majority displayed constrained diffusive movement within nuclear regions of ~ 500 nm radius and a diffusion coefficient slightly higher to that determined for nucleoplasmic *lac*O arrays in human cells. A smaller second fraction displayed diffusion also constrained but with a significantly faster movement (about five

times). In addition, an exceptionally fast telomere was observed diffusing ten times faster than a chromatin locus.

3.2.3 Mobility of nuclear bodies

Most of the studies on nuclear bodies' mobility have been conducted on PML and Cajal bodies. The two bodies display in average an analogue mobility that can be fitted with the so called "moving corral model" (Görisch et al., 2004). Both display fast movements of $6\text{-}7 \cdot 10^{-3}$ μm^2 s^{-1} over a 300 nm confinement radius and further slower translocation with a mobility coefficient of $1.1 \cdot 10^{-4}$ μm^2 s^{-1}. Nevertheless, three kind of mobility can be observed for PML bodies from very fast translocation to almost complete immobility suggesting that these bodies can associate at least transiently with the chromatin. Interestingly, the mobility of the faster species can be greatly reduced by a sodium azide treatment indicating that it is ATP dependent (Muratani et al., 2002). For the Cajal body it is the chromatin association that was, on the contrary, shown to be ATP-dependent (Platani et al., 2002).

4 The promyelocytic leukemia-associated (PML) body

Among the multiple sorts of "bodies" that were so far identified in the mammalian nucleus the PML nuclear body appears to be distinct with regards to the number of the different proteins which are shown to interact with it as well as the number of its associated functions. Indeed, PML bodies are shown to be involved in processes as different as apoptosis, senescence, cell proliferation, chromatin remodeling, DNA damage reparation, transcription or telomere lengthening. Interestingly, PML bodies are involved in telomere lengthening of telomerase-negative tumor cells through the so-called alternative telomere lengthening (ALT) pathway. The ALT pathway involves a particular sort of PML bodies that are found to co-localize with telomeric DNA (see paragraph 4.4).

4.1 The PML Protein family

The PML protein is the major and central structural component of PML bodies (Ishov et al., 1999; Zhong et al., 2000). Seven PML splicing variants have been identified so far. All of them harbor the same N terminus but differ in the central core domain as well as the C terminus (Fagioli et al., 1992) as shown in Figure I.7.

PML IV was found to interact directly with the tumor suppressor p53 (Bischof et al., 2002) but the specific function of the other isoforms remain however unknown.

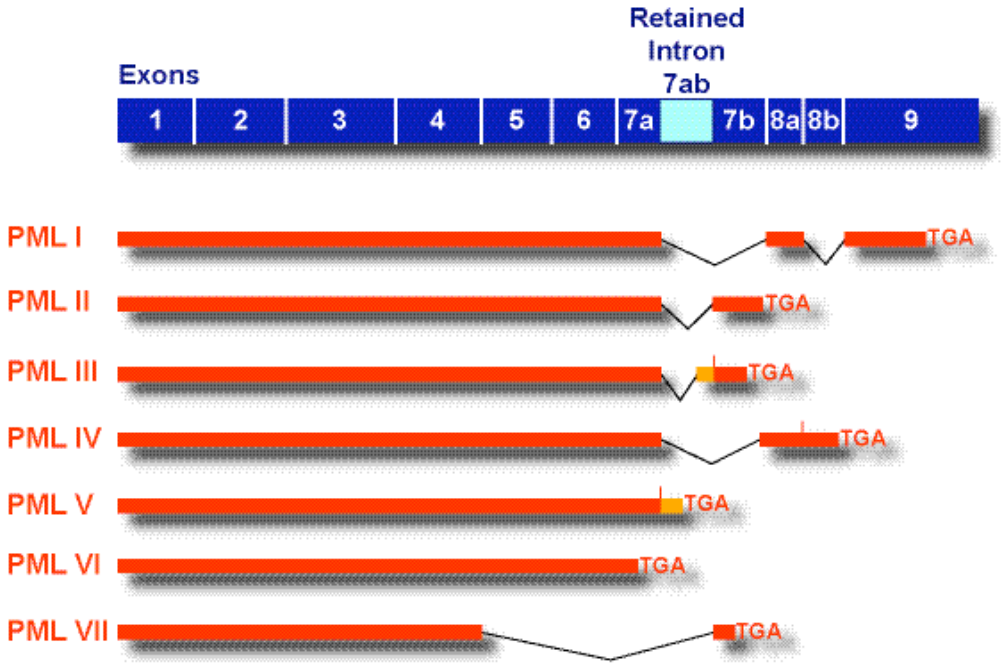

Figure I.7: The PML isoforms
The PML family is composed of seven splicing variants that all share the same N-terminal part but differ in their respective C-terminus.

The N-Terminus of PML harbors three cystein-rich metal binding motifs (Goddard et al., 1991), a RING finger and two B-boxes (Borden et al., 1996), followed by a coiled coil homooligomerization domain (Kastner et al., 1992; Perez et al., 1993), which together are essential for the formation of PML bodies (Fig. I.7). These three motifs are called together RBCC domains (also known as TRIM). The RBCC pattern is common to the sub-group of RING finger proteins among which many proto-oncogenes can be found. Finally PML is modified by SUMO-1 (small ubiquitine-like modifier), a protein that can be found in PML bodies, at lysines 65,160 and 490 (Fig. I.8).

4.2 Structure of the PML body

Although the PML body is often described as a doughnut-shaped structure, it rather displays a hollow-spherical shape (Salomoni and Pandolfi, 2002) of 0.1 to 1 µm in diameter. Typically, 10-30 PML bodies are contained in a single cell (Ascoli and Maul, 1991), but their sizes and numbers change dramatically in various

situations (Dellaire et al., 2006). The PML protein is a major component of PML bodies together with the protein Sp100. In addition, a high number of proteins are found to co-localize with PML bodies in a constant fashion or, for the major part, only transiently depending on the context. These include Sp100 related proteins, SUMO that modifies the PML protein, the heterochromatin protein 1 (HP1), p53, pRb, Daxx, and CBP. Recent observations made on extremely large PML bodies that are found to be associated with the centromeric instability and facial dysmorphy (ICF) syndrome indicate that PML bodies are highly organized and composed of several layers of protein compartments in an onion-like structure (Luciani et al., 2006).

Figure I.8: The structure of PML protein
Only one splice variant (PML III) is shown. The positions of the RING finger domain, the B-Box motifs and the coiled coil, as well as a serine-rich region are indicated. The SUMO-1 modification places are shown in red.

4.3 The multiple functions of the PML body

PML bodies have been implicated in multiple biological functions through the large number and function of their interacting factors and can therefore be described as a “mobile molecular toolbox” of the nucleus. The following list describes some of the most important functions of the PML bodies and is not exhaustive.

4.3.1 PML bodies and senescence, apoptosis and tumor suppression

PML acts as a potent growth suppressor by inducing a block in the G1 phase of the cell cycle (Le et al., 1998) and $PML^{-/-}$ mouse embryonic fibroblasts (MEFs) are known to grow faster than their wild type counterparts. PML bodies are also reported to be involved in premature senescence. This phenomenon appears to be mediated by the PML IV isoform that stabilize and activates p53 phosphorylation and acetylation (Bischof et al., 2002; Salomoni and Pandolfi, 2002). PML has also been shown to physically interact with the retinoblastoma

protein (pRb), which is found in PML bodies and is involved in the control of cell cycle entry and cellular senescence (Alcalay et al., 1998). PML is finally suspected to act as a tumor suppressor (Salomoni and Pandolfi, 2002).

4.3.2 PML bodies and transcription

Together with Daxx, the PML protein plays a central role in p53-mediated apoptosis. For example $PML^{-/-}$ cells are resistant to the lethal effects of γ irradiation and CD95-induced apoptosis (Guo et al., 2000; Wang et al., 1998). One of the major components of the PML bodies, the protein Sp100, is suspected be involved in transcription regulation and known transcription regulators such as Daxx, Bright or HSF2 are found to co-localize with it. PML bodies play a direct role in transcription through the recruitment of p53, the acetyl-transferase CREB-binding protein (CPB), HIPK2 (Kim et al., 1999) and MDM2 (Louria-Hayon et al., 2003). Transcriptionally active genes are found to associate preferentially with PML bodies (Wang et al., 2004) and nascent transcript have been shown to accumulate at their surface (Boisvert et al., 2000).

4.3.3 PML bodies and DNA metabolism

Interestingly, proteins involved in DNA metabolism, such as Rad51, RP-A, hRad9 BLM, Mre11, and NBS1 can be found in PML bodies (Lombard and Guarente, 2000; Mirzoeva and Petrini, 2001; Nabetani et al., 2004; Zhong et al., 1999). BLM is a RecQ-type helicase encoded by the gene mutated in the Bloom syndrome, which is characterized by high frequencies of sister chromatid exchanges and cancer susceptibility. NBS1 is encoded by the gene mutated in the Nijmegen breakage syndrome that is associated with genetic instability and cancer predisposition. NBS1, Mre11, and Rad50 form a complex called the MRN complex, which plays a critical role in DNA damage sensing, repair, and checkpoint. Altogether, these results suggest that PML bodies are also involved in genomic stability. PML bodies are moreover found to co-localize with unscheduled DNA synthesis loci in damaged cells suggesting they play a direct role in DNA repair (Dellaire and Bazett-Jones, 2004).

4.3.4 PML bodies and chromatin

PML bodies have been shown to associate tightly with chromatin (Eskiw et al., 2003; Muratani et al., 2002) at least transiently and their functional interactions

appear to be very complex. On the one hand chromatin modifying proteins such as acetyltransferases (Boisvert et al., 2001; Doucas et al., 2000; von Mikecz et al., 2000) and de-acetylases (Wu et al., 2001) as well as the heterochromatin protein 1 (HP1) (Hayakawa et al., 2003; Ishov et al., 1999) accumulate in PML bodies, implying a role in chromatin structure regulation. PML bodies are in addition suspected to play a central role in the establishment of the constitutive heterochromatin at DNA satellites (Luciani et al., 2006). On the other hand chromatin itself has been shown to play a direct role in PML bodies structural integrity as for example DNAse treatments of the nucleus or apoptosis induction leads to their destabilization (Eskiw et al., 2004). Moreover a recent study has shown that PML bodies number is increasing in early S phase by a fission process suggesting that PML bodies, tightly bound to several chromatin domains are thorn apart by the replication machinery (Dellaire et al., 2006).

4.4 The ALT-associated PML body (APB)

One remarkable feature of the PML body is the role that it plays in the alternative lengthening pathway. A fraction of cells in a given ALT population possess enlarged PML bodies called ALT associated PML bodies or APBs (Yeager et al., 1999). APBs display the unique feature to enclose a large amount of telomeric repeats as revealed by fluorescence in situ hybridization (FISH) or the immunological detection of telomeric DNA-binding proteins TRF1 and TRF2. APBs contain PML protein variants along with Sp100, Mre11, NBS1, Rad50, and BLM that normally exist in PML bodies. In addition, APBs contain the telomere-associating protein Rap1 and the recombination proteins Rad51, Rad52, and BRCA1, which are not normally present in PML bodies, as well as many protein involved in double stand break detection and reparation machinery such as hRad9, hHus1, hRad1 and hRad17 (Nabetani et al., 2004; Naka et al., 2002; Wu et al., 2003; Wu et al., 2000; Yeager et al., 1999). Furthermore, 5-bromo-2'-deoxyuridine (BrdUrd) incorporation was detected in U2OS cells at foci where the APB marker hRad9 and telomere DNA co-localize indicating that DNA is synthesized at APBs. This DNA synthesis appears to be caffeine dependant (Nabetani et al., 2004; Wu et al., 2000).

5 Approaches to study the dynamics of nuclear components

5.1 *In vivo* labeling of nuclear proteins

The major breakthrough in the study of dynamic processes in the cell was the introduction of the green fluorescent protein (GFP), isolated from a jellyfish (Prasher et al., 1992; Tsien, 1998). Using GFP fusion proteins it became possible to monitor the localization and the dynamics of proteins in living cells by simply stably or transiently transfecting the corresponding DNA constructs (Chalfie et al., 1994; Wang and Hazelrigg, 1994). Later, improved variants of the GFP (eGFP), new fluorescent protein with different absorption and emission spectra were generated (eBFP, eCFP, eYFP) (Heim et al., 1994) or isolated from different species (DS red, mRFP1) allowing the observation of multiple proteins simultaneously (Campbell et al., 2002).

5.2 Global protein mobility (FRAP/FCS)

As a technique to study nuclear protein dynamics, fluorescence fluctuation approaches have been proven to be highly valuable. These involve fluorescence recovery after photobleaching (FRAP) and fluorescence correlation spectroscopy (FCS). In a FRAP experiment, a pulse of high intensity light from a laser is used to photobleach fluorophores, typically GFP-fused proteins. Subsequently, fluorescence recovers due to diffusion of unbleached fluorophores into the bleached region and concomitant movement of bleached fluorophores out of the region (Lippincott-Schwartz et al., 2001). Under optimal conditions, the recovery kinetics depends only on the molecular mobility, which is usually determined by the diffusion as well as the binding kinetics of the fluorescent molecules to anchored or slowly moving structures. In most cases, a diffusion coefficient and/or flow velocity and mobile fraction can be determined. FCS is another technique that can be used to study protein mobility. Similar to FRAP, this method requires molecules of interest to either be fluorescent or, alternatively, be conjugated to a fluorescent dye or protein. In this method, the fluctuations in the fluorescence intensity from sample observation volume are recorded and temporally autocorrelated to reveal information about the concentration and dynamics of the fluorescent species (Hess and Webb, 2002; Thompson et al., 2002). Both

methods have been extensively used to measure the diffusion speed, the time of residence and the relative proportion between bound and free fraction of chromatin-associated proteins such as core histones, histone H1 (Kimura, 2005) or heterochromatin protein 1 (HP1) (Schmiedeberg et al., 2004). However they are not suited to analyze the mobility of a specific chromatin locus.

5.3 *In vivo* labeling of chromosomal loci

5.3.1 The *lac* operator/Lac inhibitor technique

An elegant technique to trace individual chromosomes during interphase in living eukaryotic cells, the *lac*O/LacI-GFP system, was introduced by Belmont and co-workers (Robinett et al., 1996; Straight et al., 1996), and its application is reviewed in (Hediger et al., 2004). This method is based on the high affinity binding of a bacterial Lac repressor (LacI) protein fused with an autofluorescent protein domain to its recognition sequence, the *lac* operator (*lac*O). A schematic representation of the method is given in Figure I.9. A plasmid containing up to 256 repeats of the *lac*O sequence is stably transfected in mammalian cells. As for a standard stable transfection the integration occurs in a random and multiple-copy fashion. The integration loci are then detected by transiently transfecting the cells with a LacI construct. In a similar approach the *tet*O/TetR-GFP system was used to study the segregation behavior of chromosomes in yeast cells (Michaelis et al., 1997). The *lac*O/LacI-GFP system has been applied in a number of studies of chromatin structure and dynamics (Cabal et al., 2006; Chubb et al., 2002; Heun et al., 2001; Janicki et al., 2004; Taddei et al., 2006; Thomson et al., 2004; Tumbar et al., 1999). It can be extended by using a combination of *lac*O and *tet*O arrays for a two color label to examine the relative position of two genomic loci as shown in studies of *E. coli* (Lau et al., 2003) and yeast (Bystricky et al., 2004).

5.3.2 *In vivo* labeling with PNAs

A novel approach for the visualization of chromatin specific loci, based on peptide nucleic acid (PNA) labeling, was recently introduced (Molenaar et al., 2003). Due to their pseudo-peptidic backbone, PNA probes are not charged and are therefore not submitted to the repulsion forces involved in DNA/DNA interaction. PNAs display such an affinity for their complementary sequence that they do not require the denaturation of their target DNA to hybridize. When loaded inside a living cell,

fluorescently labeled PNAs can thus hybridize *in vivo* at specific sequences. Unfortunately, PNAs are synthetic sequences and only small size probes can be generated. Therefore the application of PNA for *in vivo* chromatin labeling is so far limited to long repetitive sequences like the telomeres.

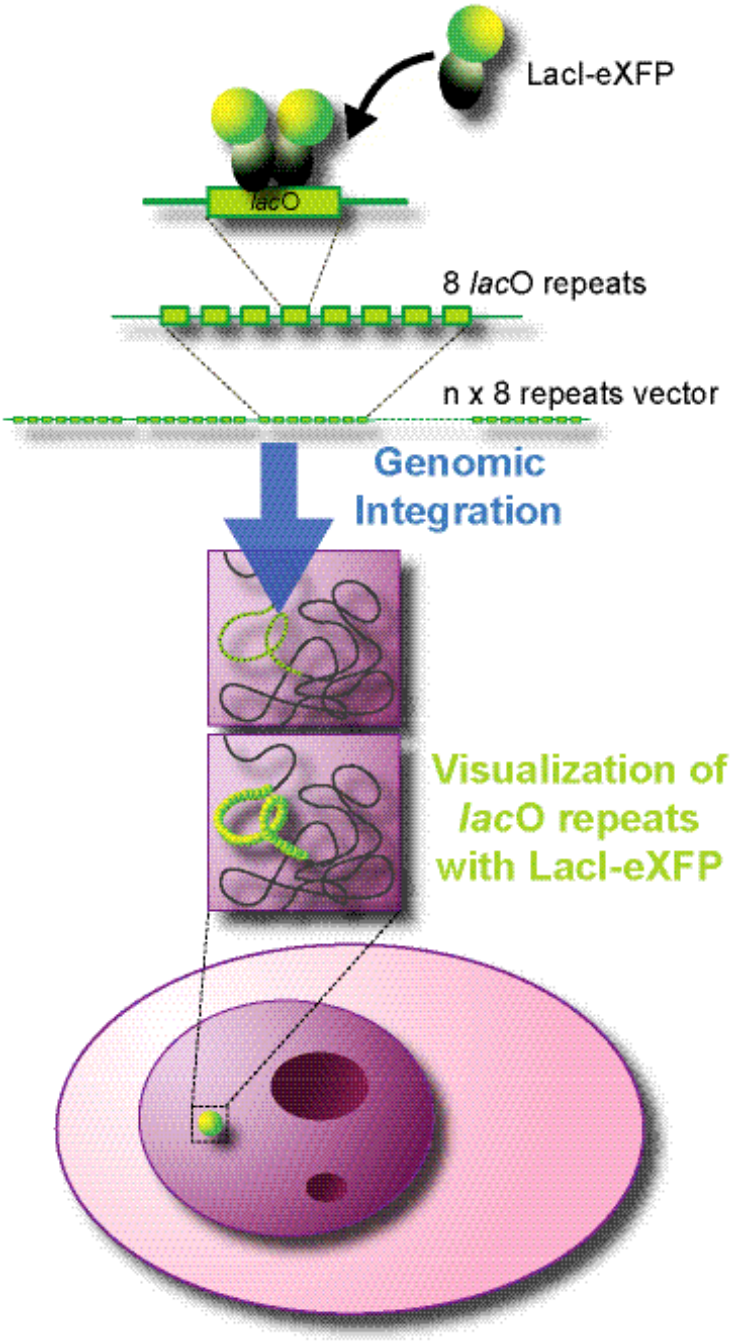

Figure I.9: Description of the *lac* operator/ Lac inhibitor *in vivo* chromatin labeling method.

A vector containing up to 256 repeats of the *lac*O is stably transfected in a mammalian cell. The repeats are integrating in a random and multiple copy fashion and in most of the cases at a single locus. The arrays are then visualized in living cells by transiently transfecting a construct coding for LacI fused to an autofluorescent protein.

6 Scope of the thesis

About 10 to 15 % of the human tumors, including very aggressive forms, are using the ALT telomere lengthening pathway. Understanding the ALT mechanism could provide much valuable information in the treatment of these particular tumors. Telomere lengthening constitutes indeed a target of choice in cancer treatment, as the telomere maintenance is crucial for the growth of the tumor cells. If this one is stopped or impeded cells would rapidly undergo replicative senescence. Targeting the ALT pathway would moreover allow to treat specifically tumor cells since even the fast growing healthy tissues are using the telomerase to maintain their telomere length and would therefore not be affected by the treatment. The ALT mechanism is based on DSB repair and recombination, which involves dynamic telomere-telomere interaction, as well as the association of telomeres with PML bodies in the APB structure, which is thought to be the siege of the lengthening.
With this regards, the first purpose of this thesis was to describe the overall mobility of telomeres in the osteosarcoma cell line U2OS which uses the alternative telomere lengthening pathway. We have therefore generated a large amount of cell lines with telomeric *lac*O arrays inserts that were characterized with respect to insert number and chromosomal insertion loci. A particular cell line with three different *lac* operator arrays stably inserted at telomeric sites was obtained. The three coordinates system provided by the three different *lac*O arrays allowed us to study the mobility of telomeric regions regardless of cell mobility on a time scale ranging from the millisecond to the hour by using high-performance live cell imaging systems. Previous telomere dynamics studies were conducted with *in vivo* PNA telomere labeling, a method that allows to visualize only the telomere displaying the longest repeats (Molenaar et al., 2003). On the contrary, the *lac*O/LacI system allows to label a telomere regardless of the repeats length. We therefore investigated if a correlation could be established between telomere length and mobility by using combination of live cell imaging and FISH experiments. Finally, the *lac*O labeled telomeres allowed us to characterize the PML bodies relative mobility towards telomeres as well as the dynamics of the formation as well as the structure of the APBs was investigated.

II. Material and Methods

1 Material

1.1 Biological material

1.1.1 Bacterial strains

Bacteria are used in molecular biology for amplification and preparation of plasmid-DNA. Commercially available chemocompetent bacteria *E. coli* XL1 blue, XL10 gold and Sure (Stratagene, Germany) were used in this thesis.

1.1.2 Cultured cell lines

The following cell lines were used for creating stable clones with *lac*O arrays integration or were directly used:

- Human osteosarcoma cell line U2OS, ATCC n° HTB 96, was used to generate all *lac*O array cell lines described in this study.
- HeLa H2A-eYFP cell line was kindly provided by T.A. Knoch (Fejes Tóth et al., 2004; Knoch et al., 2000).

1.1.3 Expression vectors

Plasmids are constructs used for the bacterial amplification of DNA fragments. Some plasmids also allow the expression of a cDNA coupled to an autofluorescent protein in mammalian cells by transfection.

Usual name	Insert	XFP	Ref.	Size (bp)	Selections	
p3'SS	LacI-NLS-eGFP	eGFP	1	± 7400	Amp	Hygro
TetR-eGFP	TetR-eGFP	eGFP	**2**	5384	Kan	Neo
pSV2-LacI-XFP	LacI XFP	mRFP1	3	5506	Kan	Neo
		eGFP	**2**	5506	Kan	Neo
		eCFP	**2**	5506	Kan	Neo
		eYFP	**2**	5506	Kan	Neo
pLAU53	LacI-eCFP + TetR-eYFP bacterial expression vector	eCFP eYFP	4	7674	Amp	-
pLAU25	30-40 *lac*O repeats	-	4	± 4090	Amp	-
pLAU29	30-40 *tet*O repeats	-	4	± 4090	Amp	-

pLAU41	About 120 *lac*O repeats	-	4	7946	Amp	-
pLAU42	About 120 *tet*O repeats	-	4	7564	Amp	-
pLAU43	About 240 *lac*O repeats	-	4	12290	Amp	-
pLAU44	about 240 *tet*O repeats	-	4	11704	Amp	-
pSVHIII-H1.0 XFP	Histone H1.0	eGFP	5	5900	Kan	Neo
		eCFP	5	5900	Kan	Neo
		eYFP	5	5900	Kan	Neo
pSVHIII-H2A.i XFP	Histone H2A.i	eCFP	5	5700	Kan	Neo
		eGFP	5	5700	Kan	Neo
		eYFP	5	5700	Kan	Neo
		mRFP1	**2**	5700	Kan	Neo
PML III GFP	Nuclear protein PML III	GFP	6	± 7000	Amp	n.k.
PMLIII XFP	Nuclear protein PML III	eGFP	7	6814	Kan	Neo
		mRFP1	**2**	6814	Kan	Neo
PMLV eGFP	Nuclear protein PML V	eGFP	7	6570	Kan	Neo
PCNA XFP	Nuclear protein PCNA	eGFP	**2**	± 6500	Amp	n.k.
		eYFP	**2**	± 6500	Amp	n.k.
		mRFP1	**2**	± 6500	Amp	n.k.
		eCFP	6	± 6500	Amp	n.k.
pcDNA 3.1 (+)	Empty vector	-	8	5428	Amp	Neo
pcDNA 3.1 (+) Hygro	Empty vector	-	8	5600	Amp	Hygro
pRSET B-mRFP1	Expression vector	mRFP1	3	3590	Amp	-
pEGFP-N1	Expression vector	eGFP	9	4700	Kan	Neo
pEYFP-N1	Expression vector	eYFP	9	4700	Kan	Neo
pEGFP-C1	Expression vector	eGFP	9	4700	Kan	Neo
pEYFP-C1	Expression vector	eYFP	9	4700	Kan	Neo
pECFP-N1	Expression vector	eCFP	9	4700	Kan	Neo

Table II.1: Plasmids used in this study

Kan: Kanamycin prokaryotic resistance; Amp: Ampicilin prokaryotic resistance; Hygro: Hygromycin eukaryotic selection marker; Neo: Neomycin (G418) eukaryotic selection marker; n.k.: not known.

References: 1: A. Belmont, (Belmont et al., 1999); **2: This thesis**; 3: C. Cardoso; 4: D. Sherrat, (Lau et al., 2003); 5: T. A. Knoch, (Knoch et al., 2000); 6: S. Görisch,(Görisch et al., 2004); 7: P. Hemmerich,(Kiesslich et al., 2002); 8: Invitrogen, USA; 9: Clontech, TaKaRa Bio inc., Japan.

1.1.4 DNA oligonucleotides

Synthetic DNA oligonucleotides are used as primers for sequencing and polymerase chain reaction (PCR) or, when they are directly coupled with a fluorescent dye, for fluorescent *in situ* hybridization (FISH) assays. All DNA oligonucleotides were purchased from Thermo Fisher scientific.

Primers used for DNA sequencing

Name	Sequence	Hybridization locus
eXFP rev	CTTGTGGCCGTTTACGTC	+23 for all *X*FP cDNAs
eXFP seq For	GTCCTGCTGGAGTTCGTGAC	+665 for all *X*FP cDNAs
PeXFP-C1 MCS Rev	GATCAGTTATCTAGATCCG	+1399 in the MCS of pE*X*FP-C1 plasmid family
Histone For	CCTCTGAGCTATTCCAGAAG	70bp before Histone insert in pSV-HIII Hx-XFP vectors
pUC18 ins For	CTCTTCGCTATTACGCCAGC	+290 on PUC18 vector
pUC18 ins Rev	CCGGCTATGTTGTGTGG	+508 on PUC18 vector
TetR For	CATCGCGATGGAGCAAAAG	+277 on TetR cDNA
TetR Rev	GCGCTGAGTGCATATAATGC	+388 on TetR cDNA
LacI For	CGATAGCGGAACGGGAAG	+699 on LacI cDNA
PML III.2 For	CAGATGCACGCGGCCGTCGG	+792 on PML IIII cDNA
PML III.3 For	GCAACCACGTGGCCAGTGGC	+1639 on PML III cDNA

Table II.2: List of sequencing primers used in this Thesis

DNA oligonucleotides used for FISH experiments

Name	Sequence	Fluorescent dye
*lac*O Cy3	AATTGTTATCCGCTCACAATT	Cy3
*lac*O Fluo	AATTGTTATCCGCTCACAATT	Fluo 6 Fam

Table II.3: List of fluorescent-labeled FISH oligonucleotide probes used in this Thesis

Primers used for cloning

Name	Sequence	Remarks
TetR Bgl II ATG NLS For	AAAGATCTCACCATGGTGGATCCAAAAAAGA AGAGAAAGGTAGCCATGGTGTCTAGATTAC	Bgl II cloning site followed by ATG and a NLS
TetR Eco RI rev	ATGAATTCCGTCAGACCCACTTTCAC	Eco RI cloning site

Table II.4: List of cloning primers used in this Thesis

1.1.5 Enzymes

The following enzymes were used for the generation, the modification or the analysis of the plasmids used in this thesis:

Restriction enzymes	MBI Fermentas, Lithuania
T4 DNA ligase	MBI Fermentas, Lithuania
Calf intestine phosphatase	New England Biolabs, USA
Pwo DNA polymerase	Peqlab, Germany

1.1.6 Antibodies

Antibodies were used in this thesis for immunolabeling of fixed cells. The primary antibody is specific for the protein of interest. The secondary antibody is specific for the primary antibody and is coupled to a fluorescent dye.

Primary antibodies

Antibody	Specificity	Origin specie	Provider
Anti-PML	Human	Mouse	Santa Cruz Biotechnology, USA

Table II.5: List primary antibodies used in this Thesis

Secondary antibodies

Antibody	Origin specie	Coupled fluorescent dye	Provider
Anti-mouse IgG	Goat	Alexa 488	Molecular Probes, USA
Anti-mouse IgG	Goat	Alexa 568	Molecular Probes, USA

Table II.6: List secondary antibodies used in this Thesis

1.2 Media and solutions

1.2.1 Cell culture reagents

DMEM, low glucose, without phenol red	Invitrogen, USA
DMSO	Sigma-Aldrich, Germany
Fetal calf serum (FCS) “Gold”	PAA, Germany
L-glutamine	PAA, Germany
Trypsin	PAA, Germany
G418 solution	PAA, Germany
Hygromycin B solution	PAA, Germany
Colcemid “Caryo max”	Invitrogen, USA

1.2.2 Cell coloring dyes and mounting reagents

Vectashield	Linaris, Germany
Vectashield with DAPI	Linaris, Germany
To-Pro 3 iodine	Molecular Probes-Invitrogen, USA

1.2.3 Bacteria culture media

Luria Bertani (LB) medium	1 % (w/v) Bacto tryptone 0.5 % (w/v) yeast extract 86 mM NaCl
LB-media with antibiotics	LB + 100 µg/ml ampicillin LB + 50 µg/ml kanamycin
SOC	2 % (w/v) Bacto tryptone 0.5 % (w/v) yeast extract 4.3 mM NaCl 2.5 mM KCl 10 mM MgCL2 20 mM Glucose (sterile filtered)
LB-agar plates	15 g agar was added to 1000 ml LB Antibiotics added to cooled medium

1.2.4 Buffers

6 x gel electrophoresis loading buffer	0.25 % (v/v) Bromophenol blue 30 % Glycerol in water
1 x PBS (pH 7.4)	2.7 mM KCL 1.7 mM KH_2PO_4 137 mM NaCl 10 mM Na_2HPO_4

1 x TBE (Tris/borate/EDTA; pH 8.0)	89 mM Tris 89 mM H_3BO_3 2 mM EDTA
20 x SSC	0.15 M NaCl 0.015 M $C_6H_8O_7Na_3$

1.3 Kits

The following kits were used in this thesis for standard molecular biology, cell transfection and PNA-FISH assays:

Effectene transfection reagent	Qiagen, Germany
Fugene transfection reagent	Roche, Germany
Nucleospin miniprep kit	Macherey-Nagel, Germany
Nucleobond PC 500 Plasmid Maxi Kit	Macherey-Nagel, Germany
Qiaquick PCR Purification System	Invitrogen, Germany
Qiaquick gel Extraction Kit	Invitrogen, Germany
Telomere PNA FISH Kit	DakoCytomation, Denmark

1.4 Instruments

Spectrophotometer	V 530	Jasco, Japan
Inverted fluorescence microscope	DMIRB	Leica Microsystems, Germany
Laser scanning microscope (LSM)	TCS-SP2	Leica Microsystems, Germany
Spinning Disk LSM	Ultra view	Perkin-Elmer, USA
	ERS-FRET	Perkin-Elmer; USA
Thermocycler	Mastercycler	Eppendorf, Germany
Gel documentation system	GD/Chemi Doc	Bio Rad, Germany

1.5 Software

Image J	1.36b	National Institutes of Health, USA
Adobe Photoshop	CS	Adobe Systems, USA
Adobe Illustrator	CS	Adobe Systems, USA
Mat Lab	7.3.0	The Mathworks, Inc., USA
Excel	11.3.5	Microsoft, USA
Kaleida Graph	4.0	Synergy Software, USA

4 Peaks	1.5	Mek&Tosj, The Netherlands Cancer Institute, Holland
DNA Strider	1.46f	Commissariat à l'énergie atomique (CEA), France

2 Methods

2.1 Molecular biology techniques

2.1.1 Transformation of competent bacteria

E.coli cells were used to amplify plasmid DNA. The transfer of plasmids into bacteria requires that the cell membrane is permeable for the plasmids. 30 µl of competent *E.coli* were thawed on ice, mixed with 3 µl of the ligation reaction, or, in case of a re-transformation, with 0.1 ng plasmid DNA and incubated on ice for 30 minutes. For the plasmid uptake, the bacteria were heat-shocked at 42°C for 90 s and briefly equilibrated back on ice. 270 µl pre-warmed SOC media was added to the cells and the cells were incubated for 30 to 60 minutes at 37°C with shaking. 250 µl of the bacteria suspension was plated onto agar-plates containing the appropriate antibiotic. Cells were incubated over night at 30 to 37°C depending on the nature of the transformed plasmid. It appeared that growing large (> 10 kb) plasmids or vectors containing repetitive sequences (*lac*O or *tet*O arrays) in standard bacterial strain (XL1 or XL10) at 37°C highly increased the probability of unwanted DNA recombination. Therefore those constructs were systematically transformed in recombinase-negative *E.coli* "Sure" cells and grown at ~ 30°C.

2.1.2 Isolation of plasmid DNA

E. coli containing the plasmid of interest were grown on agar plates. Colonies were picked from the plates and grown for minipreps in 5 ml LB-medium in the presence of the appropriate antibiotic in a shaking incubator at 37°C over night.
For maxipreps a 5 ml pre-culture in LB-medium was grown for 6 hours and transferred to an overnight culture (100 ml for low-copy and 500 ml for high-copy plasmids). Isolation of plasmid DNA was performed according to the manufacturers protocol (Nucleospin Miniprep Kit and Nucleobond PC500 Plasmid Maxi Kit).

2.1.3 Agarose gel electrophoresis

Agarose gel electrophoresis is used to separate DNA-fragments in an electric field according to their size. The concentration of the agarose is dependent of the size

of the DNA fragments. The agarose was melted by boiling in 1 x TBE buffer. The solution was poured into a gel sled and was allowed to harden. For electrophoresis, the gel was placed in a gel chamber and covered with 1 x TBE buffer. The samples were mixed with loading buffer and loaded into the well of the gel. Electrophoresis was run for 30 to 90 min at 90-120 V and 500 mA. The DNA was stained by soaking the gel for 5 minutes in 1 µg/ml ethidium bromide at room temperature. Images were taken with the digital camera device of the Gel Documentation System.

2.1.4 Determination of DNA concentration

The concentration of DNA was determined from absorbance measurements with a spectrophotometer (Jasco GmbH, Germany). The absorbance of the nucleic acid solution was determined of a wavelength of λ = 260 nm. Contaminations with proteins or phenol can be detected by calculating the ratio of OD_{260}/OD_{280}, as protein or phenol increase the A_{280}. A ratio of 1.8 to 2.0 indicates low protein contamination of the DNA. In general, the higher the ratio, the purer the nucleic acids are. A ratio $<$ 1.6 might show residual amounts of proteins or phenol, whereas a ratio $>$ 2 occurs if the sample is too diluted. An absorbance unit of the optical density of 1 at λ = 260 nm (OD_{260} = 1) corresponds to a concentration of 50 µg/ml of dsDNA.

2.1.5 Restriction digestion

Restriction endonucleases are nucleases from bacteria, which cut DNA sequences at specific recognition sites, often containing a palindromic sequence. For cloning purposes, using two different restriction nucleases that produce 5' overhangs ('sticky ends') is advantageous, since sticky ends prevent re-ligation of the vector without insert DNA and produce sense-orientated inserts. Double restriction digests can be performed in many cases in the same buffer system.

Analytical restriction digestion

Analytical digestions were performed in 10 µl volume with 50 ng to 1 µg DNA for 1 hour with 5 Units (U) of enzyme at the required temperature (37°C for the large majority of the enzymes). DNA fragments were analyzed by agarose gel electrophoresis.

Preparative restriction digestion

For preparative purpose up to 10 µg DNA was digested in a final volume of 50 µl with up to 40 U enzyme for 2 hours to overnight. In case of impossible double digestion for buffer incompatibility reasons only one enzyme was used first. The restricted fragment was then gel-purified and subsequently cut with the second enzyme and finally purified again the same way.

Partial restriction digestion

4-5 µg of plasmid DNA was digested with 5-10 units of the single cutting enzyme at 37°C in a final volume of 40 µl. After 1-2 hours, 5-10 units of the multi cutting enzyme were added and the final volume was adjusted to 85 µl. Digests were incubated at 37°C. 10 µl samples were taken after 2, 5, 10, 15, 20, 25, 30, and 40 minutes and mixed with 2 µl of 6 x DNA loading buffer with 100 mM EDTA and kept on ice. Subsequently, 2 µl of each sample were subjected to agarose gel electrophoresis. Samples containing the desired DNA fragment were pooled and purified on an agarose gel.

2.1.6 Gel purification

After digestion of vector and/or PCR products, restriction enzymes and side products need to be removed from the samples to enable ligation. The DNA was separated in a 1-2 % agarose gel. As the exposition to 254 nm UV light leads to pyrimidine dimmers in the DNA that can cause mutation the gel observation and handling time was kept as short as possible and reduced UV light source was used (“preparative light” modus on the gel documentation device). The bands of interest were cut out carefully with a sharp scalpel blade on the UV table and DNA was extracted from the agarose gel with a gel purification kit according to the manufacturer’s instructions (Qiaquick gel extraction kit).

2.1.7 Primer design

Primers are short, single stranded, DNA sequences used for sequencing, PCR reactions and fluorescent *in situ* hybridization (FISH). Typically 19-20 base-long primers were designed. As the annealing temperature is depending from the base composition the primer were designed to contain a minimum of 50% G/C content when possible. For cloning purposes it is often required to add a restriction site on the 5’ end of the primer. It is then necessary to add one or two more bases

upstream to the enzyme site to assure a good cleavage. It is moreover possible to add all kind of short sequences (Nuclear Localization Signal, stop codons, protein recognition tags…) between the restriction site and the complementary sequence. For all the PCR primers designed for the cloning of a sequence in an expression plasmid a particular attention to the conservation of the reading frame is given.

2.1.8 PCR

In order to amplify a specific DNA target sequence, a forward and a reverse primer were designed as described in the previous paragraph. The target sequences were amplified with Pwo DNA polymerase. According to the enzyme provider protocol the standard PCR reaction volume is 50 µl and is divided in two master-mixes from 25 µl each (final concentration is given for the whole mix). Both master-mixes are kept on ice.

Master-mix I:

	Volume	Final concentration
dNTP (10 mM each)	1 µl	200 µM
Downstream Primer (20 pM/µl)	1,5 µl	600 nM
Upstream Primer (20 pM/µl)	1,5 µl	600 nM
Template DNA	-	0,1-0,5 µg
H_2O	Fill to 25 µl	-

Master-mix II:

10 x reaction mix	5 µl	1 X
Pwo DNA polymerase	2,5 µl	2,5 U
H_2O	Fill to 25 µl	-

Table II.7: PCR mix composition

The following PCR cycling program was used:

1 cycle	initial denaturation	1+3 minutes	94°C
25-35 cycles	denaturation	1 minute	94°C
	annealing	45 seconds	50 to 65°C
	extension	1 minute/kbp	72°C
1 cycle	final extension	10 minutes	72°C

Table II.8: Typical PCR cycling program

When starting only master-mix I is present in the thermocycler. The master-mix II is added after the first minute of the initial denaturation. This method is an adaptation of the technique known as “hot start” that is used to reduce the probability of unspecific DNA amplification. The annealing temperature was modified according to the primers used. Extension time was calculated in function of the expected amplified fragment length to one minute for each 1 kb amplified. PCR products were then analyzed on a 1 % agarose gel.

2.1.9 Purification of PCR products

The PCR products were purified from primers and nucleotides before restriction digestion. Purification was performed according to the protocol of a PCR purification kit (Qiaquick PCR purification kit). The purified fragments were finally dissolved in 50 µl TE buffer.

2.1.10 Removal of 5-phosphate residues from DNA fragments

In order to prevent re-ligation of a linearised vector, the phosphate groups that deliver the reactive phosphor required for the sugar-phosphate bonds of the DNA, were removed by an alkaline phosphatase (Calf Intestine Phosphatase, CIP). The digested vector DNA was dephosphorylated for 1 hour with 1 unit CIP at 37°C and subsequently inactivated for 15 minutes at 70°C.

2.1.11 Ligation

For the ligation reaction, insert DNA and vector DNA were mixed, such that the molecular ratio between insert and vector was 6:1 for inserts smaller than 2 kb and 3:1 up to 1:1 for inserts greater than 2 kb. The ligation mix was prepared in a final volume of 10 µl containing 1 U T4 DNA ligase and the appropriated buffer, on ice. For small fragments (<1kb) ligation mix was incubated 1 hour at room temperature and for bigger fragments (>1 kb) at 16°C overnight in a thermoblock.

2.1.12 Sequencing

All cloned expression plasmids were sent to Seqlab GmbH (Göttingen, Germany) for sequencing to verify the DNA sequence.

2.1.13 DNA sequences computing

The software DNA Strider (see paragraph 1.5) was used for routine DNA sequences analysis, handling and archiving. The automatic sequencing of DNA

leads sometimes to imprecision. Therefore sequencing raw data, provided as chromatograms, were checked with 4Peaks (see paragraph 1.5) in order to solve these imprecision.

2.1.14 Generation of mammalian expression plasmid

TetR-eGFP

A mammalian expression vector coding for the Tet receptor fused at the N-terminus with the autofluorescent protein eGFP was generated. The TetR cDNA was first amplified by PCR using the vector pLAU 53 (Lau et al., 2003) as a template with the upstream primer "TetR Bgl II ATG NLS For" (see paragraph 1.1.4) that codes for the Bgl II restriction site and a nuclear localization signal (NLS) and the downstream primer "TetR Eco RI Rev" (see paragraph 1.1.4) that codes for the Eco RI restriction site. After purification the PCR fragment and was digested by Eco RI and Bgl II. The mammalian expression vector pEGFP-N1 (Clontech) was digested with the same enzymes. Both DNA fragments were purified on gel and ligged together with the T4 DNA ligase enzyme.

Replacement of autofluorescent proteins

It is possible to observe multiple autofluorescent-coupled proteins in living or fixed cells by transfection if the autofluorescent proteins are emitting in a different spectrum area. Therefore a large palette of XFP proteins is available. Depending on the desired protein combination the substitution of the autofluorescent protein coupled with one or the other is often required. The substitution of the autofluorescent protein was performed as follow: The vector of interest is digested with Nhe I (or Age I) and Bsr GI (a partial digestion is sometimes required if one of the chosen enzymes has more than one digestion site in the vector). The required XFP is extracted from a peXFP plasmid family vector (Clontech) with the same enzymes. The fragments of interest are purified on gel and ligged together with the T4 DNA ligase.

2.2 Cell culture techniques

2.2.1 Cultivation of culture cell lines

Human osteosarcoma cell line U2OS was grown in tissue culture flasks in an incubator providing a constant 37°C temperature, 97 % relative humidity and 5 %

CO_2 in low glucose D-MEM medium, without phenol red supplemented, with 10% FCS, freshly added L-glutamine (2 mM final) and penicillin/streptomycin antibiotic mixture (100 µg/ml final). Medium was renewed every three days.
Cells were passaged by using trypsin in PBS (0.02-0.05 % W/V) (typically 2 ml for a T75 flask) for 5 to 10 min at 37°C after a short PBS wash. When the cells were detached from the flask bottom fresh medium was immediately given in order to inactivate the enzyme. Cells were separated by vigorously pipetting up and down, diluted in an appropriated manner and transferred in a fresh flask. Cells were typically passaged in a one to six fashion each week.

2.2.2 Freezing of cells

The freezing procedure was conducted as follow: A healthy looking, 80 % confluence culture was detached from flask bottom by trypsin treatment and cells were re-suspended in DMEM. Cells were then pelleted at 1200 rpm for 5 min. Supernatant was discarded and cells were re-suspended in ice cold freezing solution (10 % DMSO, 30 % FCS, 60 % D-MEM) at a final concentration of 2-4 million cells per 1 ml (typically 3 ml for a T75 flask). This cell suspension was then alliquoted in 1 ml pre-cooled cryo-vials and directly stored at –80°C over months. For long time conservation (over years) aliquots were transferred the following day to a –150°C freezer.

2.2.3 Thawing of cells

Cells were thawed by rapidly warming the cryo-vials at 37°C in a water bath. When the freezing solution was almost completely thawed (only one last small ice cube visible) the cryo-vials were sprayed with 70 % ethanol to avoid contamination and the whole aliquot was transferred to a T75 flask containing fresh pre-warmed medium. The medium was renewed as soon as the cells were attached to the flask bottom.

2.2.4 Transient transfection

Cells were splitted one or two days before and settled in order to reach 80 % confluence for the transfection day. For subsequent fixation, cells were grown in a 12 or a 24 well plate on autoclaved coverslips. For live cell imaging cells were grown on coverslips for scanning with Leica TS-SP2 or in Lab-Tech chamber (Nunc, USA) for spinning disk Laser scanning microscopy (see paragraph 2.3).

Cells were transfected either with Fugene 6 (Roche) or Effectene (Qiagen). Amount of transfection medium and DNA was empirically optimized for each vector but in a general manner the half of the amount of the manufacturer protocol was used. Cells were studied 12 to 17 hrs after transfection. Medium was renewed 1 to 2 hrs prior to use.

2.2.5 Fixation and mounting of the cells

The cells were washed three times for 2 min with PBS. The fixation was made with 4% Paraformaldehyde in PBS for 12 min at room temperature (RT) followed by three times 2 min PBS washing. Chromatin counterstaining was done either by mounting fixed cells in DAPI-containing Vectashield or by incubation with 1 µM To-Pro 3 iodide solution for 2 min followed by a 2 to 5 min PBS wash and mounting in Vectashield.

2.2.6 Generation of cell lines with stably integrated *lac*O arrays and/or *tet*O arrays

Cell lines with stably integrated *lac*O arrays were obtained by co-transfection with a plasmid containing 240 repeats of *lac* operator (pLAU 43, kindly provided by David Sherrat, Oxford) (Lau et al., 2003) sequence together with a neomycin resistance coding vector (pcDNA3.1). Both vectors were linearised and mixed in a 1:5 or 1:10 ratio. U2OS cells growing in a 12-well plate were then transfected. After 24 hrs cells were trypsinized and transferred to a 12 cm tissue culture dish and 750 µg/ml G418 was added after 24 additional hours. The non-stably transfected cells died after 4-5 days and the complete selection procedure lasted for 10 days. During the selection phase the medium was exchanged daily in order to remove the dead cells. About two to three weeks after beginning of the selection single colonies were visible. Ideally the colonies were 1-1.5 mm in diameter and separated. To ease the cloning procedure, the bottom of the dish was divided in sectors and colony position was marked with a circle using a marker pen. 100-200 clones were then picked with a 10 µl pipette tip and transferred to a 48-well plate. After one more week each surviving clones (30 to 50 %) were trypsinized and transferred to two wells of a 24 well-plates. One of the plates, containing a glass coverslip in each well, was transiently transfected with LacI-eGFP in order to screen the clones after fixation. The corresponding positive clones were grown

from the other 24-well plate. A schematic representation of the cloning strategy is given in Figure II.1.

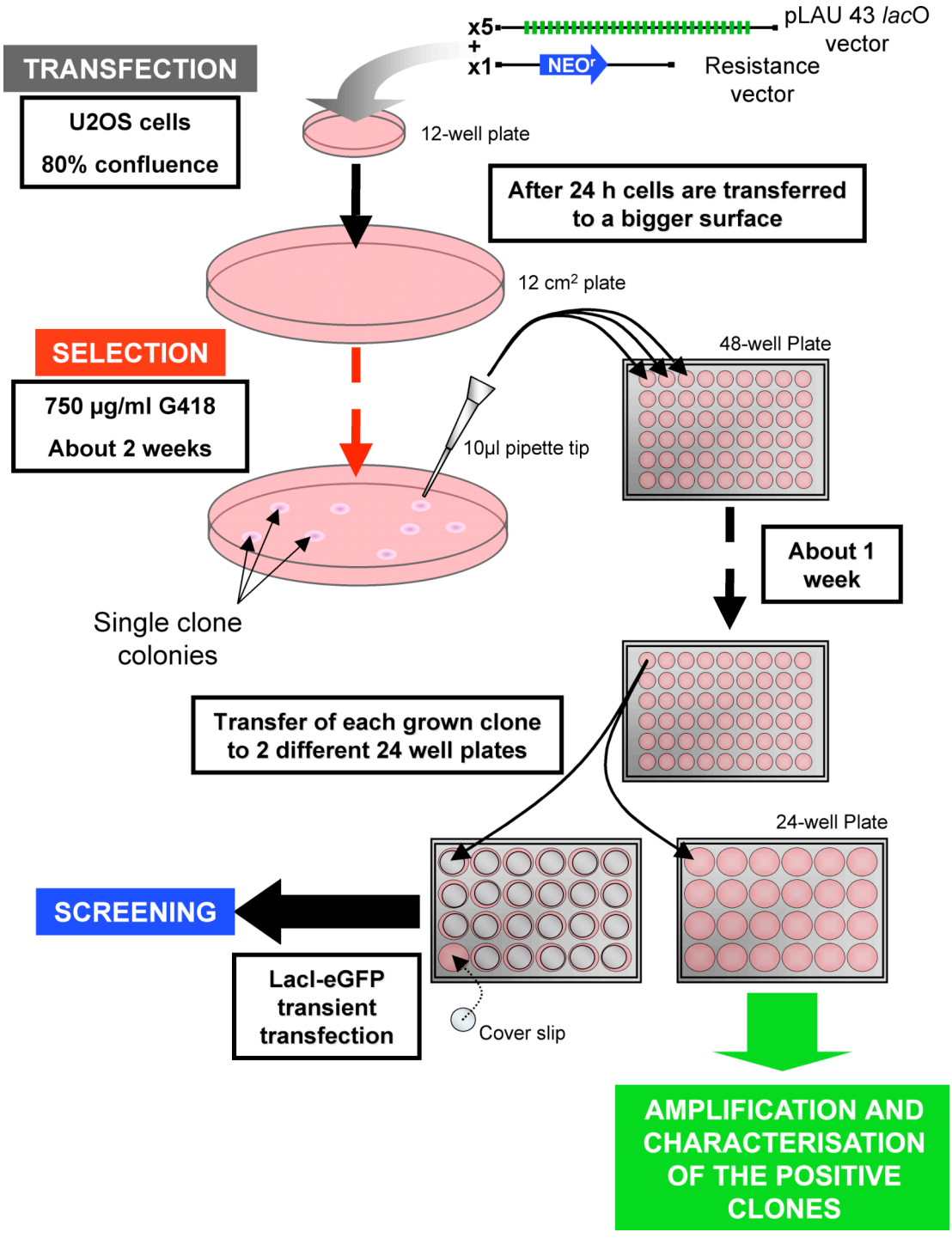

Figure II.1: Schematic representation of the strategy used for the *lac*O array stable cloning in U2OS

Double *lac*O and *tet*O clones were generated following the same procedure by using a U2OS-*lac*O stable cell line and co-transfecting a 240 *tet*O repeats plasmid (pLAU 44) together with a Hygromycin resistance coding plasmid (pcDNA3.1

Hygro). Cells were then selected wit 500µg/ml Hygromycin. For all experiments LacI-XFP (or/and TetR-XFP) was transiently transfected with Effectene 12 to 18 hrs before observation or fixation.

2.3 Microscopy methods

2.3.1 Fixed cells microscopy

For fixed cell imaging purpose a Leica TCS SP2 was used with a 63 x oil objective. Typically a zoom x 6 was used and cells were scanned in Z-axis with a distance of 0.3 µm between the pictures.

2.3.2 Live cell imaging

Two different Laser Scanning Microscope types were used depending on the experimental requirements:

Long time cell imaging

For long time cell imaging (up to 15 hours) a Leica TCS SP2 was used with an objective heating and an environmental chamber (Helmut Sauer) providing heating and CO_2.

- Z stacks of 12 to 20 pictures with 0,3 µm distance were collected every 5 minutes.

High speed microscopy

For an optimal resolution in time a Perkin-Elmer Ultra-View or a Perkin Elmer ERS-FRET spinning disk confocal microscope was used. A Tokai Hit chamber for inverted microscope was used to ensure stable temperature and required humidity to the cells. Experiments were conducted without CO_2 with medium containing 10 mM HEPES buffer pH 7.4.

- For minute scale experiments Z stacks of 10 to 16 pictures with 0.3 µm distance were collected every 8 to 15 s for 15 minutes.
- For second scale experiments cells where the three *lac*O loci were visible in the same focal plan were searched. A single scan was performed every 70 to 150 ms for 5 minutes.

2.3.3 Image treatment and spot tracking

For the single particle tracking all 3D stacks were submitted to maximum intensity projection along the *Z*-axis. The coordinates for the translocation of the *lac*O spots visualized by binding of LacI-GFP were determined with the SpotTracker software kindly provided by Daniel Sage (EPFL, Lausanne) (Sage et al., 2005) that determines the centre of mass of the tracked particle. From the X-Y coordinates of the tracked spots the mean squared displacement (MSD) over time was determined according to Eq. 1.

$$MSD = \left\langle d^2(\Delta t) \right\rangle = \left\langle \left[d\left(t\right) - d\left(t + \Delta t\right) \right]^2 \right\rangle \qquad \text{(Eq. 1)}$$

The squared distance d^2 between the two positions $d(t)$ and $d(t + \Delta t)$ of the particle before and after a time Δt is measured, averaged for all identical values of Δt and then plotted against the time difference Δt from the start point. It is noted that for an isotropic movement of the particle in three dimensions (n = 3) the value determined for D from projections to two dimensions (n = 2) will be the same as that obtained from the analysis of 3-dimensional data sets.

2.4 Metaphase spreads

Cells were splitted the previous day in order reach 80 % confluence. The medium was renewed and 0.5 µg/ml colcemid was added (CaryoMax). After 1 h 30 min incubation at 37°C the culture flask was vigorously shaken and the supernatant was collected. Remaining adherent cells were trypsinized, pooled together with the previously collected supernatant and pelleted by centrifugation at 1000 x g for 10 min at RT. The pellet was re-suspended in 300 to 500 µl fresh medium and pre-warmed (37°C) 75 mM KCl was added drop wise to a final volume equal to the original culture volume. Cells were then incubated for 30 min at 37°C in a water bath, pelleted by centrifugation and re-suspended in 300 to 500 µl KCl solution. Ice cold fixation solution (freshly prepared methanol/glacial acetic acid, 3:1 V/V) was added drop wise to a final volume equal to the original culture volume and cells were incubated 30 min at –20°C. Cells were then pelleted at 1000 rpm for 5 min at RT and re-suspended in 2 ml fixation solution. This step was repeated five times. Microscope slides were carefully washed with ethanol and water. After the

last washing step cells were re-suspended in 100 to 500 µl fixation solution and dropped from 10 to 30 cm height on the inclined slides. Breathing on the slides prior to the dropping facilitated chromosome spreading. After drying slides were submitted to a series of 5 min ethanol washes (70 %, 90 %, 100 %) and used immediately or stored at –80 °C.

2.5 Fluorescent *in situ* hybridization (FISH) technique

2.5.1 Oligo-FISH

Chromosome spreads from each clone were prepared. After a 2-3 min treatment with 250 µg/ml Pepsin in 10 mM HCL slides were washed with PBS and re-fixed 10 min in 4 % Paraformaldehyde in PBS at RT. After an additional PBS wash slides were dehydrated by a series of 5 min ethanol washes (70 %, 90 %, 100 %). For DNA denaturation cells were dipped in 70 % deionized formamid (Applichem), 2 x SSC, pH 7 at 72°C for 5 min and immediately dehydrated with a series of 3 min ethanol washes. After complete drying of the slide 30 µl of 1.5 M NaCl, 0.25 M NaAC, pH 7 containing 200 ng of fluorescent labeled (fluorescein or Cy3) *lac*O oligonucleotide probe was given on the sample, a coverslip was applied and sealed with Fixogum. The slides were incubated overnight at 37°C in a humid chamber. The next day cells were washed in 4 x SSC, 0.2 % Tween 20 at RT for 5 min, mounted in Vectashield and pictures were taken by laser scanning microscopy.

2.5.2 *Lac*O oligo-FISH and Telomere PNA-FISH double hybridization

For telomere length estimation, chromosome spreads were prepared as described in the previous paragraph. A small grid was drowned on the hybridization field on the back of the slide with a diamond pen. Chromosome spreads were then scanned and, for each one, the position on the grid was noted. Fixogum was removed and slides were incubated in PBS to remove the coverslip. Telomere PNA FISH (DakoCytomation) was then performed according to the manufacturers protocol with an hybridization time extended from 2 h to overnight. Previously scanned chromosome spreads were relocated by using the grid coordinate system and scanned with a laser scanning microscope.

2.5.3 Multicolor FISH (mFISH) and second hybridization

Multicolor FISH assays were done using the SpectarVysion (Vysis, Inc.) 24 color chromosome paint assay. Chromosome spreads were treated prior to hybridization: 1 ml 0.1µg/ml RNAse A (Sigma), in 2 x SSC was dropped directly on the region of interest and the slides were incubated 30 min at 37°C. After two 5 min washes in 2 x SSC slides were incubated in a Pepsin (Amresco) solution (20µg/ml in 0,1N HCl) for 5 min at 37°C. Pepsin was subsequently inactivated by washing twice for 5 min in PBS at RT. The slides were then incubated 2 min in a 1% Formaldehyde (sigma), 0.05M $MgCl_2$ PBS solution, washed twice 5 min in PBS at RT and dehydrated by a series of 5 min ethanol washes (70 %, 90 %, 100 %). Denaturation, hybridization and slide washing were conducted according to the manufacturers protocol.

Images were acquired using a Axioplan 2 (Zeiss, Germany) microscope together with a Sensys CCD camera (Photometrix) and the Smart Capture acquisition software (Vysis, Inc.). For each chromosome spread acquisition the coordinates on the microscope table were noted. Images were processed and karyotype was composed using the Quips SpectraVysion software (Vysis, Inc.).

After mFISH picture acquisition, slides were incubated in PBS for 5 min and coverslip was carefully removed. The slides were then incubated twice 10 min in a 4 x SSC solution containing 0.1 % Tween 20 (Roth), washed twice 5 min in 2 x SSC and dehydrated in series of 5 min ethanol washes (70 %, 90 %, 100 %). A *lac*O oligo-FISH was then conducted on the slides. From the previously noted coordinates the mFISH-analyzed chromosome spreads were relocated and images were taken using the same settings as for the mFISH.

2.6 Immunofluorescence

Cells were grown to 80 % confluence on 18 mm diameter coverslips. If required cells were transiently transfected 12-18 h prior to fixation. Cells were fixed with 4 % PFA/PBS, washed and permeabilized by incubating the coverslips for 5 min with ice cold 0.1 % (V/V) Triton X100 solution in PBS. After three PBS washes, cells were incubated for 5 – 15 minutes with 10 % goat serum in PBS to block unspecific antibody binding. After removal of the blocking solution, the cells were incubated with 20 µl of the appropriate primary antibody adequately diluted in PBS for 30 – 60 minutes. Coverslips were washed three time five minutes with PBS

containing 0.002 % (V/V) NP40. The secondary antibody was diluted according to the manufacturer instructions in PBS. A total volume of 20 µl was applied to the cells and incubated for 30 to 60 minutes. After rinsing three times in PBS, the coverslips were dipped briefly into ddH_2O and were either directly mounted or incubated for 1 minute in ethanol and air dried. Coverslips were mounted with Vectashield on microscope slides. Slides were stored at 4°C.

III. Results

1 Characterization of global chromatin mobility

The chromatin dynamics was analyzed *in vivo* in a global manner by fluorescence recovery after photobleaching (FRAP) experiments. For these experiments a HeLa cell line stably expressing H2A-eYFP was used (Fejes Tóth et al., 2004). The H2A histone protein incorporates in the nucleosomes and provides an *in vivo* labeling of the chromatin. A grid pattern was bleached onto labeled chromatin at t=0 and the recovery of the fluorescence in the bleached region was observed over a period of 20 minutes. At the same time, the influence of chromatin remodeling on the fluorescence recovery was monitored (Fig. III.1). From previous experiments we know that sodium Azide treatment leads to an ATP depletion and a compacting of the chromatin whereas treatment with TSA, a chromatin deacetylase inhibitor, leads to a global decondensation (Fejes Tóth et al., 2004).

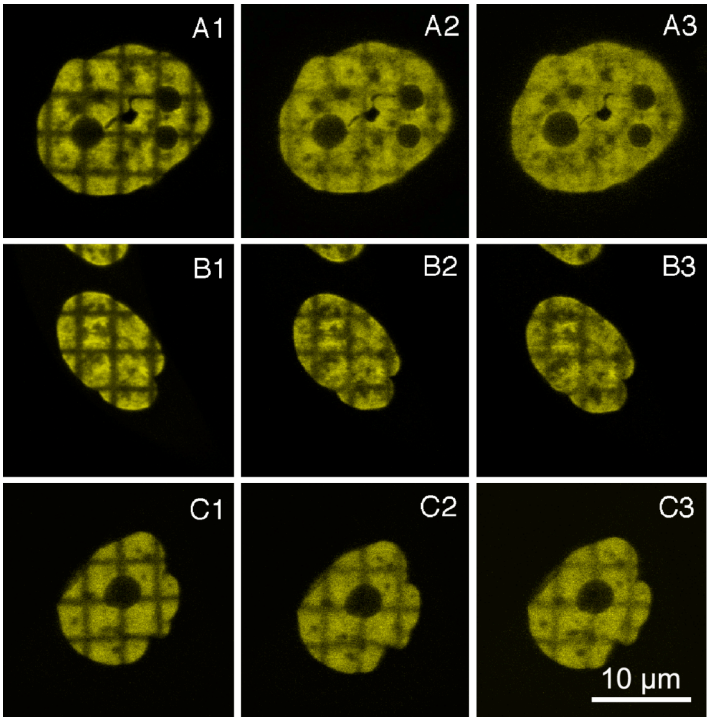

Figure III.1: Effect of chromatin modifying factors on global chromatin dynamics

HeLa cells with autofluorescent histone H2A-eYFP (Fejes Tóth et al., 2004) are studied. The H2A-eYFP fluorescence was bleached in a 5 x 5 µm grid with a line width of 0.5 µm. Then the recovery of the fluorescence was monitored. Images acquired directly after the bleach (1), after 10 minutes (2) and after 20 minutes (3) are shown. (A) Control cells (B) ATP was depleted by adding 10mM sodium azide to the medium and incubating the cells for 30 minutes. (C) Cells treated with 100 ng/ml TSA for 24 h.

In these experiments it can be seen that upon ATP depletion (Fig. III.1B) or increased histone acetylation (Fig. III.1C) the chromatin is somewhat more static than in the control cells as indicated by a more prolonged visibility of the grid after 20 minutes (Fig. III.1, panel 3). This suggests, that the differences observed are due to variations in chromatin mobility on a length scale of a few hundred nanometers and in the exchange rate of histone H2A-eYFP.
The analysis of bleaching experiments revealed the difficulty of studying chromatin dynamics on a global scale and the need for a more specific system. The *lac*O LacI in vivo chromatin labeling system introduced in mammalian cells for the first time by the laboratory of A. Belmond (Robinett et al., 1996) was therefore used to carry out further investigations on chromatin dynamics.

2 Generation of cell lines with stably integrated *lac*O and/or *tet*O arrays

2.1 Cells with stably integrated *lac*O arrays

The plasmid pLAU 43 containing 240 copies of the *lac* operator (Lau et al., 2003) was stably transfected in the human osteosarcoma cell line U2OS. The insertion loci were then visualized in stable clones by transiently transfecting the cells with a construct coding for the Lac inhibitor fused with eGFP or mRFP1. Figure III.2 is summarizing the technique. A serie of over 30 U2OS clones with stably integrated *lac*O arrays was generated by the procedure described in Figure II.1. These are distinct with respect to the chromosomal integration loci, the integration sizes and the number of integration sites per cell. A list of the most relevant clones is given in Table III.1.
The repetitive nature of the *lac*O arrays lead to a relative instability of the insert. First, in order to minimize the intrinsic instability of the sequence, the transfected constructs, pLAU 43 and pLAU 44 (respectively containing the *lac*O and the *tet*O repeats) were build with non repetitive linker sequences between the operators (Lau et al., 2003). Nevertheless some clones displayed a large heterogeneity in the *lac*O array sizes and/or numbers. These clones were systematically rejected or sub-cloned in order to obtain a stable phenotype. Thus, only highly homogenic clones were used in this thesis. Finally, a large amount of cells of each used clone

were frozen at an early stage after the cloning. After no more than 30 days of culture, the cells were discarded and a fresh culture was re-started.

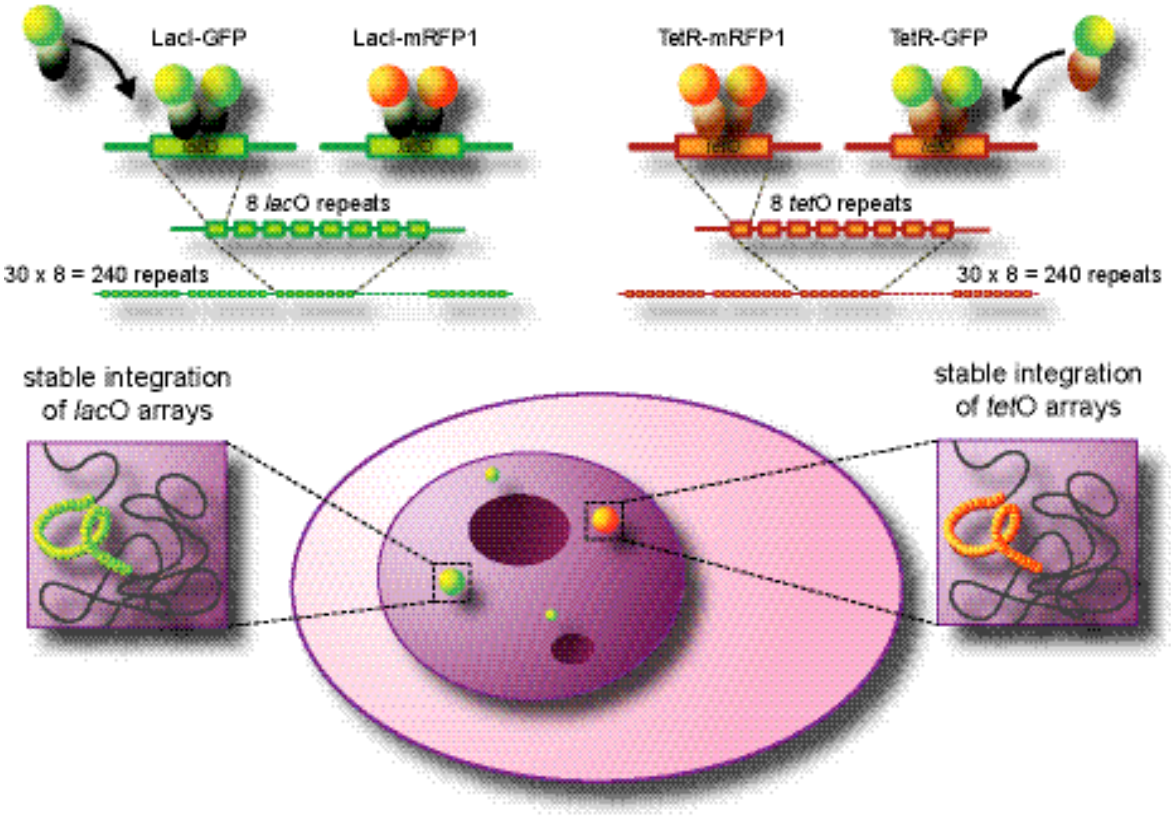

Figure III.2: In vivo labeling of specific genomic loci using *lac*O/*tet*O repeats and bound LacI-eGFP/mRFP1 and/or TetR-eGFP/mRFP1 repressor.

A plasmid with 240 copies of *lac*O and/or *tet*O is transfected into U2OS cells. The construct integrates in the genome at single or multiple loci in a random fashion. By transient transfection with LacI-eGFP/mRFP1 and/or TetR-eGFP/mRFP1 the integration site can be visualized in vivo by fluorescence microscopy

Clone designation	*lac*O Insert chromosomal localization		
EC4	3p		Telomere
FB4	3p		Telomere
FC2	11q		Telomere
F4 1B4	21p		Telomere
F4 2B8	2q		Centromere
F4 2C8	14p		Telomere
F6B2	Locus “b”	11q	Telomere
	Locus “m”	6q	Telomere
	Locus “s”	12q	Telomere

1C3	n.d.	Telomere
2A4	n.d.	Telomere
2B2	n.d.	Telomere
2C2	n.d.	Telomere

Table III.1: Generated U2OS cell lines with stably integrated *lac*O arrays.

Clones were generated by stably transfecting the *lac*O vector pLAU 43 in U2OS cells. The table displays the most relevant clones for experimental purpose. For precision on the *lac*O array chromosomal location identification see paragraph 3. n.d.: clones currently under characterization. The table lists only the clones retained for experimental purpose according to the characteristics described in the text.

The *lac*O were visualized *in vivo* by transient transfection with a LacI-eGFP or a LacI-mRFP1 construct as shown in Figure III.2. Most of the stable clones had a single insert as shown in Figure III.3A, 3.3B 3.3C and III.3D for the clones EC4, FB4 and F4 2B8 but a small number displayed several stable inserts like, for example, the clone F6B2 (Fig. III.3E). As the unbound LacI-eGFP stays confined in the nuclear envelope it offered a convenient nuclear counter-staining during the *in vivo* observations.

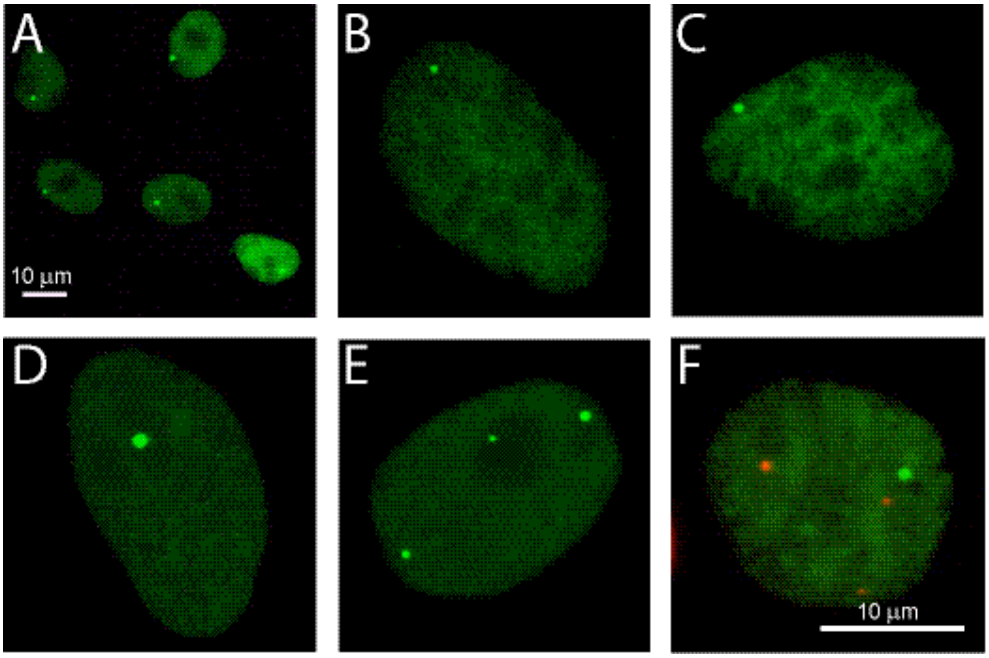

Figure III.3: Examples of generated clones with stably integrated *lac*O arrays and/or *tet*O arrays.

U2OS clones with stably integrated *lac*O arrays FB4 (A), EC4 (B), FC2 (C), F42B8 (D) and F6B2 (E) were transiently transfected with a Lac Inhibitor-eGFP vector. U2OS *lac*O array and *tet*O array double stable BiC3 (F) was transiently co-transfected with LacI-mRFP1 together with TetR-eGFP. BiC3 was obtained by stably transfecting a *tet*O array in the F6B2 cell line. Thus the three typical *lac*O inserts of the clone F6B2 are visible in BiC3 (in red) as well as a large *tet*O array insert (in green).

2.2 Generation of stable clones with *lac*O and *tet*O arrays multiple inserts

A serie of over 30 clones with *lac*O arrays and *tet*O arrays was generated using the clone F6B2 as starting cell line. The procedure used was the same as described for the *lac*O arrays by stably co-transfecting the vector pLAU 44, containing 240 *tet*O repeats, together with a different mammalian selection marker (see paragraph II.2.2.6). Like previously described, only clones displaying homogeneity with respect to arrays size and number were retained. Other clones were sub-cloned in order to get a more stable phenotype or were simply rejected. An example for the clone BiC3 is shown in Figure III.3F. BiC3 displays the three *lac*O array inserts *b*, *m* and *s* (in red), typical for F6B2, together with a single large *tet*O array. A list of the most relevant clones for experimental purpose is given in Table III.2.

Clone designation	Number of *lac*O Inserts	Number of *tet*O Inserts
Bi A4	6	1
Bi B3	3	1
Bi C2	3	2
Bi C3	3	1
Bi D2	2	2
Bi D3	3	1
Bi B3-sA4	3	1
Bi B3-sB2	3	2
Bi B3-sC2	3	1
Bi B3-sC3	3	1
Bi B3-sD2	2	2
Bi A4-sA4	5	2
Bi A4-sC4	6	1
Bi A4-sC4	4	1

Table III.2: Generated U2OS cell lines with stably integrated *lac*O arrays and *tet*O array.

The clones were generated by stably transecting the *tet*O vector pLAU 44 in the F6B2 U2OS clone that have three stably integrated *lac*O arrays. The table displays the most relevant clones for experimental purpose. The number of *lac*O and *tet*O inserts is indicated for each clones. The table lists only the clones retained for experimental purposes according to the characteristics described in the text.

3 Characterization of the clones

3.1 Determination of the chromosomal integration

3.1.1 U2OS karyotype

In order to characterize the clones, the karyotype of the U2OS cell line was determined. Metaphase chromosome spreads were submitted to Giemsa banding. Picture of the chromosome spreads were taken and the karyotype was determined from chromosome sizes, shapes (acrocentric, telocentric, *ect*...) and banding pattern as shown in Figure III.4A. Several karyotypes were determined in this way. U2OS is a human osteosarcoma cell line that has the particularity to belong to the group of telomerase-negative tumor cells. Like most of the cells of this group, the U2OS cell line displays a very complex karyotype. The number of chromosomes is between 70 and 73. U2OS is partially triploid and many chromosome rearrangements are apparent.

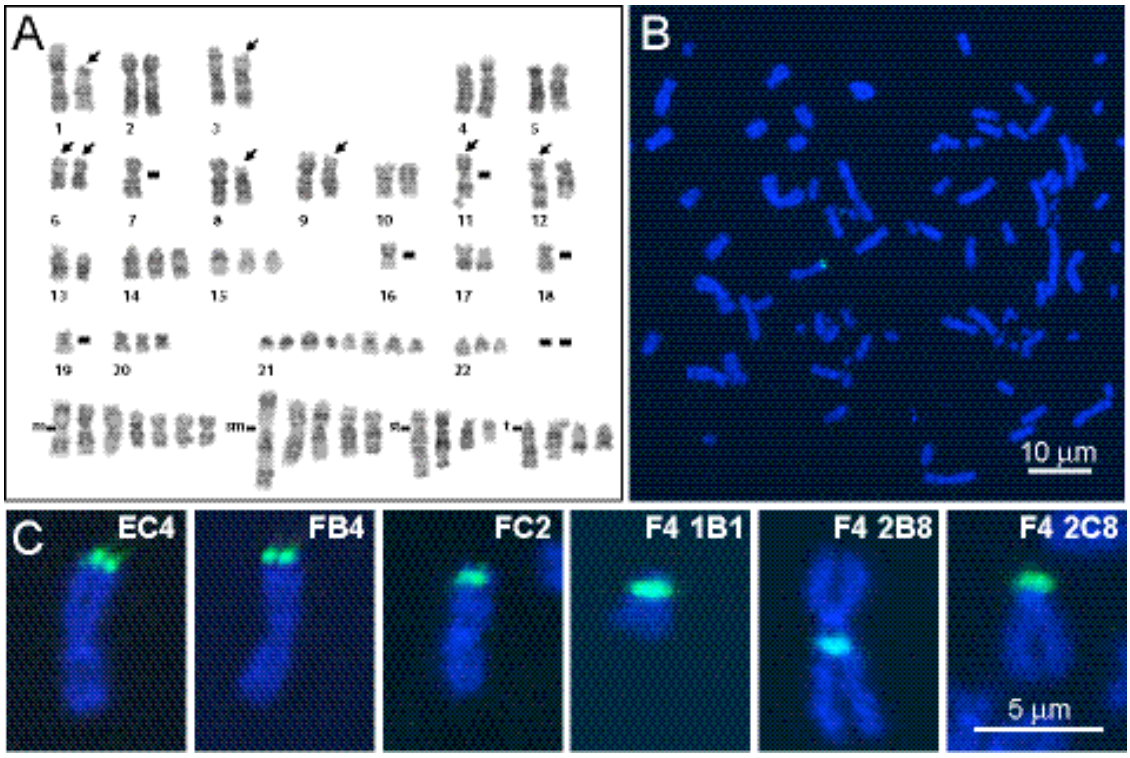

Figure III.4: Identification of the *lac*O array integration chromosomal locus by FISH.
(A) The karyotype of the U2OS cell line was constituted by the Giemsa banding technique. The image was made in collaboration with Dr. Antoaneta Mincheva. (B) The precise chromosomal integration of the arrays is determined by FISH on metaphase chromosomes using a fluorescently labeled probe coding for the *lac*O sequence. An example for the clone FB4 is given. (C) A typical set of metaphase chromosomes from different clones isolated with the stably integrated *lac*O array is shown.

3.1.2 Fluorescence *in situ* hybridization (FISH)

The *lac*O arrays chromosomal integration loci were identified by FISH on metaphase chromosomes with a fluorescently labeled oligonucleotide probe coding for the *lac*O sequence for each clones of interest. An example of chromosomal oligo FISH for the clone FB4 is shown in Figure III.4 B. Examples of several clone inserts loci are presented in Figure III.4C. Surprisingly, the large majority of clones had an integration in the telomere region. As an exception, the clone F4 2B8 displayed a peri-centromeric insert and was subsequently used as non-telomeric *lac*O array reference. The chromosome carrying the array integration was then identified by comparison with the U2OS karyotype.

3.1.3 Multicolor FISH

Since the U2OS cell line displays a complex karyotype that leads to some uncertainties in the determination of the genomic integration, a multicolor FISH experiment was conducted. The multicolor FISH or mFISH is based on the whole chromosome painting technique. Probes were generated in order to hybridize specifically each chromosome, regularly on the whole length, so that it becomes entirely visible ("painted"). With a five color combination it is not only possible to identify each chromosomes but also to observe and describe karyotype aberrations such as deletion, trisomia or translocation.

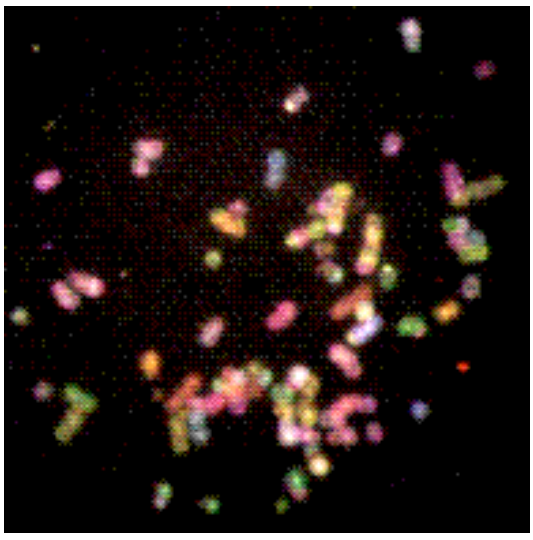

Figure III.5: Example of a multicolor FISH (mFISH) experiment conducted on metaphase chromosome spreads of the clone F6B2.

A mFISH experiment was conducted on chromosome spreads of the clone F6B2. Pictures were taken at the five wavelengths associated with the five fluorescent dyes coupled to the chromosome specific mFISH probes. The figure displays a merging of the five color channels.

The mFISH assays were done using the SpectraVysion (Vysis, Denmark) kit. The five color combination key is given in Table III.3. After hybridization, pictures of interphase chromosomes were taken at each five wavelengths corresponding to the five fluorescent dyes plus DAPI (in order to see all chromosomes at the same time). Figure III.5 displays one example of an hybridized karyotype with an overlay of all five color channels.

Chromosome	Spectrum Fred	Spectrum Aqua	Spectrum Green	Spectrum Gold	Spectrum Red
1				X	
2					X
3		X			
4			X		X
5	X			X	
6			X		
7	X				
8	X				X
9				X	X
10	X	X		X	
11		X			X
12			X	X	
13		X	X		
14			X	X	X
15		X		X	X
16	X		X		
17	X		X		X
18	X			X	X
19	X		X	X	
20	X	X			X
21		X	X	X	
22		X	X		X
X	X	X			
Y		X		X	

Table III.3: mFISH chromosome identification fluorescent dye color key.

Figure III.6A shows the results of an mFISH experiment. Each chromosome was identified with the help of the software and arranged to determine the karyotype.

The picture displays a merging of all five colors. As previously observed with the G banding experiment, the U2OS karyotype displays many aberration among which the chromosomal rearrangement became particularly visible with the mFISH technique.

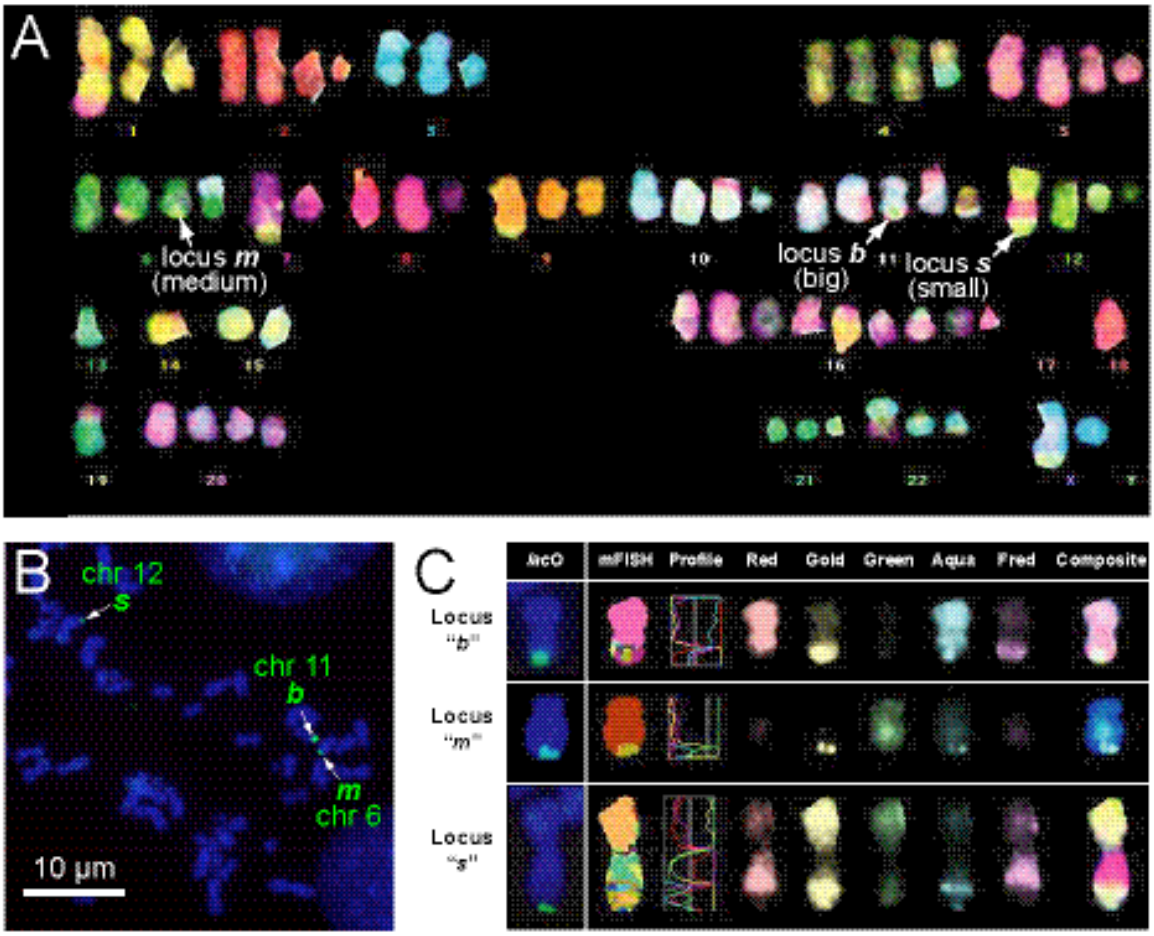

Figure III.6: Characterization of F6B2 clone carrying three integrations of chromosomal *lac*O arrays by mFISH.

(A) mFISH conducted on chromosome spreads of the clone F6B2. Chromosomes were identified and the karyotype was determined with the help of the Quips SpectraVysion software. The picture displays a merging of the five mFISH colors. The identified *lac*O array insertion locus of inserts *b*, *m* and *s* is reported on the figure. (B) Example of a *lac*O oligo-FISH re-hybridization conducted on a chromosome spread previously analyzed by mFISH. (C) The three chromosomes carrying the *lac*O array inserts *b*, *m* and *s* detected by oligo-FISH with a DAPI staining next to their respective mFISH profiles. „Red", „Gold", „Green", „Aqua" and „Fred" (far-red) are the five mFISH colors, „Composite" is the merging of these five colors and „mFISH" is a chromosome identification representation generated by the software.

In order to identify the precise genomic locations of the three *lac*O inserts of the clones F6B2 the mFISH procedure was followed by a re-hybridization with the fluorescently labeled *lac*O oligonucleotide probe. Using a coordinate system on the slides, it was possible to relocate the metaphase spreads that were previously

analyzed with mFISH to identify the insertion locus of each *lac*O arrays (Fig. III.6B). The software allowed to display the profiles in the five mFISH colors, the color overlay or composite and a computer generated chromosome identification color (mFISH) for each chromosome. The profile for the chromosomes carrying a *lac*O array insert is given in Figure III.6C next to their respective *lac*O FISH picture.

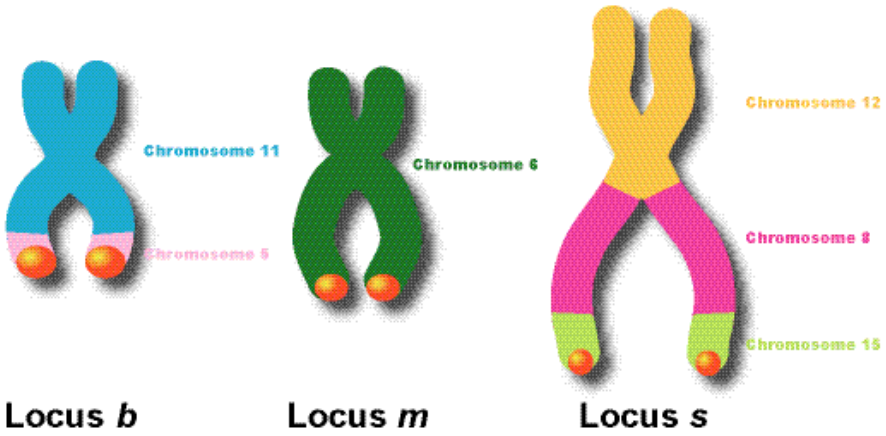

Figure III.7: Schematic representation of the structure of the chromosomes carrying the three *lac*O array inserts in the clone F6B2.

The integration sites were identified as follows:

- The biggest *lac*O array, *b,* is located at the telomere region on the *q* arm of chromosome 11, in a translocated region that belongs to chromosome 5 (Fig. III.6C, Fig. III.7).
- The medium size *lac*O array, *m,* is inserted at the telomere region on the *q* arm of chromosome 6 (Fig. III.6C, Fig. III.7).
- The smallest *lac*O array, *s,* is, like the two other inserts, located at the telomere on the *q* arm of a chromosome. This chromosome is largely composite: the *p* arm belongs to chromosome 12, the larger part of the *q* arm belongs to chromosome 8 and the last part, where the array is actually inserted, is translocated from chromosome 15 (Fig. III.6C, Fig. III.7).

A schematic representation of the structure of the three chromosomes carrying telomeric *lac*O array inserts is given Figure III.7.

The *lac*O array sequence appears to give an unspecific signal in “Gold” and “Aqua” (Fig. III.6C). The color key indicates that this combination is specific for the

"Y" chromosome. As the U2OS cell are derived from a female patient this artefact is not likely to interfere with the mFISH data interpretation.

3.2 Interphase chromatin localization

The interphase chromatin localization was also studied in fixed cells. *Lac*O arrays were detected by a LacI-eGFP transient transfection and the chromatin was stained by co-transfection with H2A-mRFP1, as shown in Figure III.8 for the clone F6B2. The observation of single as well as multiple telomeric integration clones did not show a clear preferential interphase nuclear localization. Nevertheless, arrays could often be observed at the nucleolar periphery or close to the cell membrane. Figure III.8 displays representative examples. The observation of the relative positioning of the *lac*O arrays in clones with multiple integration did not show a preferential pattern or fixed positioning of the loci with regard to each other.

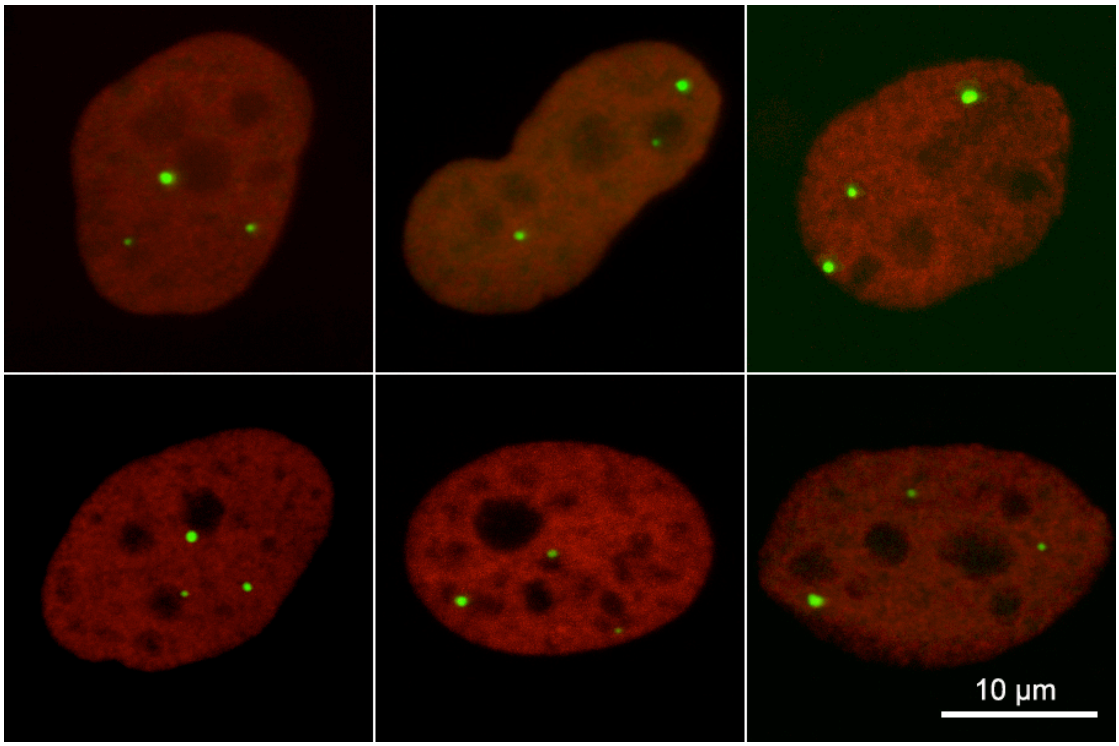

Figure III.8: Interphase chromatin localization of the three *lac*O array inserts of the clone F6B2.

Telomeres appear not to locate at a preferential region in the U2OS interphase nucleus. F6B2 cells were transiently co-transfected with LacI-eGFP together with H2A-mRFP1 and fixed with 4% paraformaldehyde after 14 hours incubation. Z axis picture stacks were recorded with a LSM. Maximum intensity projections of the Z axis picture stacks are shown for six representative cells.

3.3 Influence of cell cycle

The influence of the cell cycle on the characteristics of the *lac*O arrays with respect to appearance, localization and mobility was also observed. For this purpose the cell cycle marker protein PCNA was co-transfected, as a PCNA-eCFP construct, together with LacI-mRFP1. Figure III.9 displays two cells at different phases in the cell cycle. The lower cell is in G1 or G2 phase according to the PCNA diffuse pattern, whereas the upper cell displays the typical S phase pattern with PCNA localizing in the replication foci.

*Lac*O array labeled telomere mobility on the hour time scale was measured (see paragraph 4.5) in parallel to a PCNA pattern monitoring by co-transfecting LacI-mFRP1 together with PCNA-eCFP (Fig. III.9). No significant difference in the mobility value were observed in cells displaying G1/G2 pattern with regards to cells displaying a S phase pattern. However the cell cycle seemed to be blocked at the end of the S phase in cells transiently transfected with LacI fused to an autofluorescent protein and no cell division was observed.

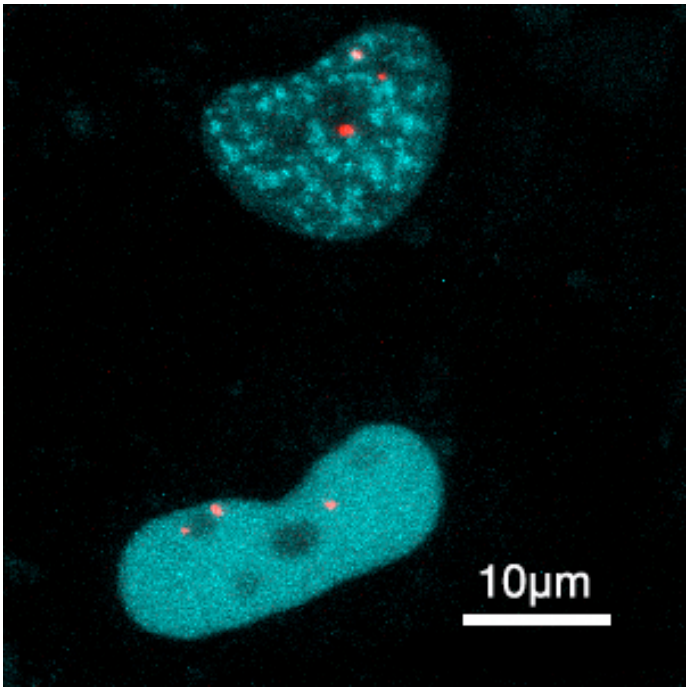

Figure III.9: Observation of the influence of then cell cycle on F6B2 cells.
F6B2 cells were co-transfected with LacI-mRFP1 together with PCNA-eCFP. The upper cell displays the typical S phase pattern as PCNA co-localizes with replication foci, whereas the lower cell displays the diffuse G1/G2 pattern.

4 Measurement of the telomere mobility on the scale of seconds, minutes and hours

4.1 The “moving corral” model

To describe the mobility of particles in the nucleus we used the so called “moving corral” (MC) model that was introduced previously (Görisch et al., 2005; Görisch et al., 2004). A careful analysis of the data on the mobility of *lac*O loci indicated that this approach is also appropriate to represent the mobility of chromatin on different time scales. The MC model describes the mobility of a particle/locus in *n* dimensions according to Eq. 1.

$$MSD = \left\langle r_c^2 \right\rangle \cdot \left(1 + \frac{2n D_{slow} \Delta t}{\left\langle r_c^2 \right\rangle} \right) \cdot \left[1 - \exp\left(- \frac{2n D_{fast} \Delta t}{\left\langle r_c^2 \right\rangle} \right) \right] \qquad \text{(Eq. 1)}$$

The overall mobility is determined by three parameters: the corral radius r_c, in which the particle experiences fast but confined diffusion with a diffusion coefficient D_{fast}. These regions of fast mobility, the corrals, can then translocate according to a free diffusion model with a diffusion coefficient D_{slow}. For the case of neglectable mobility within the corral as described by $D_{fast} = 0$ the exponential term is equal to one, and the above expression reduces to that of simple diffusion with an offset:

$$MSD = \left\langle r_c^2 \right\rangle + 2n D_{slow} \Delta t \qquad \text{(Eq. 2)}$$

On the other hand if there is no translocation of the corral, i. e. $D_{slow} = 0$ one obtains the diffusion displacement of the particle that is confined to a corral with radius r_c.

$$MSD = \left\langle r_c^2 \right\rangle \cdot \left[1 - \exp\left(- \frac{2n D_{fast} \Delta t}{\left\langle r_c^2 \right\rangle} \right) \right] \qquad \text{(Eq. 3)}$$

4.2 Chromatin mobility measurement of U2OS clone F6B2 with three *lac*O inserts

The accurate measurements of the chromatin mobility and the determination of the three parameters described by the "moving corral" model is hampered by two problems. First, the comparison between two different cells is problematic due to heterogeneities in the cell population for example with respect to the cell cycle state. Second, the cells itself move during the measurement. As also the cell shape changes the alignment to correct for this is fraught with difficulties. Accordingly, we have developed an alternative approach that uses the multiple label in clones like F6B2 (Fig. III.3E, Fig. III.10). If multiple particles/loci are present the difference in distance Δd between two particles with indices 1 and 2 can be measured to determine the diffusion coefficient:

$$MS\Delta D = \left\langle \Delta d^2(\Delta t) \right\rangle = \left\langle \left[\Delta d(t) - \Delta d(t + \Delta t) \right]^2 \right\rangle \qquad \text{(Eq. 4)}$$

Using the same approach as described previously (Görisch et al., 2004) an expression for a mobility described by the MC model is derived in Eq. 5. That is valid for $D_{fast,1}/\langle r_{c,1}^2 \rangle \approx D_{fast,2}/\langle r_{c,2}^2 \rangle$.

$$MS\Delta D = \Delta d^2(0) + \left(\left\langle r_{c,1}^{\ 2} \right\rangle + \left\langle r_{c,2}^{\ 2} \right\rangle \right) \cdot \left(1 + \frac{2n\left(D_{slow,1} + D_{slow,2}\right)\Delta t}{\left(\left\langle r_{c,1}^{\ 2} \right\rangle + \left\langle r_{c,2}^{\ 2} \right\rangle \right)} \right) \cdot \left[1 - \exp\left(- \frac{2n\left(D_{fast,1} + D_{fast,2}\right)\Delta t}{\left(\left\langle r_{c,1}^{\ 2} \right\rangle + \left\langle r_{c,2}^{\ 2} \right\rangle \right)} \right) \right]$$

(Eq. 5)

For a set of three loci with indices 1, 2, and 3 one can measure the distance between 1 and 2 (index 1-2), 2 and 3 (index 2-3) and 1 and 3 (index 1-3). For the analysis, Eq. 4 is applied with three single fit parameter for r_c, D_{slow} and D_{fast} and to obtain three values for each of these parameters by analysis of the distances 1-2, 2-3 and 1-3. The resulting values from the fit can then be decomposed according to Eq. 6 to determine the individual parameter values for each spot.

$$\left\langle r_{c,1\text{-}2}^{\,2}\right\rangle = \left\langle r_{c,1}^{\,2}\right\rangle + \left\langle r_{c,2}^{\,2}\right\rangle \quad \left\langle r_{c,2\text{-}3}^{\,2}\right\rangle = \left\langle r_{c,2}^{\,2}\right\rangle + \left\langle r_{c,3}^{\,2}\right\rangle \quad \left\langle r_{c,1\text{-}3}^{\,2}\right\rangle = \left\langle r_{c,1}^{\,2}\right\rangle + \left\langle r_{c,3}^{\,2}\right\rangle$$

$$D_{slow,1\text{-}2} = D_{slow,1} + D_{slow,2} \quad D_{slow,2\text{-}3} = D_{slow,2} + D_{slow,3} \quad D_{slow,1\text{-}3} = D_{slow,1} + D_{slow,3} \quad \text{(Eq. 6)}$$

$$D_{fast,1\text{-}2} = D_{fast,1} + D_{fast,2} \quad D_{fast,2\text{-}3} = D_{fast,2} + D_{fast,3} \quad D_{fast,1\text{-}3} = D_{fast,1} + D_{fast,3}$$

This approach has the advantage that it is insensitive to movements of the whole cell and therefore no alignment of the cell needs to be done. Furthermore, it allows a direct and faithful comparison within a single cell: For example in F6B2 clone, the loci *b*, *m* and *s*. A comparative study of individual telomere mobility is then obtained by determining changes in the distance between *b* and *m* (*b*-*m*), *b* and *s* (*b*-*s*) and *m* and *s* (*m*-*s*) (Fig. III.10).

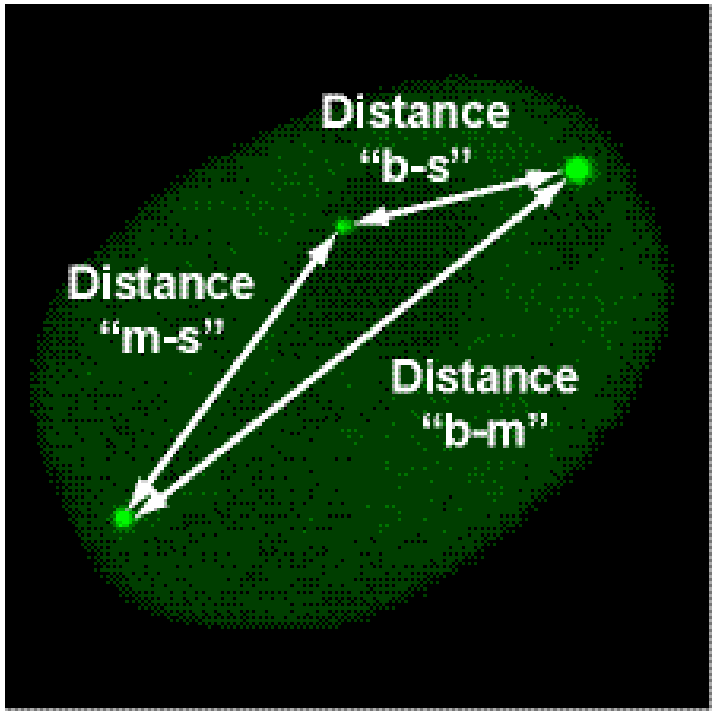

Figure III.10: The clone F6B2 is a valuable tool for chromatin mobility measurements.

U2OS clone F6B2 was used in all chromatin mobility measurements as it displayed three *lac*O array inserts easily differentiable by their apparent size. Cells were transiently transfected with LacI-eGFP. The three individual telomere mobilities were obtained by measuring changes in the distance between the loci, referred as distance "*b*-*m*", "*b*-*s*" and "*m*-*s*", over several time scales.

The analysis was conducted at three different time scales: the second, the minute and the hour with respective resolutions of milliseconds, seconds and minutes. For the hour time scale, *Z* axis stacks of pictures were collected with a laser scanning microscope (LSM). For the second and the minute scales a spinning disk laser confocal microscope was used. This particular type of LSM allowed scanning

speed in the range of 10-20 pictures per second, which over ten fold faster than a classical LSM. The quantitative analysis of telomere mobility (MSΔD versus time) according to the MC model was conducted as described in the preceding paragraph.

4.3 The second time scale

In order to minimize the scanning time, cells that had the three *lac*O arrays inserts were visible in the same focal plan were selected. A single scan was then necessary for each time point and thus an average time resolution of ~ 80 ms was obtained. Pictures were recorded for a total time of 3 to 5 min. The spots were tracked using the software ImageJ, the squared changes in distance between the loci Δd^2 was then calculated and plotted against the time. An average of 22 cells (66 telomeres) is shown in Figure III.11. The curve shows two phases: a first phase characterized by a fast increase and a second one, more moderate. The curve was fitted with the "moving corral" model. In order to calibrate the system, fixed cells were measured under the same conditions.

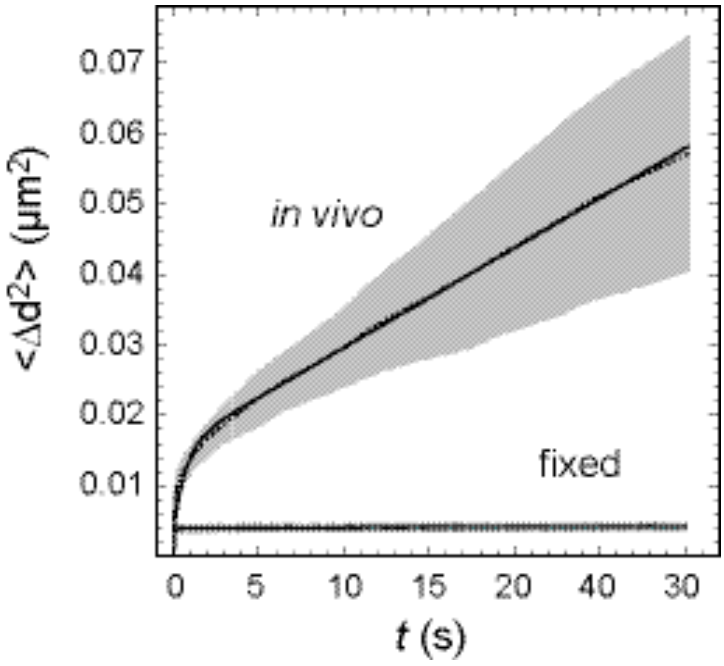

Figure III.11: Chromatin mobility analysis on the second time scale

Pictures were recorded every 70-150 ms for 3 to 5 min with a spinning disk confocal laser scanning microscope. Loci were tracked and the squared changes Δd^2 in the distance between two telomeres was plotted against the time. The data was fitted with the MC model (see text for details). An average of 66 telomere mobility measurements is displayed. The corresponding trace for fixed cells is also included.

4.4 The minute time scale

As for the second time scale, a spinning disk LSM was used. Z axis stacks were recorded each 8 to 15 s for a total time of 15 min. The maximum intensity projection was calculated for each picture stack, and the loci were tracked. The squared changes in distance between the telomeres, Δd^2, were calculated and plotted against the time. An average of 14 cells (42 telomeres) is shown in Figure III.12. Like for the second time scale, the curve comprises two different phases and was fitted using the MC model.

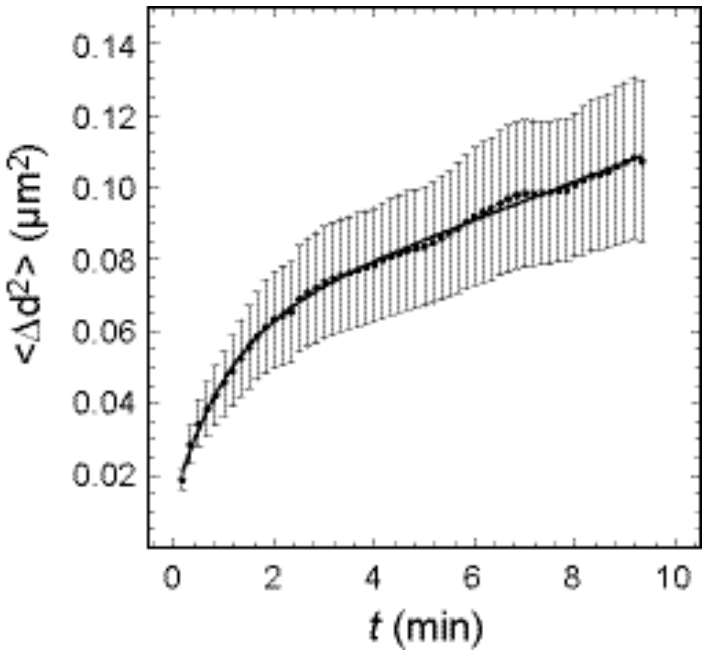

Figure III.12: Chromatin mobility analysis on the minute time scale

Image stacks were recorded every 8 to 15 s for 15 min with a spinning disk confocal laser scanning microscope. Tracking of the loci was conducted on the maximum intensity projections of each stack. The squared changes Δd^2 in the distance between two telomeres was plotted against the time. The data was fitted with the MC model. an average of 42 telomeres mobility measurements. Is displayed

4.5 The hour time scale

For the hour time scale, Z axis stacks of transiently transfected F6B2 cells were scanned every 5 minutes for a total time of up to 5 hours. The cells used for all mobility experiments at the hour time scale were from the same batch of frozen

aliquots and are therefore displaying almost the same number of divisions since the cloning of the cell line.

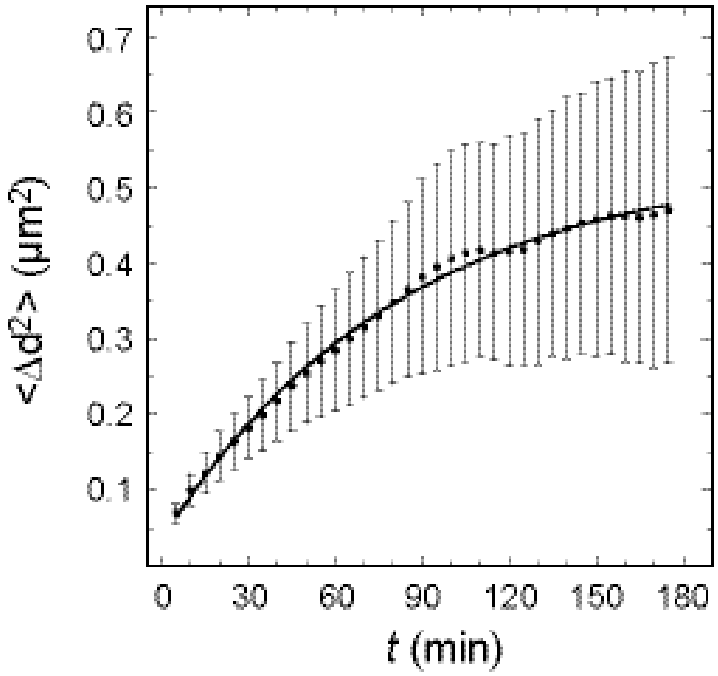

Figure III.13: Chromatin mobility analysis on the hour time scale

Image stacks were taken every 5 min for a total of 5 hours with a confocal laser scanning microscope. Tracking of the loci was conducted on the maximum intensity projections of each stack. The squared changes Δd^2 in the distance between two telomeres were plotted against the time. The data was fitted with a confined diffusion model. An average of 60 telomeres mobility measurements is displayed.

The maximum intensity projections were calculated for each picture stack and then the loci were tracked. The squared changes in distance between the telomeres, Δd^2, were calculated, plotted against the time and fitted with a confined diffusion model. An average of 20 cells (60 telomeres) is shown in Figure III.13. The end of the curve displays large fluctuations associated with an increasing standard deviation. Indeed, a closer look to the raw data revealed large differences in individual telomere mobility. A characteristic example is shown in Figure III.14. Whereas most of the time telomeres displayed a „standard“ mobility (Fig. III.14A), some telomeres, like for example telomere *b* and telomere *s* in Figure III.14B, showed, for certain periods, an additional long range translocation.

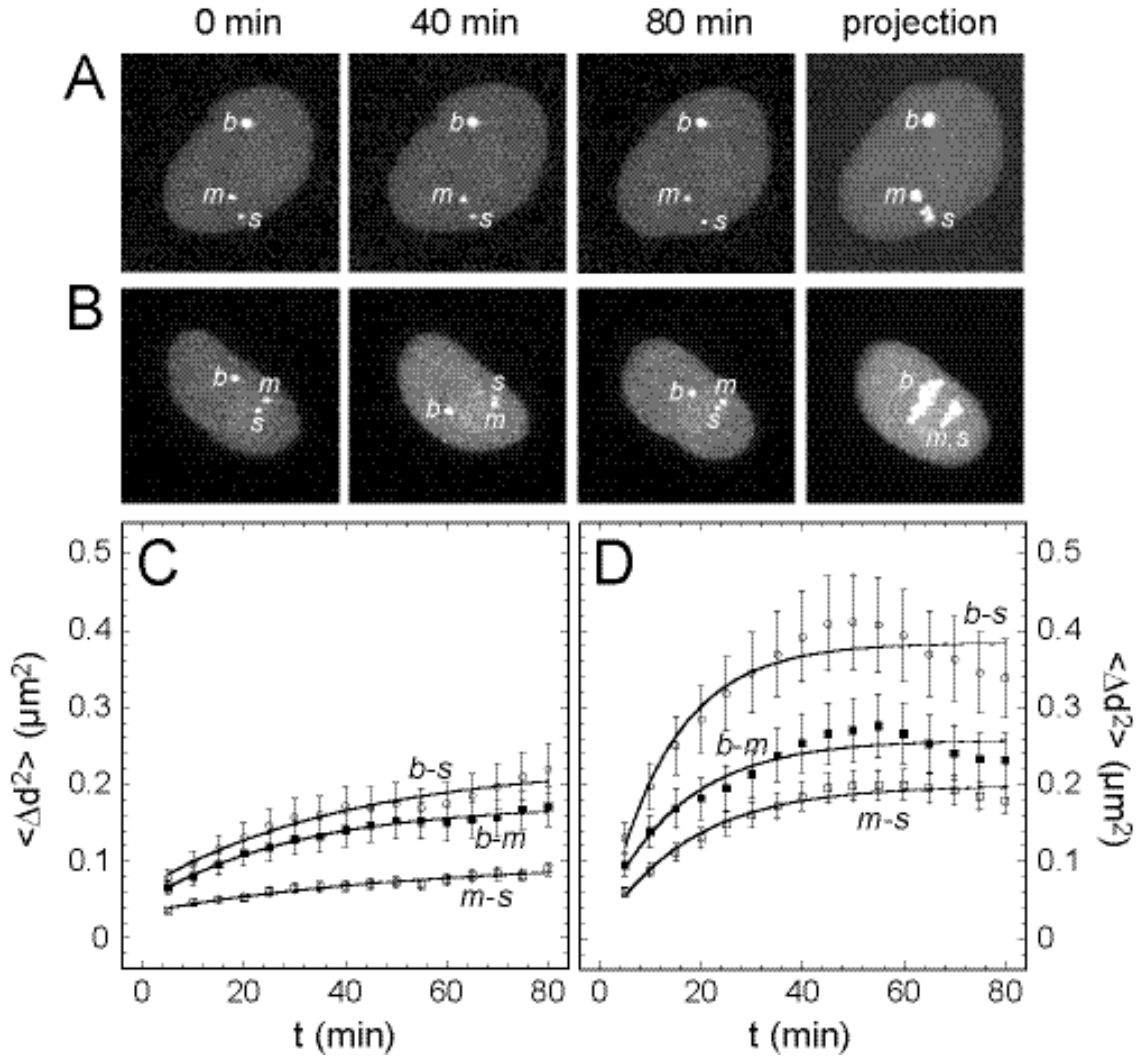

Figure III.14: Some telomeres show a dramatically enhanced mobility on the hour time scale.

Images at the indicated time points and a maximum intensity projection of all images are shown. Examples for two experiments are presented that reveal large differences in the mobility of telomeres. Individual telomere mobility can be calculated as described in the text from the plotted distance *b*-*s*, *b*-*m* and *m*-*s*. (A) A cell with slow moving telomeres, which represent the majority of our observations. (B) A cell showing three loci with dramatic differences in mobility. The telomeres *b* and *s* display a very fast motion, while telomere *m* is only moderately mobile. The quantitative analysis from distance variation between the three spots is shown in (C) for the slow and in (D) for the cell with fast moving telomeres *b* and *s*. (Movies are included on the supplementary CD under the references III-14 M1 and III-14 M2).

4.6 Quantitative description of telomere mobility

The analysis of the data obtained on the second, the minute and the hour time scale, demonstrates that all telomeres display a fast mobility D_{ms} = 2.2·10^{-3} μm^2 s^{-1} in a region ("corral") of 80 nm radius and a further slower translocations in a radius of 190 nm with D_{sec} = 2.9·10^{-4} μm^2 s^{-1} (Fig. 3.11, 3.12, 3.13 and 3.14). On the hour time scale, the telomeres are sharing the same diffusion coefficient D_{min} = 5.2·10^{-5}

$\mu m^2\ s^{-1}$ with the majority of the telomeres constricted to an average radius r_c = 0.3 µm whereas a small fraction extends to an average corral radius r_c = 0.8 µm.

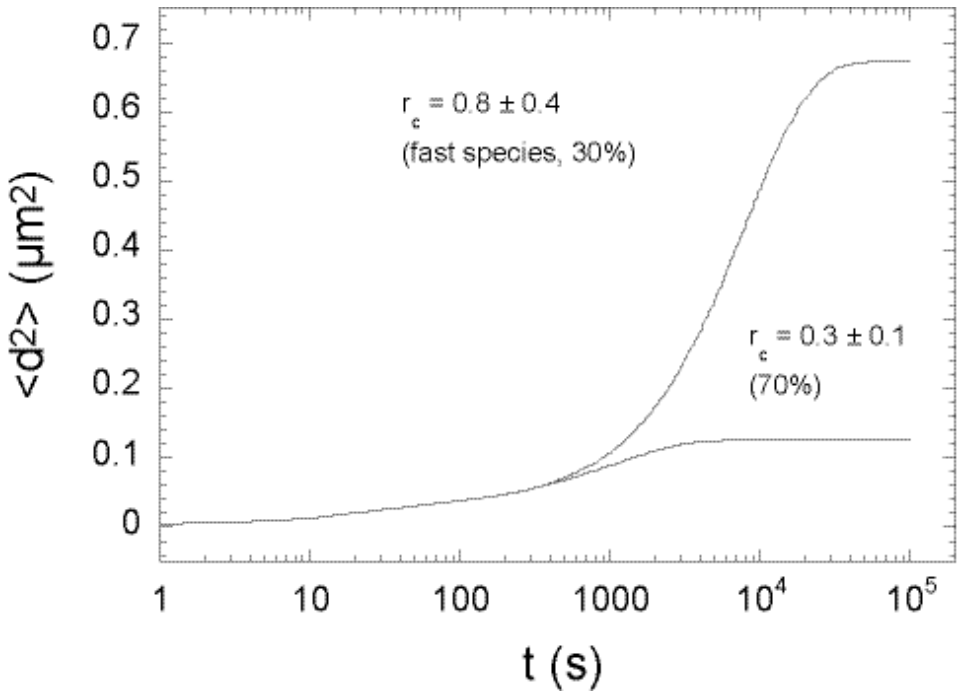

Figure III.15: Mobility of telomeres on all length scales

Combined plot of the squared changes Δd^2 in the distance between two telomeres for all the measured time scales.

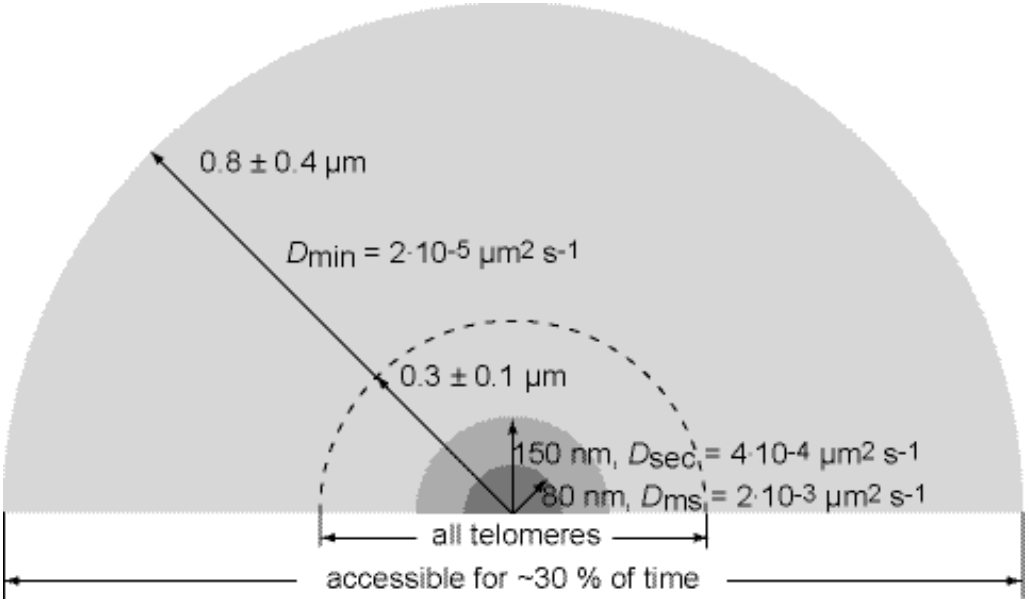

Figure III.16: Schematic representation of all collected mobility data.

Results from the analysis of telomere mobility are summarized. From experiments on different time scales the indicated diffusion coefficients and translocation ranges were determined (Fig. 3.10, 3.11, 3.12 and 3.13).

The experiments analyzed so far show that this striking increase of the mobility can be observed for a certain period of time for all three telomeres (*b, m, s*) in clone F6B2. Thus, the same telomere adopts a low-mobility state during ~70% of the time, in which its mobility is the same as that of other non-telomeric chromatin regions. A combination of the measurements at the three time scales with the "normal" and the "extended" mobility is presented in Figure III.15 and a summary of the numerical values for the telomere mobility is given in Figure III.16.

5 Alternative lengthening of telomeres

As already mentioned, U2OS cells belong to the telomerase negative tumor cell lines and maintain their telomere length through the so called "alternative" lengthening (ALT) pathway. The ALT system appears to be characterized by a high rate of telomere recombination (Laud et al., 2005; Londono-Vallejo et al., 2004; Muntoni and Reddel, 2005) and the presence of a particular class of promyelocytic Leukemia associated (PML) bodies, the ALT-associated PML bodies (APBs) that are co-localizing with the telomeres (Nabetani et al., 2004). The U2OS stable clones with telomeric *lac*O array generated in this thesis offered an interesting tool to investigate the ALT system.

5.1 Telomere length at *lac*O inserts

Because of their important chromosomes number and large telomere length variability (see below), it is very hard to monitor precisely the telomere lengthening dynamics in ALT cell lines. The *lac*O system provides the possibility to mark a specific chromosome allele and observe the variability of the telomere length at this precise locus on a whole population.

5.1.1 Telomere length in U2OS cells

Using a labeled PNA probe, the telomere repeats could be stained by FISH (Fig. III.17). PNA are peptide nucleic acid that have a pseudopeptidic backbone instead of the canonical L-desoxyribose-phosphate. Accordingly, PNA is not charged and is therefore not submitted to the repulsion forces involved in DNA/DNA interactions so that DNA/PNA hybrid is more stable than DNA duplex. These properties make PNA probes much reliable than standard DNA for the quantification of FISH experiments (Boukamp et al., 2005; Molenaar et al., 2003).

A comparison between the U2OS cells and human lymphocytes telomere length is shown in Figure III.17. Both pictures were taken with the same exposure time. Whereas in lymphocytes all telomeres are visible and display a regular size (10 to 15 kb in human cells), in the U2OS cells large variations in the repeat length of the telomeres can be observed. Some of the telomeres were not detectable and a few chromosomes with asymmetrical telomere length at one end could be observed. These characteristics are shared by all cell lines using the ALT telomere lengthening pathway.

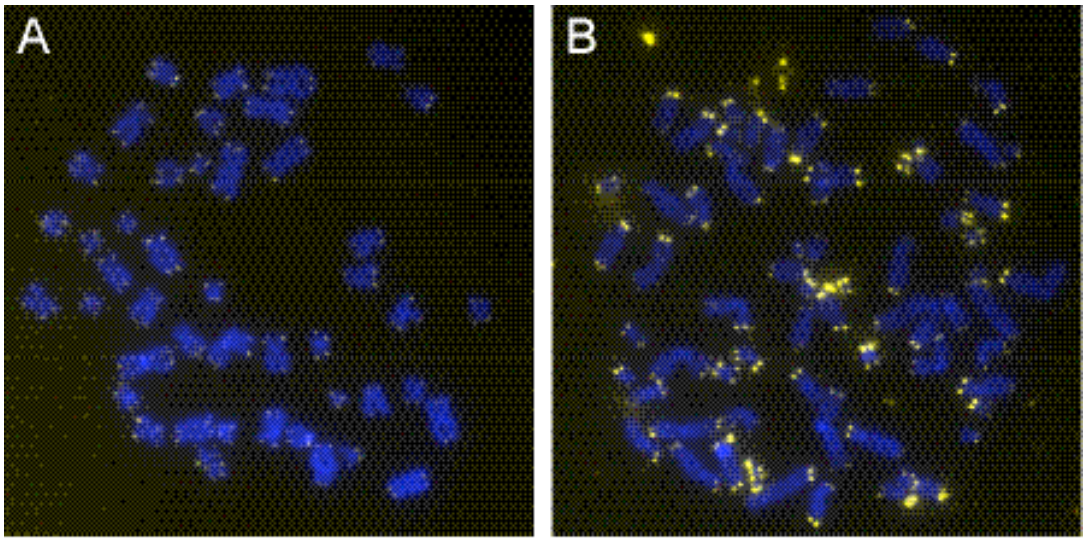

Figure III.17: ALT cells display a large variability in telomere length.
Telomere staining by FISH with a $(TTTAGG)_3$-Cy3 PNA probe of metaphase chromosome spreads. Both images were recorded with the same exposure time. (A) Human lymphocytes show an homogenous distribution of relatively short telomeres with repeats that are typically 10-15 kb in length. (B) U2OS cell line. The alternative telomere lengthening (ALT) mechanism leads to large variations in telomere length. Images in collaboration with Dr Karin Greulich-Bode.

5.1.2 Telomere repeat length of *lac*O array labeled telomere

By using a *lac*O FISH (Fig. III.18A) followed by a re-hybridization with a telomeric repeat complementary PNA probe (Fig. III.18B), we where able to observe the telomere repeats length variation at a precise telomere in a cell population. 45 metaphase spreads of the clone F6B2 were analyzed. Typical examples of telomeric repeat length variations for each loci are given in Figure III.18C.
All cells used for these experiments were from a single batch of aliquots frozen at an early stage after the clone isolation that was used also in the hour time scale telomere mobility experiments (see paragraph 4.5). Each *lac*O array labeled telomere displayed a large variety of telomere repeat length. The telomere repeat

signal was not detectable in about 20 % of the *lac*O array labeled telomere (Table III.2).

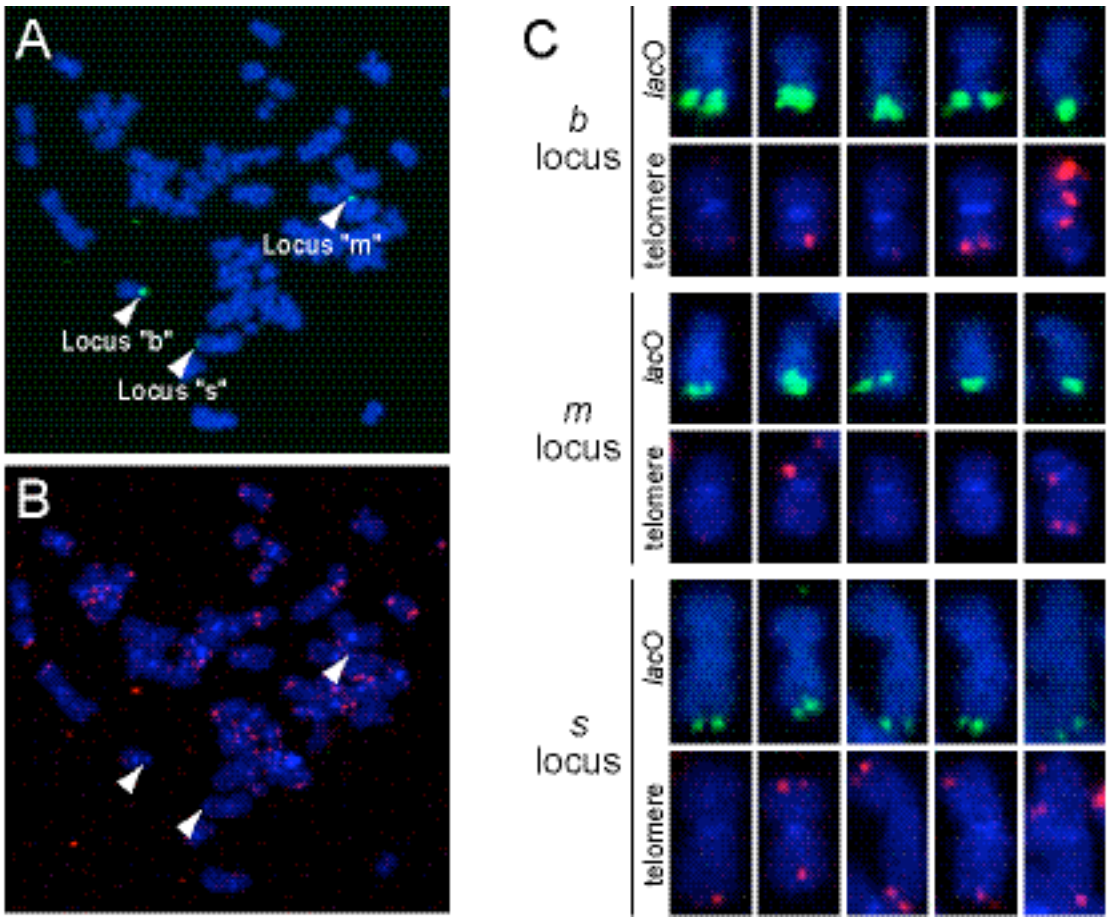

Figure III.18: Measurement of the repeat length at *lac*O array labeled telomeres.
(A) FISH experiment conducted on metaphase chromosomes of the F6B2 clone using a fluorescently labeled probe coding for the *lac*O. DNA was DAPI-stained. (B) Re-hybridization of the previous metaphase chromosome spreads with a $(TTTAGG)_3$-Cy3 PNA probe in order to visualize the telomere repeat length. The same chromosome spread as in (A) was re-located using the coordinate system. DNA is stained with DAPI. (C) Examples of evaluation of telomere length at the three different integration sites by using the same method as in (A) and (B).

Locus	b	m	s	Together
% detectable telomere repeats	81.2 ± 6.7	78.1 ± 6.7	82.7 ± 6.7	80,7 ± 11.6

Table III.4: Percentage of telomeres repeats detectable by mFISH at the loci *b*, *m* and *s* in F6B2 cells.

6 PML body mobility relative to telomeres

Promyelocytic leukemia associated (PML) bodies are nuclear protein complexes that are involved in multiple nuclear functions. Although the mobility of PML body was already precisely described recently (Görisch et al., 2004) there is little information available on the PML bodies mobility in dependence to their environment, the nuclear chromatin. Cells with stably integrated *lac*O arrays offer the opportunity to visualize PML bodies together with various well defined chromatin loci *in vivo*. Moreover in the U2OS stable clones generated in this thesis, the *lac*O arrays are inserted at the telomeres. U2OS are using the alternative telomere lengthening pathway (Nabetani et al., 2004) and, since in ALT cells PML bodies are interacting with telomeric DNA, our method appeared to be a very interesting tool for the study of PML body mobility.

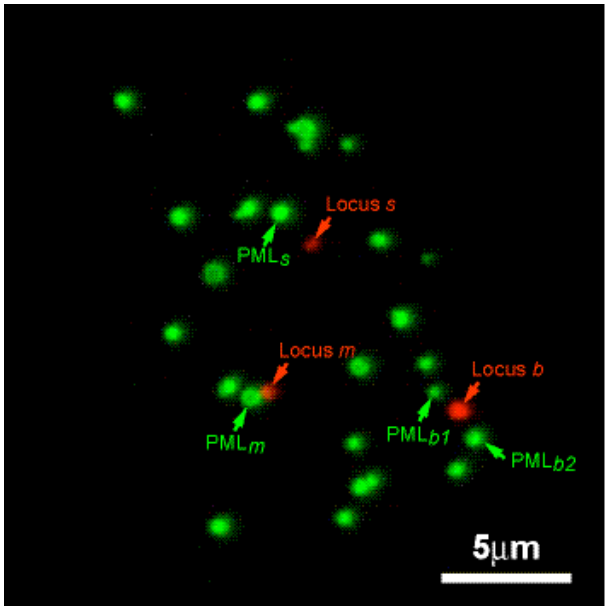

Figure III.19: Measurement of PML bodies mobility with regard to telomeres.
U2OS F6B2 clones were transiently co-transfected with LacI-mRFP1 together with PML III-GFP. For each Telomeric *lac*O arrays inserts (locus *b*, *m* or *s*) the distance changes to the respective proximal PML body was measured (PML_{b1}, PML_{b2}, PML_m and PML_s).

Cells of the F6B2 clone were co-transfected with PMLIII-GFP and LacI-mRFP1 to examine the relation between telomere and PML body mobility. Translocations of the three telomeric *lac*O inserts and that of PML bodies were monitored (Fig. III.19). The relative mobility of PML body to telomere was determined by measuring the distance changes between the closest PML body to each *lac*O

array (*b, m* or *s*). Positions of these arrays are referred to as PML_b, PML_m and PML_s. A single *lac*O array can be close to several PML bodies, like the locus *b* in Figure III.19 (PML_{b1} and PML_{b2}). In this case the distance variation to each close PML body is measured. On the contrary, PML bodies that never approached a *lac*O closer than 2 μm over the measured time were ignored.

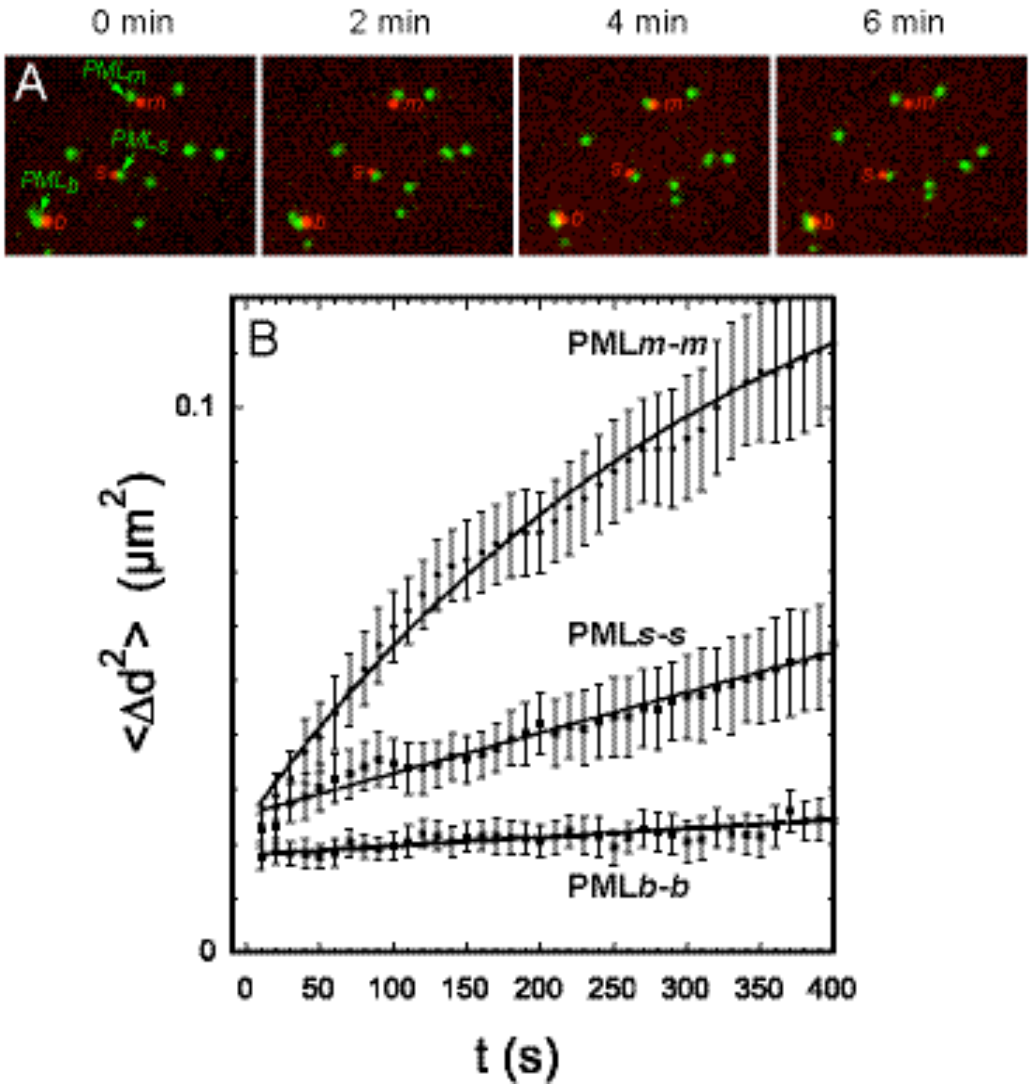

Figure III.20: Relative mobility of PML bodies and telomeres.

The U2OS cell line F6B2 was transiently co-transfected with PMLIII-GFP and LacI-mRFP1. (A) The mobility of the three *lac*O inserts (*b*, *m* and *s*) and proximal PML bodies was studied by recording changes in the relative distance between the spots and fitting these to a confined diffusion model. The figure displays a typical example (Movies is included on the supplementary CD under the reference III-20 M). (B) Mean squared distance changes, Δd^2, in the distance between PML bodies ant its proximal telomeres in the previous cell were plotted against the time.

6.1 The three classes of PML body mobility relative to the telomeres

The Figure III.20A shows a typical example of the mobility of PML bodies with respect to close *lac*O labeled telomeres. After tracking of *lac*O arrays and PML bodies, the squared distance changes, Δd^2, were plotted against time for each of three couples (Fig. III.20B). The Figure III.21 shows the averages of 30 different measurements grouped in three main categories :

- PML bodies that are independent from the proximal telomere, like PML_m in Figure III.20. theses are represented by the group 1 in Figure III.21. This quite heterogeneous PML body class displays an average mobility of $7.4 \cdot 10^{-5} \pm 1.7 \cdot 10^{-6}$ $\mu m^2 s^{-1}$ in a 280 nm confinement radius .
- PML bodies that show a completely correlated mobility relative to the telomere like PML_b in Figure III.20. These PML bodies, represented by the group 2a in Figure III.21, did not necessarily had a physical contact with the telomere and could be distant of up to 0.5-1 µm from it. These PML bodies were characterized by a very small mobility relative to the telomere ($1.3 \cdot 10^{-5} \pm 1.1 \cdot 10^{-7}$ $\mu m^2 s^{-1}$) with a confinement radius of 80 nm.
- PML bodies that show a correlated movement with the telomere with some independency, like PML_b Figure III.20, represented by the group 2b in Figure III.21. Although these PML bodies displayed a low mobility relative to the telomere, this was two times higher than the value obtained for the group 2a: $2.4 \cdot 10^{-5} \pm 7.4 \cdot 10^{-7}$ $\mu m^2 s^{-1}$ with a confinement radius of 170 nm.

The relative mobility of the PML body was independent of the telomere insert localization. Thus, all three classes of PML mobility were indifferently observed at locus *b*, *m* or *s.*

- In addition , a specific class of PML body was also observed during these experiments: PML bodies that are forming ALT-associated PML bodies or APBs (see further).

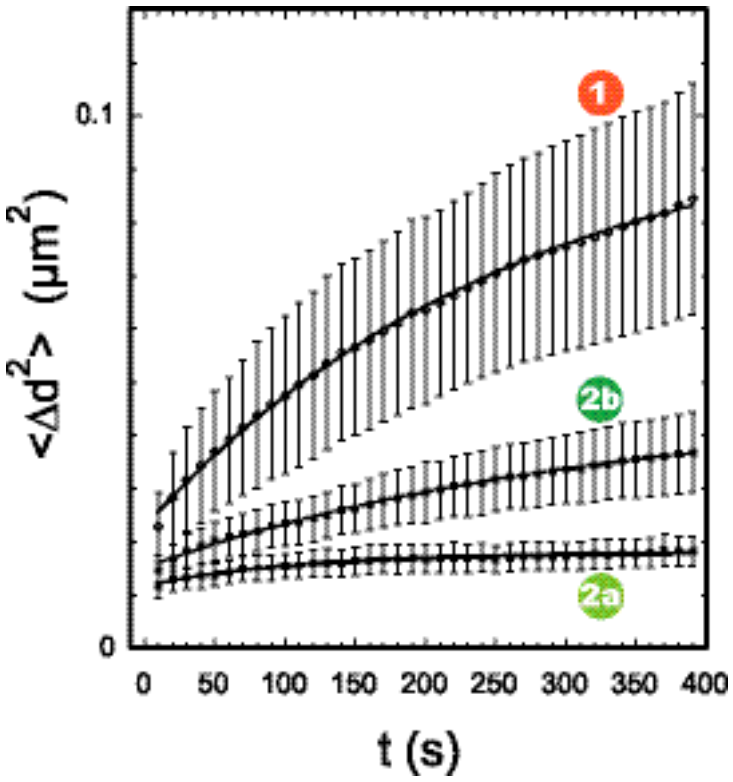

Figure III.21: PML relative mobility can be classified in three main classes.
The curves obtained by plotting the distance changes of a PML body towards the proximal *lac*O labeled telomere can be grouped in three main tendencies referred as group 1, 2a and 2b. Average of ten measurements for each curve are shown. Data were fitted with a confined diffusion model.

6.2 The ALT-associated PML body (APB)

In cell lines using the ALT telomere lengthening pathway, a special class of PML bodies can be observed: the ALT-associated PML bodies or APBs. These structures are shown to co-localize with telomeres and are thought to be the site of the telomere lengthening process of the ALT pathway (Nabetani et al., 2004).

6.2.1 Structure of the APB

Figure III.22 shows two examples of APBs forming around telomeric *lac*O inserts in F6B2 cell line at locus *b*. The APB can be observed in fixed cells with anti-PML antibody after LacI-mRFP1 transfection (Fig. III.22A) as well as *in vivo* by co-transfection of PML III-eGFP construct together with lacI-mRFP1 (Fig. III.22B). These structures can be observed at all three loci in the same proportions (see supplementary CD for more examples). The observation of the enlargement (Fig. III.22C) indicates that APBs are formed by an hollow-spherical PML body surrounding the telomeric *lac*O array. Several observations and 3D reconstitutions of the Z axis image stacks demonstrate that, in the APB, the PML body does not

form a complete sphere but rather a spherical cap sitting on the telomere (see supplementary material).

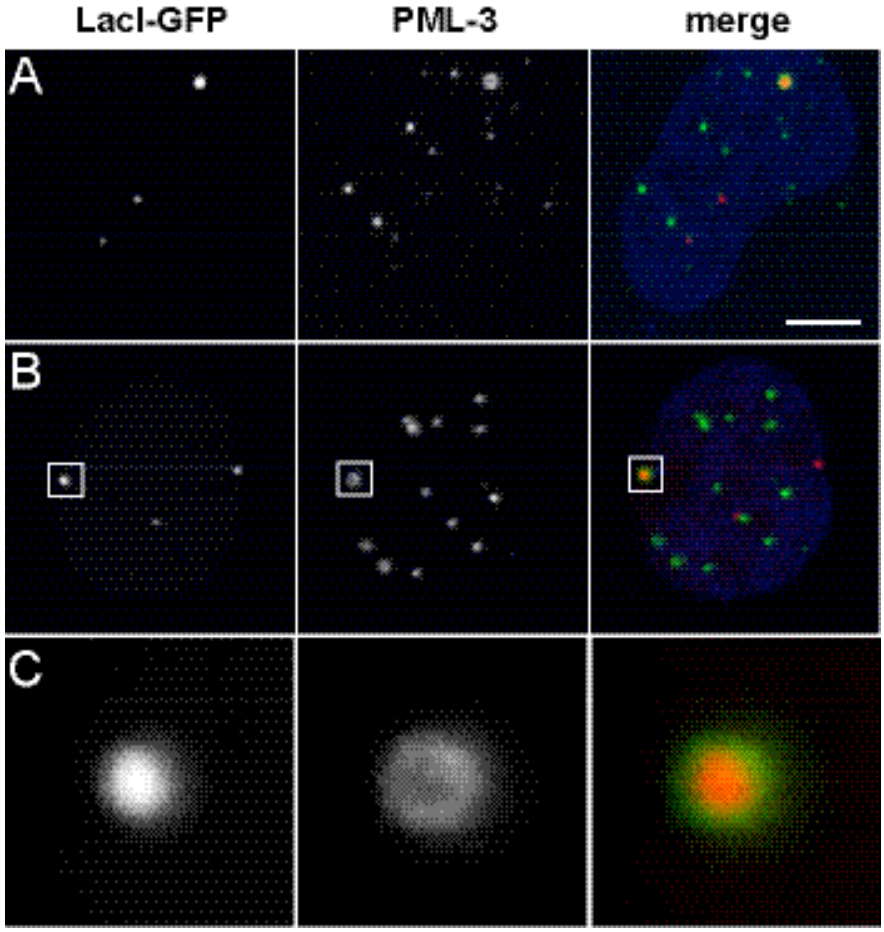

Figure III.22: Structure of an APB formed around a telomeric *lac*O insert.

The PML body forms a cap-like structure around the *lac*O/telomere label, referred to as an APB. (A) U2OS cell line F6B2 transiently transfected with LacI-mRFP1 and fixed with PFA. PML bodies are stained with antibody against PML III together with an Alexa 488-coupled secondary antibody. DNA is stained with DAPI.(B) U2OS cell line F6B2 transiently co-transfected with LacI-mRFP1 together with PML III GFP. Cells are fixed with PFA and chromatin is stained with To-pro 3. (C) Enlargement of the PML III/telomeric *lac*O array co-localization structure observed in B. Movies of 3 D reconstitutions of the Z axis image stacks the are included on the supplementary CD under the references III-22 M1 and III-22 M2.

6.2.2 Mechanism of APB formation

The study of the PML body *in vivo* was also the occasion to observe the formation of APBs. The image series shown in the Figure III.23 is a representative example of several observations. The observation of this picture sequence revealed that a pre-existing PML body is first binding to the telomere. The PML III protein is then accumulating around the telomere until it has formed a surrounding structure. A close look to the movie (included on the supplementary CD) suggest that

accumulating PML III protein is not freely diffusing but clustered in small and very mobile aggregates, previously described as PML microbodies (Eskiw et al., 2004).

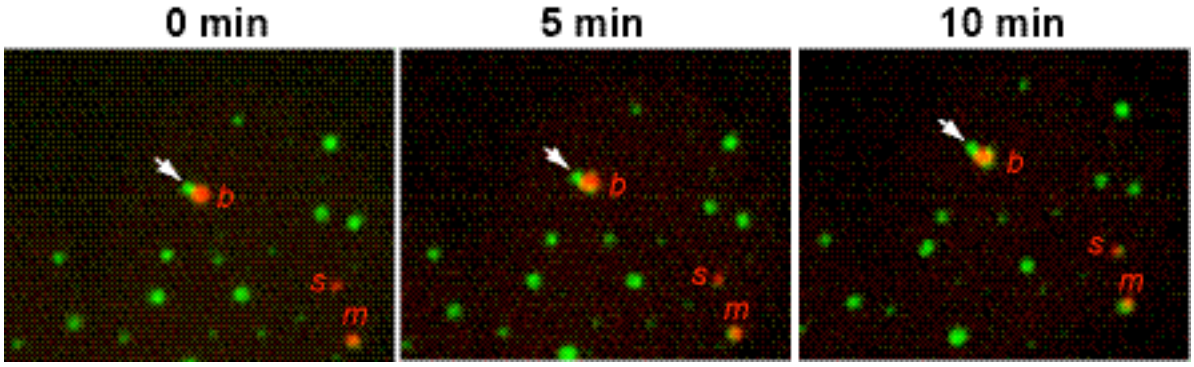

Figure III.23: Observation of the formation of an APB.

F6B2 cells were transiently co-transfected with LacI-mRFP1 together with PML III-GFP. The formation of an APB complex could be followed over time as shown here for locus *b*. Starting from an telomere bound PML body, PML III protein (under the form of PML microbody) is accumulating until it forms the typical APB surrounding structure. The movie is included on the supplementary CD under the reference III-23 M1.

7 Telomere-telomere interactions in U2OS cells

Interaction between telomere is a phenomenon hard to observe in cells using the ALT pathway. As a matter of fact, on the contrary of telomerase positive cells, in ATL cells telomeres are displaying a large variety in size. Direct estimation of telomere clustering by quantitative FISH (Q-FISH) with PNA probes (Nagele et al., 2001) is therefore not possible. For the same reasons *in vivo* labeling with PNA probe (Molenaar et al., 2003) only allows to observe the relatively long telomeres and clustering can only be observed if telomeres are aggregating or separating during the observation time.

Telomere clustering however appears to be an crucial event in ALT cells where inter- and intra-chromosomal telomere DNA recombination plays a central role in the telomere lengthening system (Laud et al., 2005; Londono-Vallejo et al., 2004; Muntoni and Reddel, 2005). First attempts of *in vivo* observation of interphase telomeres interaction in F6B2 clones appeared to be unsatisfying as it was difficult to discriminate two co-localizing loci displaying the same color.

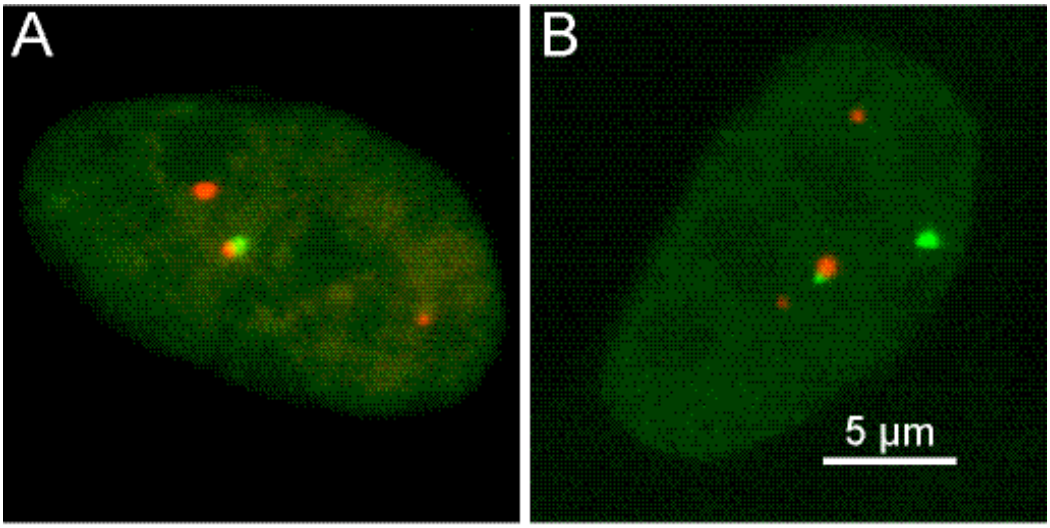

Figure III.24: The *lac*O/*tet*O double labeling system allows the observation of telomere-telomere interaction in vivo.
The *lac*O and *tet*O double stable cell lines BiC3 (A) and BiB3-sd2 (B) were transiently co-transfected with lacI-mRFP1 together with TetR-eGFP. The fixed cells were scanned with a LSM. The pictures are displaying a maximum intensity projection of the Z axis stacks. Movies of 3 D reconstitutions of the Z axis image stacks are included on the supplementary CD under the references III-24 M1 and III-24 M2.

The second generation of clone with stable *lac*O and *te*tO arrays offered a convenient tool to observe *in vivo* interaction between specifically labeled telomeres regardless to the telomere repeat length since the two arrays can be labeled with different colors. Representative examples for double *lac*O and *tet*O arrays stable cell lines are shown in Figure III.24. The clone BiC3 (Fig. III.24A) and the clone BiB3-sd2 (Fig. III.24B) were generated by stably transfecting *tet*O arrays in the clone F6B2. The *lac*O and the *tet*O arrays were visualized by transiently co-transfecting the cells with LacI-mRFP1 together with TetR-eGFP. Both cell lines are indeed displaying like F6B2 the three *lac*O arrays loci *b*, *m* and *s*, visible in red but at the same time BiC3 displays a single and BiB3-sd2 two supplementary *tet*O array inserts, visible in green. The interaction between the locus *m* and the *tet*O insert in Figure III.24A and the locus *b* and the smallest *tet*O array insert in the Figure III.24B are clearly visible. A movie of the 3D reconstitution of the Z axis image stacks is given in supplementary material (III-24 M1 and III-24 M2).

IV. Discussion

The higher order chromatin organization and its dynamic properties are directly related to gene expression, replication, DNA repair and recombination (Cremer and Cremer, 2001; Gorski et al., 2006; Horowitz-Scherer and Woodcock, 2006; Sproul et al., 2005). In this thesis, chromatin mobility was first studied using fluorescence recovery after photobleaching (FRAP) and then using the *lac*O/LacI chromatin labeling system. This chromatin labeling method allows to monitor *in vivo* dynamics of a defined locus and is therefore a powerful tool for a fine chromatin mobility analysis. For this purpose a clone of the U2OS cell line was generated with three different *lac*O arrays, stably integrated in the telomeres region of three different chromosomes. The mobility of the loci was studied at time scales ranging from the millisecond to the hour using high performance laser scanning microscopy. Based on the data obtained a model is proposed for the overall chromatin mobility in the mammalian cell nucleus. It was moreover shown that in the U2OS cells, which elongate the telomeres through the alternative telomere lengthening (ALT) pathway, a subset of about 30 % of the telomere displays an extended mobility. A correlation between this extended mobility and telomere repeat length was also demonstrated suggesting that long telomeres are anchored to a stable structure in the nucleus, whereas telomeres with too short repeats are released and therefore move more freely. The relative mobility of PML bodies with regards to telomeres was also measured. The data obtained allowed us to re-define the previous observations of the absolute PML body mobility with regard to its chromatin environment. In parallel, the structure and mechanism of formation of the ALT-associated PML body (APB) was investigated. APBs are a particular class of PML bodies that forms a distinct structure with the telomeres and that is thought to play a central role in the ALT pathway. Altogether, these data conducted to the proposal of a model for the alternative telomeric lengthening pathway dynamics.

1 Analysis of chromatin dynamics in response to histones acetylation and ATP depletion

The global chromatin mobility *in vivo* was first investigated by FRAP analysis on H2A-eYFP stably transfected HeLa cells (Fig. III.1). The relatively fast recovery of the chromatin after photobleaching (≤ 20 min) suggests a localized diffusive mobility of chromatin since core histones turnover is known to be extremely slow in the mammalian cell nucleus with a half-life time of ~200 min (Gerlich et al., 2003; Kimura et al., 2004). ATP depletion, through sodium azide treatment, as well as chromatin hyperacetylation induced by TSA, a deacetylase inhibitor, both considerably reduced the fluorescence recovery after photobleaching, suggesting that they reduce global chromatin translocations. These analogue consequences on chromatin mobility are surprising as the two treatments lead to opposite effects on chromatin folding: ATP depletion induces a global condensation of chromatin whereas hyperacetylation induces a global decondensation (Fejes Tóth et al., 2004; Görisch et al., 2004). These results demonstrate differential mobility of chromatin. However, their seemingly paradoxal nature as well as the complexity of the model do complicates a precise interpretation and sets the light on the difficulty to study chromatin mobility on the whole nucleus scale and the need for more specific analysis. The *lac* operator / Lac Inhibitor system, that provides the possibility to monitor *in vivo* a defined chromatin locus, was therefore used in order to continue the investigations on interphase chromatin mobility.

2 Mobility of telomeres in U2OS cells

The mobility measurement of nuclear sub-structures such as nuclear bodies, labeled chromatin loci as well as PNA-labeled telomeres was already the object of several publications. Data are summarized in Table IV.1. However most of theses studies are focusing on a limited time scale with often reduced accuracy and statistics. Moreover, the use of cell-nucleus alignments software to compensate for the cell mobility may have brought artifacts in the measurements. Finally, these studies were all conducted in cell lines derived from different species (human, hamster, drosophila...) what considerably complicates the comparisons between the different data sets.

In this thesis, we used the human U2OS clone F6B2 that displays three telomeric *lac*O arrays inserts of different apparent size. The measurement of the distance variation between the tree loci allowed to circumvolve all the problems linked to the cell mobility without the requirement of a cell nucleus alignment software. High-performance live cell imaging systems was used, with a time resolution ranging from the millisecond to the hour. Finally, the major achievement of this study was the comprehensive description of the overall telomeres mobility of at all relevant time scales.

2.1 Telomeres are located in the nucleus in a random manner

A preliminary observation, before studying the mobility of telomeres was conducted to get a precise picture of their starting conformation. The possible preferential location of telomeres inside the nucleus as well as their relative positioning with each other was investigated. In agreement with previous studies (Luderus et al., 1996; Molenaar et al., 2003), telomeres neither seemed to have a clear preferential location inside the nucleus nor did they displayed a conserved pattern with regard to their relative positioning.

2.2 The three levels of telomere mobility in the mammalian nucleus

Here, a model of telomere mobility in human cells is proposed, that is composed of three individual mobility levels at the second, minute and hour time scale, all associated with a specific confinement radius (r_c: corral radius).

The first level of mobility refers to the time scale of a second where all telomeres exhibit a fast movement within a region of 80 nm radius and a diffusion coefficient of D_{ms} = $2.2 \cdot 10^{-3}$ µm^2 s^{-1}. Further translocations in a radius of 150 nm and a diffusion coefficient D_{sec} = $4 \cdot 10^{-4}$ µm^2 s^{-1} are observed at the minute time scale (Fig. III.11 and III.12). Finally on the hour time scale, telomeres show two types of mobility that share the same diffusion coefficient D_{min} = $2 \cdot 10^{-5}$ µm^2 s^{-1} but differ on the accessible space. Whereas the majority of telomeres translocate within an average radius of ~0.3 µm, a subset of about 30 % displayed an extended mobility with translocations over ~0.8 µ radius (Fig. III.13, III.14, III.15 and III.16)

particle/locus	D ($\mu m^2 s^{-1}$)		r_c nm	reference
Mx1-YFP	$1.8 \cdot 10^{-4}$		280	(Görisch et al., 2004)
Cajal bodies	$1.1 \cdot 10^{-4}$		310	(Görisch et al., 2004)
PML bodies	$1.2 \cdot 10^{-4}$		260	(Görisch et al., 2004)
Nanospheres	$4 \cdot 10^{-4}$		150	(Tseng et al., 2004)
Nucleoplasmic chromatin (HT-1080 human cells)	$1.3 \cdot 10^{-4}$		300-480	(Chubb et al., 2002)
Nucleoplasmic chromatin (CHO hamster cells)	D_{fast}	$3.1 \cdot 10^{-3}$	40	(Levi et al., 2005)
	D_{slow}	$2.4 \cdot 10^{-4}$	-	
Nucleoplasmic chromatin (drosophila spermatocytes)	D_{fast}	$1.3 \cdot 10^{-2}$	500	(Vazquez et al., 2001)
	D_{slow}	$1 \cdot 10^{-3}$	-	
Dense chromatin regions	$4.8 \cdot 10^{-5}$		180	(Görisch et al., 2004)
1 Mb chromatin domain	0.5 to $1.5 \cdot 10^{-5}$		-	(Bornfleth et al., 1999)
Centromeres	$1.8 \cdot 10^{-4}$		500	(Molenaar et al., 2003)
Telomeres (*in vivo* PNA labeling, U2OS cells)	Slow species	$1.8 \cdot 10^{-4}$	500	(Molenaar et al., 2003)
	Fast species	$5.8 \cdot 10^{-4}$	1200	
Telomeres (*lac*O array labeling, U2OS cells)	$D_{/ms}$	$2.2 \cdot 10^{-3}$	80	This thesis
	$D_{/sec}$	$4 \cdot 10^{-4}$	150	
	$D_{/min}$ standard	$2 \cdot 10^{-5}$	300	
	$D_{/min}$ extended		800	

Table VI.9: Mobility of different chromatin loci and nuclear bodies.

2.3 Comparison of the mobility of the telomeres and other chromatin loci

On the minute time scale, telomeres appear to move in the same range than fluorescently tagged sub-chromosomal foci, fluorescent centromere protein clusters, or nuclear bodies for which respective diffusion coefficients between $1.1 \cdot 10^{-4}$ and $1.8 \cdot 10^{-4}$ μm^2 s^{-1} were calculated (Table IV.1) (Chubb et al., 2002; Görisch et al., 2004; Molenaar et al., 2003). The telomere mobility values calculated from measurements in this thesis are also very similar to those obtained by Levi and co-workers in the hamster CHO cell line (Levi et al., 2005) on the second and minute time scales with a comparably high time resolution imaging system (Table IV.1). Levi and co-workers interestingly observed as well several levels of mobility. Data were moreover fitted into a model similar to the “moving

corral" model used in this thesis. However, the "jumps" described in this study were not observed during our measurements. Several level of confinement in the mobility of *lac*O arrays labeled chromatin loci were also demonstrated in drosophila spermatocytes (Vazquez et al., 2001), although the telomere mobility in human U2OS cells measured here is several fold slower than the values obtained by Vazquez and co-workers. However, the different species and the extreme differentiation level of the spermatocyte cells make it hard to make more than a qualitative comparison. Interestingly, the calculated mobility value of the telomeres on the hour time scale is very close to the one observed by Bornfleth and co-workers, for 1 Mb chromatin domains labeled with Cy3-UTP on an analogue time scale (Table IV.1) (Bornfleth et al., 1999), suggesting a general ground state of slow mobility for large chromatin domains in the nucleus, in the range of $1\text{-}2\cdot10^{-5}$ $\mu m^2\ s^{-1}$.

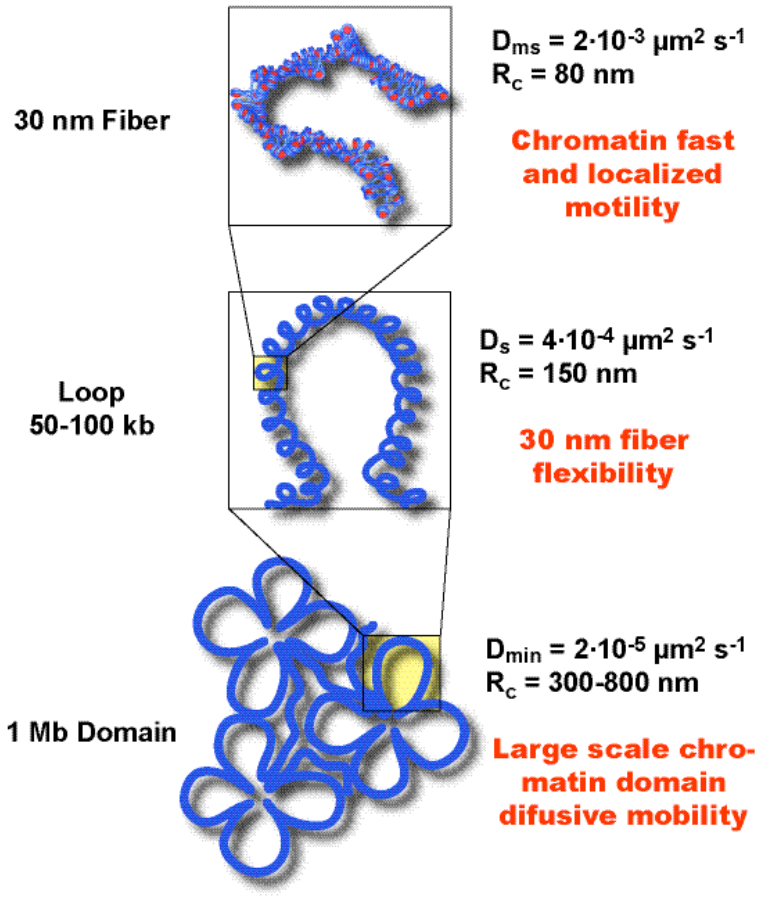

Figure IV.1: Schematic representation of the proposed model for the three levels of chromatin mobility.

The first level of very fast and localized mobility observed on the second time scale corresponds in this model to the chromatin fiber motility. The second level of mobility is induced by the flexibility of the 30 nm fiber. Finally the third level of slow mobility observed on the hour time scale corresponds to a slow diffusion of large chromatin domains.

Thus, comparison with previous studies indicates that telomeres behave similarly to other chromatin loci, although apparently slightly faster on the minute time scale. The particular extended mobility of about 30 % of the telomere population on the hour time scale is discussed in paragraph 2.5. The description derived here and depicted schematically in Figure IV.1 of a single chromatin locus is the first comprehensive description that correlates the different levels of chromatin mobility and chromatin compaction.

2.4 *Lac*O array telomere labeling allows a more accurate measurement of telomere mobility than PNA labeling

The mobility measured in this study on the minute time scale appears to be very similar to the results previously obtained by labeling telomeres *in vivo* with PNA probes (Molenaar et al., 2003). With this method, Molenaar and co-workers observed two classes of telomeres with regards to their mobility (Table IV.1): a slow telomere population displaying a diffusion coefficient of $1.8 \cdot 10^{-4}$ μm^2 s^{-1} and a relatively fast moving population representing about 10 % of the telomeres with a diffusion coefficient of $5.8 \cdot 10^{-4}$ μm^2 s^{-1}. The mobility calculated for the same time scale in this thesis, D_{sec}, appears to be in the same range although slightly faster than the main slow population. Variability in the single telomere mobility was observed in our measurements, but statistical analysis did not show two distinct groups. The estimated radius of constraint calculated for PNA-labeled telomeres appears to be on the contrary much higher than the value we obtained for the same time scale and correspond to 0.5 µm for the slow population and 1.2 µm for the fast subset of telomeres. These values are however close to the corral radius values calculated in this thesis for the two telomeres groups observed on the hour time scale. A first explanation for this discrepancy could be that Molenaar and co-workers measurements were conducted on a limited time scale, and the telomere mobility was described with a simple constrained diffusion model. Accordingly, the higher level of telomere mobility on the hour time scale may actually have interfered with the analysis. A second explanation for these differences may be related to the different telomere labeling techniques: *in vivo* PNA labeling allows to monitor a larger amount of telomeres in a single nucleus but limits the observation species that display the longer repeats. More than the half of the telomere population is thus not detectable. In this thesis, only three telomeres were

measured but in a specific manner and regardless of their repeats length, which might reflect the whole telomere population more accurately.

2.5 Possible mechanisms for different mobility rates on the hour time scale

Analysis of telomeres mobility on the hour time scale demonstrated that these are divided in two groups that differ by the accessible space but had the same mobility coefficient. The majority of the telomeres displayed a ~0.3 µm radius corral whereas a sub-population of about 30 % freely moved in an ~0.8 µm radius corral. This observation suggests that human telomeres are mostly constrained in their movements by association or anchoring with other structures in the nucleus, but can be released and freely diffuse about 30 % of the time. A further clue for telomere anchoring comes from observations in yeast: unlike in the mammalian cells, yeast telomeres are known to be anchored at the nuclear envelope and to be clustered there together with the silent subtelomeric chromatin (Gotta et al., 1996; Laroche et al., 1998; Laroche et al., 2000). Interestingly the behavior of *lac*O labeled telomeres in yeast is, at least in the G1 phase (Hediger et al., 2002), very close to our observation in human cells for the putative bound fraction: fast movements of the telomeres were observed in a constrained area of 150 to 300 nm on the minute time scale. Although telomeres are positioned randomly in the mammalian cell nucleus, the similarity of behavior between yeast and human telomeres observed using the same *in vivo* labeling system, suggests that human telomeres are also anchored to a stable structure. A recent study in mammalian cells provides another interesting comparison (Soutoglou et al., 2007): Soutoglou and co-workers generated a cell line with stably integrated *lac*O and *tet*O arrays inserts at a single locus and separated by a cleavage site. When the DNA cleavage is induced both arrays are released and undergo a slow diffusive mobility. The DNA fragments that flank the cleavage site resemble to short telomeres with disrupted telosome ones the cleavage is induced. The behavior of the two fragments is indeed similar to the telomeres that show an extended mobility observed in this thesis. The observation of Soutoglou and co-workers thus confirms the relatively slow mobility of telomeres on long time scale. It moreover corroborates the assumption that the releasing of the telomeres from the anchoring only increases the accessible space but not the mobility.

The nature of the telomere anchoring support is subject to speculations. Association of telomeres with the nuclear matrix was suggested by using biochemical approaches (Luderus et al., 1996; Weipoltshammer et al., 1999). However the possible existence of the nuclear matrix remains itself controversial (Pederson, 2000). Another possibility could be the association of the telomeres with a stable heterochromatin clusters. Indeed, the behavior as well as the measured mobility value of the telomere displaying the extended mobility on the hour time scale is very analogue to what was observed by Chuang and co-workers in the long range transition mobility of a VP16 inducible gene locus in CHO cells (Chuang et al., 2006). The activation of a *lac*O labeled gene region triggers a dramatic increase of its mobility, presumably by inducing its de-clustering from a stable heterochromatin region. Telomeres as well as sub-telomeric regions display constitutive heterochromatin markers. Interestingly, when the telomere repeats are shortened over a given limit, the telosome is disrupted and theses markers are lost (Benetti et al., 2007). A third possibility, non exclusive from the previous one, is that telomeres could cluster together, at least in small groups, and thus restricting their mobility. *In vivo* PNA labeling in U2OS cells (Molenaar et al., 2003), quantitative FISH observation in human fibroblast (Nagele et al., 2001) as well as observation of the *lac*O and *tet*O arrays double stable clones (Fig. III.24) as described in this thesis have indeed shown that telomeres can directly interact with each other. Moreover, the ALT pathway system is assumed to function through DNA recombination and therefore requires physical contact between the telomeres.

2.6 The size of the *lac*O insert does not interfere with telomere mobility

One potential source of artifacts in the *lac*O/LacI *in vivo* chromatin labeling system lies on the nature of the DNA insert itself. The inserted *lac* operator array is indeed composed of the repetition of a bacterial DNA sequence and could be susceptible to influence its environment. The clone F6B2 was used as the main tool for telomere mobility studies. This clone displays three different *lac*O arrays inserts that could easily be recognized by their apparent sizes *in vivo,* trough a LacI-XFP transfection (Fig. III.10), as well as in fluorescence *in situ* hybridization (FISH, Fig. III.12). All three loci had a spherical appearance. The locus *b* has an average

diameter of ~ 1 µm, the locus *m* ~ 0.6 µm and the locus *s* ~ 0.4 µm, which means that the apparent volume of the locus *b* is about 16-fold bigger than the volume of the locus *s*. The mobility of the three individual loci was calculated on the time scale of the second, the minute and the hour. No statistically significant differences were observed, strongly suggesting that the size of *lac*O array inserts does not influence telomere mobility and dynamic properties in the cell nucleus.

3 The three types of PML body mobility in regards to telomeres

The parallel study of telomere and PML body mobility is of multiple interests. First, it offers the possibility to compare the behavior of two sub-nuclear structures of very dissimilar nature, in the same model and with the same setting: a DNA strand and a large protein cluster. The absolute mobility of PML and Cajal bodies was already the object of several studies (Görisch et al., 2004; Muratani et al., 2002; Platani et al., 2002; Platani et al., 2000). This mobility appeared to be very dependant on the nuclear bodies chromatin environment. In addition, chromatin has been shown to play a critical role in the structural integrity of PML bodies (Eskiw et al., 2004; Eskiw et al., 2003) Therefore we took advantage of the F6B2 cell line with *lac*O-labeled telomeres to observe a possible mobility correlation and/or interactions between the PML body and a defined chromatin locus. Finally, as already mentioned, in ALT cells, PML bodies appear to play a central role by forming a particular structure with telomeres, the APB, in which the elongation process is thought to take place. A dynamic study of the relationship between telomeres and PML bodies would therefore bring valuable information on the mechanism of the ALT system.

With regard to their mobility, three types of PML bodies can be distinguished in U2OS cells on the minute time scale: (i) PML bodies with translocations that are independent from a close *lac*O-labeled telomere. These PML bodies are confined in areas with an average radius of 280 nm where they diffuse freely. This observation indicates that the nucleus contains surprisingly large areas where the chromatin density allows the free diffusion of large protein clusters. (ii) One group of PML bodies showed a correlated mobility with a nearby chromatin region. The group is constituted of two different sub-category: 2a and 2b shown on Figure III.21. The data suggest that these PML bodies are either confined to a very small

interchromatin region, literally trapped, or (at least transiently) associated with chromatin. The data suggests that PML bodies of the category 2a are associated directly with the chromatin region where the *lac*O array is inserted. In contrast, the category 2b associates with a different but spatially close region. Even if some PML bodies of this class show some contact to the nearby telomere (but no co-localization), this does not seem to be necessary to lead to a coordinated movement. Thus, some PML bodies from the category 2a were distant by 0.5-1 µm to the nearby telomere, suggesting that the chromatin region where the telomeres are associated is rather large. (iii) A significant group of PML bodies forms distinct complexes with telomeres, the APBs as discussed further.

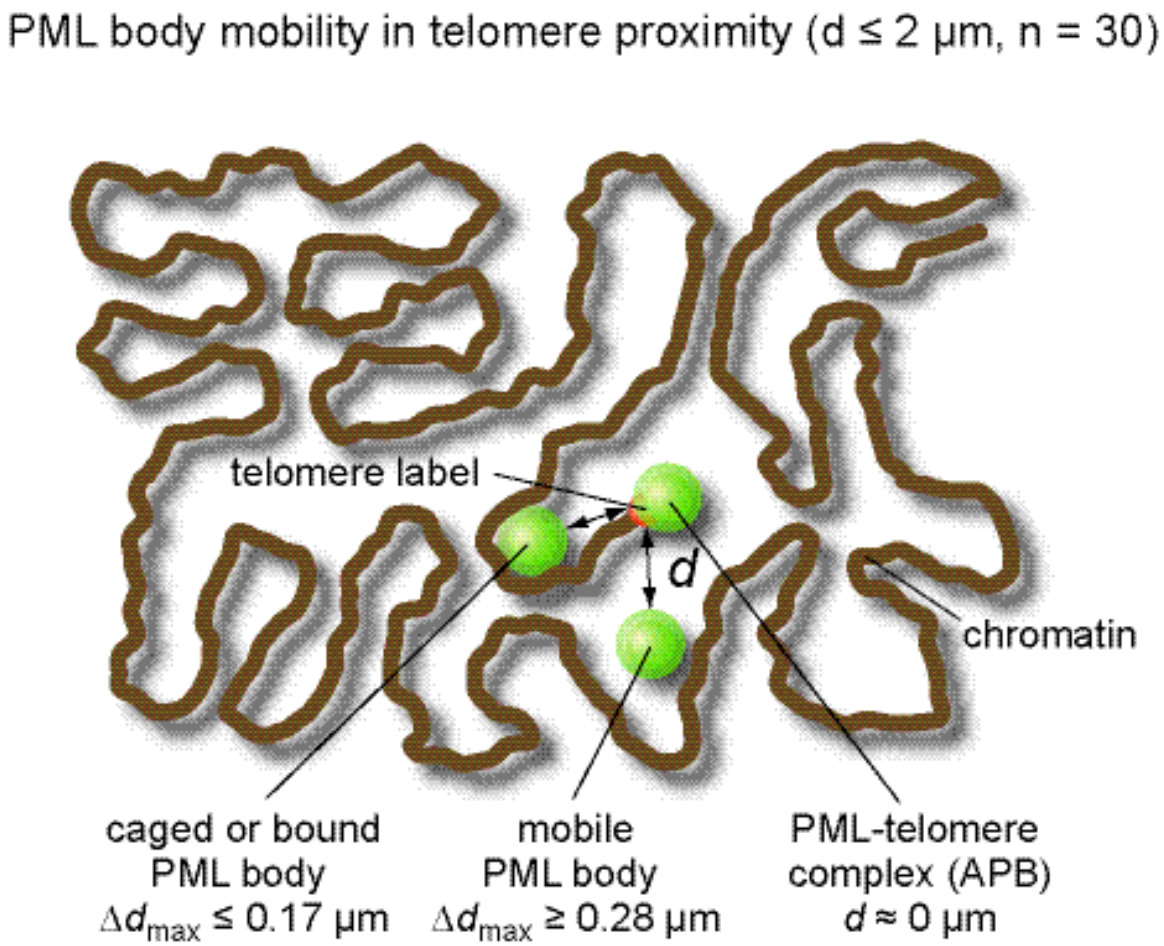

Figure IV.2: Three different PML bodies mobility classes in relation to telomeres.
A model for the three different classes of PML bodies with regard to telomeres observed in this thesis is given. The first class is constituted by PML bodies that move freely in the interchromatin space and therefore does no show any correlation with telomere mobility. In the second class, PML bodies are mechanically trapped in or associated with the same chromatin region than the telomere and therefore display a large mobility correlation with it. Finally, PML bodies that form distinct structures with telomeres: the APBs.

However, the diffusion coefficients derived here do not describe the absolute mobility of the PML body but its relative mobility with regard to a proximal chromatin locus or in other words the chromatin-independent part of the total PML mobility. This explains why, the relative mobility of the PML bodies measured in this thesis is significantly lower than previously published mobility values to which they can not be directly compared (Görisch et al., 2004; Muratani et al., 2002). The observations made in this thesis appear however to correlate with the observation made previously on the several regimes of PML mobility. Our measurements allowed us to better understand their significance in with respect to chromatin mobility: Thus chromatin-associated PML bodies are not necessarily immobile and represent the largest fraction of PML bodies in the nucleus. Our measurements furthermore allowed it to calculate the average confinement radius (~280 nm) of a freely diffusing nuclear body within the nucleus. This indicates interchromatin space can display a surprisingly large accessible area at certain time or locations within the nucleus. This observation can be related with the relatively slow large scale chromatin domain diffusion quantified in this thesis. Thus our observations emphasize the picture of a nucleus as a dynamic environment, in which large mobile chromosomal domains define the accessible space.

4 A model for the mechanism of alternative lengthening of telomeres

The clones used for this thesis are all based on the human osteosarcoma cell line U2OS which to belongs to the group of telomerase-negative tumor cells that maintain their telomeres with the ALT system. Only little is known about the ALT system. Tumor cell lines of this group display a large variability in telomere length and exhibit a very complex karyotype (Fig III.4 and Fig III.6). The ALT mechanism is associated with a special class of PML bodies designated APBs that are shown to co-localize with telomeric DNA (Yeager et al., 1999). Although DNA synthesis was demonstrated to occur in APBs (Nabetani et al., 2004) it is thought that the central mechanism of the ALT system is based on inter- or intra-chromosomal telomere recombination (Muntoni and Reddel, 2005).

4.1 Telomeres are recombination “hot spots” In U2OS cells

Analysis of the chromosomal insertion sites of the *lac*O inserts in the stable clones showed that all inserts except a single one are located at the telomeres. Moreover, these inserts are sometimes surprisingly large in comparison to stable clones obtained with other human cell lines (Chubb et al., 2002). Thus, our data indicate that in U2OS cells telomeres are recombination “hot spots”. This observation strongly supports the assumption that the ALT system is based on recombination-mediated telomere lengthening (Dunham et al., 2000; Laud et al., 2005; Londono-Vallejo et al., 2004; Muntoni and Reddel, 2005). This indicates that the plasmid containing the *lac*O arrays may have used the recombination machinery already present at telomeres to integrate in the host genome.

4.2 The APB display a hollow-spherical shape with telomeric and sub-telomeric DNA at the center

The APBs is clearly identifiable in Figure III.22. The *lac*O array appears to be included into the internal compartment of the PML body. The structure is very similar to the observation made in centromeric instability and facial dysmorphy (ICF) patients cells (Luciani et al., 2006). The ICF syndrome is associated with extremely large hollow-spherical PML bodies that offer a valuable structural model. Interestingly, large amount of satellite DNA can be detected in the internal compartment of these giant PML bodies. The presence of satellite DNA is noteworthy as it displays the same repetitive nature as the telomeres. Satellite DNA is moreover displaying the epigenetic markers of constitutive heterochromatin that also characterize the telomeres and sub-telomeric regions.
Immunolabeling experiments on of PML proteins show that the transient transfection of cells with LacI-mRFP1 does not modify number, size or shape of PML bodies. Experiments indicate that APBs do not only include telomeric DNA but also a large part of the sub telomeric region. Moreover 3D reconstitution of Z axis scans of APBs forming with large *lac*O arrays (for example the locus *b* of the clone F6B2) shows that the structure does not enclose the whole array but rather forms a sort of cap. This observation indicates that APB does not have an affinity for the *lac*O array *per se* as it was suggested by Tsukamoto and co-workers (Tsukamoto et al., 2000), but includes a large part of the chromatin which flanks the telomere. Moreover Tsukamoto and co-workers also used U2OS cells for their

work but did not characterize their clones with respect to the *lac*O array insertion locus. Our experimental data suggest that these clones had telomeric *lac*O array inserts as well.

Finally, PML bodies were shown to play a critical role in the establishment of the constitutive heterochromatin markers in satellite DNA (Luciani et al., 2006). Moreover, the heterochromatin protein 1 (HP1), one important factor in the establishment of constitutive heterochromatin, is known to be one of the prominent components of PML bodies. With respect to this analogy it would be of great interest to investigate the possible relationship between telomeric and subtelomeric DNA chromatin folding and the PML body in the ALT as well as in telomerase positive cells.

4.3 The formation of APBs occurs in a two steps fashion

The *lac*O array labeling of the telomeres *in vivo* was also used to investigate the mechanism of APB formation (Fig. III.23). In contrast to previous reports (Molenaar et al., 2003) that indicated only transient contacts between PML bodies and telomeres, the data presented here demonstrates that the APBs form in two steps: the first step is the binding of a pre-existing PML body to the telomere. In a second step the PML protein accumulates at the locus until the typical telomere surrounding structure of the APB has formed. In this step, the PML protein seemed not to accumulate as freely diffusing protein but under the form of small and very mobile aggregates already referred in the literature as PML microbodies (Eskiw et al., 2004).

4.4 The alternative telomere lengthening is a slow process that does not show preferences for certain telomeres

All the telomere length analysis experiments were carried out with cells from the same batch that have the same number of passages since the isolation of the clone. As a consequence, the experiment constitutes a sort of snapshot in the clone history with respect to the telomeres.

The analysis of the repeat length by PNA FISH combined with *lac*O arrays oligo-FISH re-hybridization demonstrated that the repeats are not detectable in about 20 % of the cases for the telomeres located at the loci *b*, *m* and *s* (Fig. III.18 and Table III.2). As this proportion appears to be representative of the whole telomere

population (Fig. III.17 and III.18), this indicates that the ALT telomere lengthening pathway does not seem to preferentially elongate specific telomeres. Moreover, the relatively high proportion of undetectable telomeres indicates that the ALT pathway is a rather slow process. Finally, the absence of differences in the telomere lengthening between the observed telomeres with each other and with the rest of the population confirms that the *lac*O arrays inserts do not interfere with the neighboring sequences in nature and/or function.

4.5 Proposed model for the ALT pathway

One valuable advantage of the *lac*O array telomere labeling for the study of the ALT system is the possibility to follow a single telomere over time in a manner independent of its TTAGGG repeats length. With this construct, we were able to observe the mobility of the *lac*O array labeled telomeres in the clone F6B2 in parallel with the monitoring of telomere repeat.

On the one hand, the study of the mobility of the *lac*O array loci *b*, *m* and *s* shows that, at the hour scale, telomeres have an extended mobility in about 30% of the time. On the other hand investigations of the telomere repeats length of the same three telomeres indicates that telomeric repeats are undetectable in a correlated fraction in cells from the same cell batch (Fig III.14, Fig III.18 and Table III.2). This observation conducted us to propose a working model for principal determinants of the ALT mechanism as depicted in Figure IV.3. Telomeres are bound to stable structure in 70% of the cases (or 70% of the time). We propose here that these are bound through the action of the constituted telosome, the protein complex forming with the intact telomere, by associating with a stable (hetero)chromatin domain. Under these conditions, the mobility of the *lac*O array is very constrained. With the successive divisions, the telomere repeat is shortening. When a certain length is reached the telosome is disrupted, thereby releasing the telomere from its anchoring point. The *lac*O array diffusion area is subsequently increased. The telomeric DNA appears at this point naked, resembling thus a double–strand break. Interestingly, many proteins involved in the detection and repair of double stand breaks, like for example Rad51, are found to accumulate (at least transiently) in PML bodies in general and in APBs in particular (Nabetani et al., 2004). A PML body then associates with the naked telomeres and PML protein is accumulating at the locus until it forms an APB where the telomere is re-

elongated. Finally, telomeric proteins accumulate at the newly synthesized telomere repeat, reforming the telosome that mediates the telomere to re-anchoring. The *lac*O array constrained mobility is then recovered.

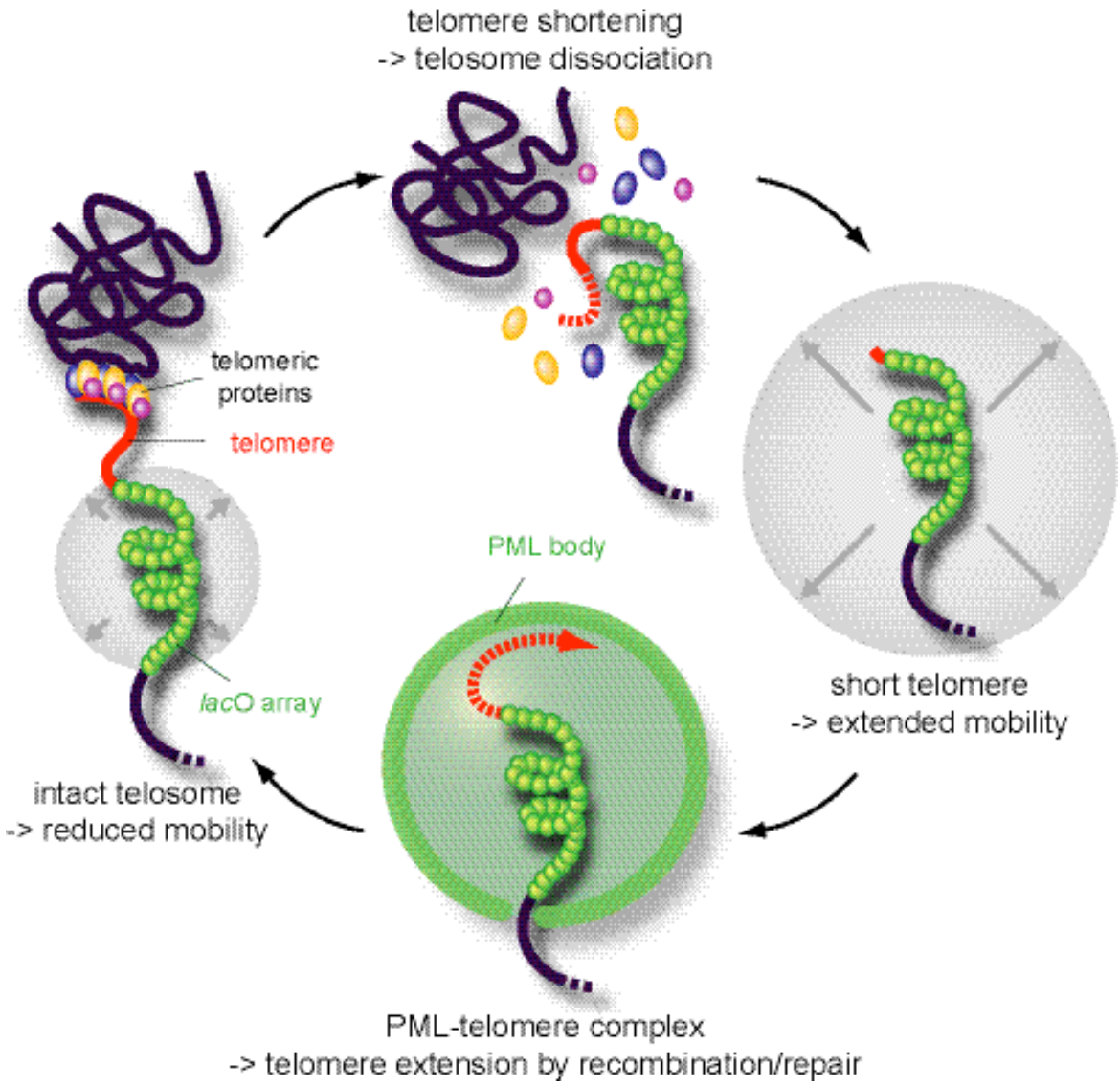

Figure IV.3: Schematic representation of the proposed model for the ALT pathway.
In 70% of the telomeres of U2OS cells the repeat length is sufficient for the formation of the telosome that mediates the anchoring to a stable (hetero)chromatin structure with restricted mobility. The telomere repeats length is reduced with each cell division. When the telomere become to short the telosome is disrupted and the anchoring lost. At this point, telomeres move freely and the accessible space is increased. The short telomere then associates with a PML body and form an APB where the repeats are re-elongated. The telosome can at this point be re-established and promote a new telomere anchoring.

5 Perspectives

The telomeric *lac*O array labeling system provides a valuable tool to further study the ALT pathway mechanism as well as the telomere structure itself. The first step to extend the work achieved in this thesis would be to combine the two available *in vivo* telomere labeling techniques by microinjecting PNAs coding for telomeric sequences in our F6B2 cell line. This would allow to directly correlate telomere length to enhanced mobility at the hour time scale *in vivo* an therefore to validate our hypothesis. In a similar approach the co-localization of *lac*O-labeled telomeres with proteins involved in the detection and the reparation of double-strand breaks could be examined *in vivo* by co-transfection. The possible correlation with telomere mobility could also be investigated. The double stable clones, with multiple *lac*O and *tet*O telomeric inserts would give us the opportunity to monitor the dynamics of telomere interactions, which is one of the key aspects of the ALT pathway. As the elongation in the alternative pathway is based on recombination, it requires direct telomere-telomere interactions. A possible co-localization of two telomeres in a single APB could be therefore investigated to observe if the recombination event involved in the ALT pathway takes actually place in this structure.

The recent cloning of single-chain antibodies isolated from camels provides a very interesting new tool to the field of cell biology research (Rothbauer et al., 2006). These single-chain antibodies, called nanobodies, can indeed be transfected into cells like any other protein and display the binding affinity of a normal antibody. An anti-eGFP nanobody construct is already available. By transfecting this nanobody fused to the LacI into our cell lines with telomeric *lac*O arrays it should be possible to recruit any eGFP-coupled protein specifically at the telomeric/sub-telomeric region. This strategy is analogue to the one used by Chuang and co-workers that targeted transcriptional activators to *lac*O arrays in CHO cells (Chuang et al., 2006). The nanobody strategy is however much more convenient as it does not require the generation of specific LacI-fusion proteins. A schematic representation of this experimental strategy is given in Figure IV.4. Our attention would particularly focus on chromatin modifying proteins. This method could thus allow to study the complex relationships that exist between the telomere, sub-telomere, constitutive heterochromatin formation and telomere lengthening that appears to be tightly related in ALT cells as well as in telomerase-positive cell lines.

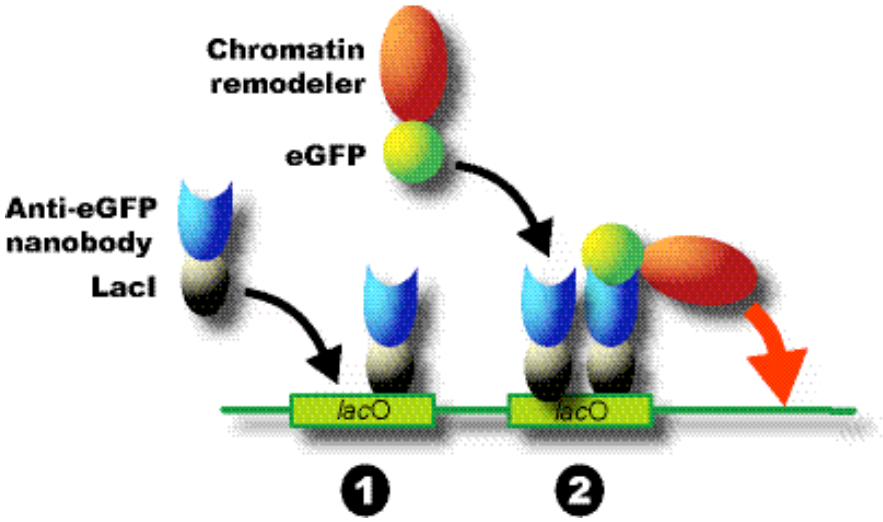

Figure IV.4: Recruitment of chromatin modifying proteins at specific chromatin loci by using an anti-eGFP nanobody/LacI fusion.

Cells with stably integrated *lac*O arrays are transiently co-transfected with the LacI/anti-eGFP nanobody fusion protein together with a chromatin remodeler fused to eGFP. The LacI/nanobody fusion protein binds first at the *lac*O site. The eGFP binds then to the nanobody recruiting chromosomal proteins to the *lac*O array. The eGFP fluorescence allows to visualize the array and to monitor the effects of the recruited protein *in vivo*.

V. References

Abney, J. R., Cutler, B., Fillbach, M. L., Axelrod, D., and Scalettar, B. A. (1997). Chromatin dynamics in interphase nuclei and its implications for nuclear structure. *J Cell Biol* **137**, 1459-1468.

Alberts, B., Bray, D., Lewis, J., Raff, M., Roberts, K., and Watson, J. D. (1994). Molecular biology of the cell, 3rd Edition edn (New York & London, Garland Publishing, Inc.).

Alcalay, M., Tomassoni, L., Colombo, E., Stoldt, S., Grignani, F., Fagioli, M., Szekely, L., Helin, K., and Pelicci, P. G. (1998). The promyelocytic leukemia gene product (PML) forms stable complexes with the retinoblastoma protein. *Mol Cell Biol* **18**, 1084-1093.

Allers, T., and Lichten, M. (2001). Differential timing and control of noncrossover and crossover recombination during meiosis. *Cell* **106**, 47-57.

Ascoli, C. A., and Maul, G. G. (1991). Identification of a novel nuclear domain. *J Cell Biol* **112**, 785-795.

Baur, J. A., Zou, Y., Shay, J. W., and Wright, W. E. (2001). Telomere position effect in human cells. *Science* **292**, 2075-2077.

Becker, P. B., and Horz, W. (2002). ATP-dependent nucleosome remodeling. *Annu Rev Biochem* **71**, 247-273.

Belmont, A. S., Li, G., Sudlow, G., and Robinett, C. (1999). Visualization of large-scale chromatin structure and dynamics using the lac operator/lac repressor reporter system. *Methods Cell Biol* **58**, 203-222.

Benetti, R., Garcia-Cao, M., and Blasco, M. A. (2007). Telomere length regulates the epigenetic status of mammalian telomeres and subtelomeres. *Nat Genet* **39**, 243-250.

Bertuch, A. A., and Lundblad, V. (2006). The maintenance and masking of chromosome termini. *Curr Opin Cell Biol* **18**, 247-253.

Bischof, O., Kirsh, O., Pearson, M., Itahana, K., Pelicci, P. G., and Dejean, A. (2002). Deconstructing PML-induced premature senescence. *Embo J* **21**, 3358-3369.

Blackburn, E. H. (2000). Telomere states and cell fates. *Nature* **408**, 53-56.

Blasco, M. A. (2005). Telomeres and human disease: ageing, cancer and beyond. *Nature reviews* **6**, 611-622.

Blasco, M. A. (2007). The epigenetic regulation of mammalian telomeres. *Nat Rev Genet* **8**, 299-309.

Bodnar, A. G., Ouellette, M., Frolkis, M., Holt, S. E., Chiu, C. P., Morin, G. B., Harley, C. B., Shay, J. W., Lichtsteiner, S., and Wright, W. E. (1998). Extension of life-span by introduction of telomerase into normal human cells. *Science* **279**, 349-352.

Boisvert, F. M., Hendzel, M. J., and Bazett-Jones, D. P. (2000). Promyelocytic leukemia (PML) nuclear bodies are protein structures that do not accumulate RNA. *J Cell Biol* **148**, 283-292.

Boisvert, F. M., Kruhlak, M. J., Box, A. K., Hendzel, M. J., and Bazett-Jones, D. P. (2001). The transcription coactivator CBP is a dynamic component of the promyelocytic leukemia nuclear body. *J Cell Biol* **152**, 1099-1106.

Borden, K. L., Lally, J. M., Martin, S. R., O'Reilly, N. J., Solomon, E., and Freemont, P. S. (1996). In vivo and in vitro characterization of the B1 and B2 zinc-binding domains from the acute promyelocytic leukemia protooncoprotein PML. *Proc Natl Acad Sci U S A* **93**, 1601-1606.

Bornfleth, H., Edelmann, P., Zink, D., Cremer, T., and Cremer, C. (1999). Quantitative motion analysis of subchromosomal foci in living cells using four-dimensional microscopy. *Biophys J* **77**, 2871-2886.

Boukamp, P., Popp, S., and Krunic, D. (2005). Telomere-dependent chromosomal instability. *J Investig Dermatol Symp Proc* **10**, 89-94.

Branco, M. R., and Pombo, A. (2006). Intermingling of chromosome territories in interphase suggests role in translocations and transcription-dependent associations. *PLoS Biol* **4**, e138.

Branco, M. R., and Pombo, A. (2007). Chromosome organization: new facts, new models. *Trends Cell Biol* **17**, 127-134.

Bryan, T. M., Englezou, A., Gupta, J., Bacchetti, S., and Reddel, R. R. (1995). Telomere elongation in immortal human cells without detectable telomerase activity. *Embo J* **14**, 4240-4248.

Bystricky, K., Heun, P., Gehlen, L., Langowski, J., and Gasser, S. M. (2004). Long-range compaction and flexibility of interphase chromatin in budding yeast analyzed by high-resolution imaging techniques. *Proc Natl Acad Sci U S A*.

Bystricky, K., Laroche, T., van Houwe, G., Blaszczyk, M., and Gasser, S. M. (2005). Chromosome looping in yeast: telomere pairing and coordinated movement reflect anchoring efficiency and territorial organization. *J Cell Biol* **168**, 375-387.

Cabal, G. G., Genovesio, A., Rodriguez-Navarro, S., Zimmer, C., Gadal, O., Lesne, A., Buc, H., Feuerbach-Fournier, F., Olivo-Marin, J. C., Hurt, E. C., and Nehrbass, U. (2006). SAGA interacting factors confine sub-diffusion of transcribed genes to the nuclear envelope. *Nature* **441**, 770-773.

Campbell, R. E., Tour, O., Palmer, A. E., Steinbach, P. A., Baird, G. S., Zacharias, D. A., and Tsien, R. Y. (2002). A monomeric red fluorescent protein. *Proc Natl Acad Sci U S A* **99**, 7877-7882.

Chalfie, M., Tu, Y., Euskirchen, G., Ward, W. W., and Prasher, D. C. (1994). Green fluorescent protein as a marker for gene expression. *Science* **263**, 802-805.

Chan, S. W., and Blackburn, E. H. (2002). New ways not to make ends meet: telomerase, DNA damage proteins and heterochromatin. *Oncogene* **21**, 553-563.

Cheutin, T., McNairn, A. J., Jenuwein, T., Gilbert, D. M., Singh, P. B., and Misteli, T. (2003). Maintenance of stable heterochromatin domains by dynamic HP1 binding. *Science* **299**, 721-725.

Chuang, C. H., Carpenter, A. E., Fuchsova, B., Johnson, T., de Lanerolle, P., and Belmont, A. S. (2006). Long-range directional movement of an interphase chromosome site. *Curr Biol* **16**, 825-831.

Chubb, J. R., Boyle, S., Perry, P., and Bickmore, W. A. (2002). Chromatin motion is constrained by association with nuclear compartments in human cells. *Curr Biol* **12**, 439-445.

Collins, I., and Newlon, C. S. (1994). Meiosis-specific formation of joint DNA molecules containing sequences from homologous chromosomes. *Cell* **76**, 65-75.

Collins, K., and Mitchell, J. R. (2002). Telomerase in the human organism. *Oncogene* **21**, 564-579.

Cremer, T., and Cremer, C. (2001). Chromosome Territories, Nuclear Architecture and Gene Regulation in Mammalian Cells. *Nat Rev Genet* **2**, 292-301.

Cremer, T., Cremer, M., Dietzel, S., Muller, S., Solovei, I., and Fakan, S. (2006). Chromosome territories - a functional nuclear landscape. *Curr Opin Cell Biol* **18**, 307-316.

Cremer, T., Kurz, A., Zirbel, R., Dietzel, S., Rinke, B., Schrock, E., Speicher, M. R., Mathieu, U., Jauch, A., Emmerich, P., and et al. (1993). Role of chromosome territories in the functional compartmentalization of the cell nucleus. *Cold Spring Harbour Symp Quant Biol* **58**, 777-792.

Cremer, T., Lichter, P., Borden, J., Ward, D. C., and Manuelidis, L. (1988). Detection of chromosome aberrations in metaphase and interphase tumor cells by in situ hybridization using chromosome specific library probes. *Hum Genet* **80**, 235-246.

Dellaire, G., and Bazett-Jones, D. P. (2004). PML nuclear bodies: dynamic sensors of DNA damage and cellular stress. *Bioessays* **26**, 963-977.

Dellaire, G., Ching, R. W., Dehghani, H., Ren, Y., and Bazett-Jones, D. P. (2006). The number of PML nuclear bodies increases in early S phase by a fission mechanism. *J Cell Sci* **119**, 1026-1033.

Dillon, N. (2004). Heterochromatin structure and function. *Biol Cell* **96**, 631-637.

Dillon, N., and Festenstein, R. (2002). Unravelling heterochromatin: competition between positive and negative factors regulates accessibility. *Trends Genet* **18**, 252-258.

Doucas, V., Shi, Y., Miyamoto, S., West, A., Verma, I., and Evans, R. M. (2000). Cytoplasmic catalytic subunit of protein kinase A mediates cross-repression by NF-kappa B and the glucocorticoid receptor. *Proc Natl Acad Sci U S A* **97**, 11893-11898.

Dunham, M. A., Neumann, A. A., Fasching, C. L., and Reddel, R. R. (2000). Telomere maintenance by recombination in human cells. *Nat Genet* **26**, 447-450.

Eskiw, C. H., Dellaire, G., and Bazett-Jones, D. P. (2004). Chromatin contributes to structural integrity of promyelocytic leukemia bodies through a SUMO-1-independent mechanism. *J Biol Chem* **279**, 9577-9585.

Eskiw, C. H., Dellaire, G., Mymryk, J. S., and Bazett-Jones, D. P. (2003). Size, position and dynamic behavior of PML nuclear bodies following cell stress as a paradigm for supramolecular trafficking and assembly. *J Cell Sci* **116**, 4455-4466.

Fagioli, M., Alcalay, M., Pandolfi, P. P., Venturini, L., Mencarelli, A., Simeone, A., Acampora, D., Grignani, F., and Pelicci, P. G. (1992). Alternative splicing of PML transcripts predicts coexpression of several carboxy-terminally different protein isoforms. *Oncogene* **7**, 1083-1091.

Fejes Tóth, K., Knoch, T. A., Wachsmuth, M., Stöhr, M., Frank-Stöhr, M., Bacher, C. P., Müller, G., and Rippe, K. (2004). Trichostatin A induced histone acetylation causes decondensation of interphase chromatin. *J Cell Sci* **117**, 4277-4287.

Festenstein, R., Pagakis, S. N., Hiragami, K., Lyon, D., Verreault, A., Sekkali, B., and Kioussis, D. (2003). Modulation of heterochromatin protein 1 dynamics in primary Mammalian cells. *Science* **299**, 719-721.

Flores, I., Benetti, R., and Blasco, M. A. (2006). Telomerase regulation and stem cell behaviour. *Curr Opin Cell Biol* **18**, 254-260.

Gerlich, D., Beaudouin, J., Kalbfuss, B., Daigle, N., Eils, R., and Ellenberg, J. (2003). Global chromosome positions are transmitted through mitosis in mammalian cells. *Cell* **112**, 751-764.

Gerlich, D., and Ellenberg, J. (2003). Dynamics of chromosome positioning during the cell cycle. *Curr Opin Cell Biol* **15**, 664-671.

Goddard, A. D., Borrow, J., Freemont, P. S., and Solomon, E. (1991). Characterization of a zinc finger gene disrupted by the t(15;17) in acute promyelocytic leukemia. *Science* **254**, 1371-1374.

Gonzalo, S., Jaco, I., Fraga, M. F., Chen, T., Li, E., Esteller, M., and Blasco, M. A. (2006). DNA methyltransferases control telomere length and telomere recombination in mammalian cells. *Nat Cell Biol* **8**, 416-424.

Görisch, S. M., Wachsmuth, M., Fejes Tóth, K., Lichter, P., and Rippe, K. (2005). Histone acetylation increases chromatin accessibility. *J Cell Sci* **118**, 5825-5834.

Görisch, S. M., Wachsmuth, M., Ittrich, C., Bacher, C. P., Rippe, K., and Lichter, P. (2004). Nuclear body movement is determined by chromatin accessibility and dynamics. *Proc Natl Acad Sci USA* **101**, 13221-13226.

Gorski, S. A., Dundr, M., and Misteli, T. (2006). The road much traveled: trafficking in the cell nucleus. *Curr Opin Cell Biol* **18**, 284-290.

Gotta, M., Laroche, T., Formenton, A., Maillet, L., Scherthan, H., and Gasser, S. M. (1996). The clustering of telomeres and colocalization with Rap1, Sir3, and Sir4 proteins in wild-type Saccharomyces cerevisiae. *J Cell Biol* **134**, 1349-1363.

Griffith, J. D., Comeau, L., Rosenfield, S., Stansel, R. M., Bianchi, A., Moss, H., and de Lange, T. (1999). Mammalian telomeres end in a large duplex loop. *Cell* **97**, 503-514.

Guo, A., Salomoni, P., Luo, J., Shih, A., Zhong, S., Gu, W., and Pandolfi, P. P. (2000). The function of PML in p53-dependent apoptosis. *Nat Cell Biol* **2**, 730-736.

Hayakawa, T., Haraguchi, T., Masumoto, H., and Hiraoka, Y. (2003). Cell cycle behavior of human HP1 subtypes: distinct molecular domains of HP1 are required for their centromeric localization during interphase and metaphase. *J Cell Sci* **116**, 3327-3338.

Hediger, F., Neumann, F. R., Van Houwe, G., Dubrana, K., and Gasser, S. M. (2002). Live imaging of telomeres: yKu and Sir proteins define redundant telomere-anchoring pathways in yeast. *Curr Biol* **12**, 2076-2089.

Hediger, F., Taddei, A., Neumann, F. R., and Gasser, S. M. (2004). Methods for visualizing chromatin dynamics in living yeast. *Methods Enzymol* **375**, 345-365.

Heim, R., Prasher, D. C., and Tsien, R. Y. (1994). Wavelength mutations and posttranslational autoxidation of green fluorescent protein. *Proc Natl Acad Sci U S A* **91**, 12501-12504.

Henson, J. D., Hannay, J. A., McCarthy, S. W., Royds, J. A., Yeager, T. R., Robinson, R. A., Wharton, S. B., Jellinek, D. A., Arbuckle, S. M., Yoo, J.*, et al.* (2005). A robust assay for alternative lengthening of telomeres in tumors shows the significance of alternative lengthening of telomeres in sarcomas and astrocytomas. *Clin Cancer Res* **11**, 217-225.

Hess, S. T., and Webb, W. W. (2002). Focal volume optics and experimental artifacts in confocal fluorescence correlation spectroscopy. *Biophys J* **83**, 2300-2317.

Heun, P., Laroche, T., Shimada, K., Furrer, P., and Gasser, S. M. (2001). Chromosome dynamics in the yeast interphase nucleus. *Science* **294**, 2181-2186.

Horowitz-Scherer, R. A., and Woodcock, C. L. (2006). Organization of interphase chromatin. *Chromosoma* **115**, 1-14.

Ishov, A. M., Sotnikov, A. G., Negorev, D., Vladimirova, O. V., Neff, N., Kamitani, T., Yeh, E. T., Strauss, J. F., 3rd, and Maul, G. G. (1999). PML is critical for ND10 formation and recruits the PML-interacting protein daxx to this nuclear structure when modified by SUMO-1. *J Cell Biol* **147**, 221-234.

Janicki, S. M., Tsukamoto, T., Salghetti, S. E., Tansey, W. P., Sachidanandam, R., Prasanth, K. V., Ried, T., Shav-Tal, Y., Bertrand, E., Singer, R. H., and Spector, D. L. (2004). From silencing to gene expression: real-time analysis in single cells. *Cell* **116**, 683-698.

Jiang, W. Q., Zhong, Z. H., Henson, J. D., and Reddel, R. R. (2007). Identification of candidate alternative lengthening of telomeres genes by methionine restriction and RNA interference. *Oncogene*.

Kastner, P., Perez, A., Lutz, Y., Rochette-Egly, C., Gaub, M. P., Durand, B., Lanotte, M., Berger, R., and Chambon, P. (1992). Structure, localization and transcriptional properties of two classes of retinoic acid receptor alpha fusion proteins in acute promyelocytic leukemia (APL): structural similarities with a new family of oncoproteins. *Embo J* **11**, 629-642.

Kiesslich, A., von Mikecz, A., and Hemmerich, P. (2002). Cell cycle-dependent association of PML bodies with sites of active transcription in nuclei of mammalian cells. *J Struct Biol* **140**, 167-179.

Kim, N. W., Piatyszek, M. A., Prowse, K. R., Harley, C. B., West, M. D., Ho, P. L., Coviello, G. M., Wright, W. E., Weinrich, S. L., and Shay, J. W. (1994). Specific association of human telomerase activity with immortal cells and cancer. *Science* **266**, 2011-2015.

Kim, Y. H., Choi, C. Y., and Kim, Y. (1999). Covalent modification of the homeodomain-interacting protein kinase 2 (HIPK2) by the ubiquitin-like protein SUMO-1. *Proc Natl Acad Sci U S A* **96**, 12350-12355.

Kimura, H. (2005). Histone dynamics in living cells revealed by photobleaching. *DNA Repair (Amst)* **4**, 939-950.

Kimura, H., and Cook, P. R. (2001). Kinetics of core histones in living human cells: little exchange of H3 and H4 and some rapid exchange of H2B. *J Cell Biol* **153**, 1341-1353.

Kimura, H., Hieda, M., and Cook, P. R. (2004). Measuring histone and polymerase dynamics in living cells. *Methods Enzymol* **375**, 381-393.

Knoch, T. A., Waldeck, W., Müller, G., Alonso, A., and Langowski, J. (2000). DNA-Sequenz und Verfahren zur in vivo Markierung und Analyse von DNA/Chromatin in Zellen. In Deutsche Patentanmeldung 100 13 204.9 (Germany).

Kornberg, R. D. (1974). Chromatin structure: a repeating unit of histones and DNA. *Science* **184**, 868-871.

Lamond, A. I., and Sleeman, J. E. (2003). Nuclear substructure and dynamics. *Curr Biol* **13**, R825-828.

Laroche, T., Martin, S. G., Gotta, M., Gorham, H. C., Pryde, F. E., Louis, E. J., and Gasser, S. M. (1998). Mutation of yeast Ku genes disrupts the subnuclear organization of telomeres. *Curr Biol* **8**, 653-656.

Laroche, T., Martin, S. G., Tsai-Pflugfelder, M., and Gasser, S. M. (2000). The dynamics of yeast telomeres and silencing proteins through the cell cycle. *J Struct Biol* **129**, 159-174.

Lau, I. F., Filipe, S. R., Soballe, B., Okstad, O. A., Barre, F. X., and Sherratt, D. J. (2003). Spatial and temporal organization of replicating Escherichia coli chromosomes. *Mol Microbiol* **49**, 731-743.

Laud, P. R., Multani, A. S., Bailey, S. M., Wu, L., Ma, J., Kingsley, C., Lebel, M., Pathak, S., DePinho, R. A., and Chang, S. (2005). Elevated telomere-telomere recombination in WRN-deficient, telomere dysfunctional cells promotes escape from senescence and engagement of the ALT pathway. *Genes Dev* **19**, 2560-2570.

Le, X. F., Vallian, S., Mu, Z. M., Hung, M. C., and Chang, K. S. (1998). Recombinant PML adenovirus suppresses growth and tumorigenicity of human breast cancer cells by inducing G1 cell cycle arrest and apoptosis. *Oncogene* **16**, 1839-1849.

Lever, M. A., Th'ng, J. P., Sun, X., and Hendzel, M. J. (2000). Rapid exchange of histone H1.1 on chromatin in living human cells. *Nature* **408**, 873-876.

Levi, V., Ruan, Q., Plutz, M., Belmont, A. S., and Gratton, E. (2005). Chromatin dynamics in interphase cells revealed by tracking in a two-photon excitation microscope. *Biophys J* **89**, 4275-4285.

Lichter, P., Cremer, T., Borden, J., Manuelidis, L., and Ward, D. C. (1988). Delineation of individual human chromosomes in metaphase and interphase cells by in situ suppression hybridization using recombinant DNA libraries. *Hum Genet* **80**, 224-234.

Lippincott-Schwartz, J., Snapp, E., and Kenworthy, A. (2001). Studying protein dynamics in living cells. *Nat Rev Mol Cell Biol* **2**, 444-456.

Lombard, D. B., and Guarente, L. (2000). Nijmegen breakage syndrome disease protein and MRE11 at PML nuclear bodies and meiotic telomeres. *Cancer Res* **60**, 2331-2334.

Londono-Vallejo, J. A., Der-Sarkissian, H., Cazes, L., Bacchetti, S., and Reddel, R. R. (2004). Alternative lengthening of telomeres is characterized by high rates of telomeric exchange. *Cancer Res* **64**, 2324-2327.

Louria-Hayon, I., Grossman, T., Sionov, R. V., Alsheich, O., Pandolfi, P. P., and Haupt, Y. (2003). The promyelocytic leukemia protein protects p53 from Mdm2-mediated inhibition and degradation. *J Biol Chem* **278**, 33134-33141.

Luciani, J. J., Depetris, D., Usson, Y., Metzler-Guillemain, C., Mignon-Ravix, C., Mitchell, M. J., Megarbane, A., Sarda, P., Sirma, H., Moncla, A.*, et al.* (2006). PML nuclear bodies are highly organised DNA-protein structures with a function in heterochromatin remodelling at the G2 phase. *J Cell Sci* **119**, 2518-2531.

Luderus, M. E., van Steensel, B., Chong, L., Sibon, O. C., Cremers, F. F., and de Lange, T. (1996). Structure, subnuclear distribution, and nuclear matrix association of the mammalian telomeric complex. *J Cell Biol* **135**, 867-881.

Lundblad, V., and Blackburn, E. H. (1993). An alternative pathway for yeast telomere maintenance rescues est1- senescence. *Cell* **73**, 347-360.

Manders, E. M., Kimura, H., and Cook, P. R. (1999). Direct imaging of DNA in living cells reveals the dynamics of chromosome formation. *J Cell Biol* **144**, 813-821.

Marshall, W. F., Straight, A., Marko, J. F., Swedlow, J., Dernburg, A., Belmont, A., Murray, A. W., Agard, D. A., and Sedat, J. W. (1997). Interphase chromosomes undergo constrained diffusional motion in living cells. *Curr Biol* **7**, 930-939.

McEachern, M. J., and Haber, J. E. (2006). Break-induced replication and recombinational telomere elongation in yeast. *Annu Rev Biochem* **75**, 111-135.

Meshorer, E., Yellajoshula, D., George, E., Scambler, P. J., Brown, D. T., and Misteli, T. (2006). Hyperdynamic plasticity of chromatin proteins in pluripotent embryonic stem cells. *Dev Cell* **10**, 105-116.

Michaelis, C., Ciosk, R., and Nasmyth, K. (1997). Cohesins: chromosomal proteins that prevent premature separation of sister chromatids. *Cell* **91**, 35-45.

Michel, B., Grompone, G., Flores, M. J., and Bidnenko, V. (2004). Multiple pathways process stalled replication forks. *Proc Natl Acad Sci U S A* **101**, 12783-12788.

Mirzoeva, O. K., and Petrini, J. H. (2001). DNA damage-dependent nuclear dynamics of the Mre11 complex. *Mol Cell Biol* **21**, 281-288.

Misteli, T., Gunjan, A., Hock, R., Bustin, M., and Brown, D. T. (2000). Dynamic binding of histone H1 to chromatin in living cells. *Nature* **408**, 877-881.

Molenaar, C., Wiesmeijer, K., Verwoerd, N. P., Khazen, S., Eils, R., Tanke, H. J., and Dirks, R. W. (2003). Visualizing telomere dynamics in living mammalian cells using PNA probes. In Embo J, pp. 6631-6641.

Muntoni, A., and Reddel, R. R. (2005). The first molecular details of ALT in human tumor cells. *Hum Mol Genet* **14 Spec No. 2**, R191-196.

Muratani, M., Gerlich, D., Janicki, S. M., Gebhard, M., Eils, R., and Spector, D. L. (2002). Metabolic-energy-dependent movement of PML bodies within the mammalian cell nucleus. *Nat Cell Biol* **4**, 106-110.

Nabetani, A., Yokoyama, O., and Ishikawa, F. (2004). Localization of hRad9, hHus1, hRad1, and hRad17 and caffeine-sensitive DNA replication at the alternative lengthening of telomeres-associated promyelocytic leukemia body. *J Biol Chem* **279**, 25849-25857.

Nagele, R. G., Velasco, A. Q., Anderson, W. J., McMahon, D. J., Thomson, Z., Fazekas, J., Wind, K., and Lee, H. (2001). Telomere associations in interphase nuclei: possible role in maintenance of interphase chromosome topology. *J Cell Sci* **114**, 377-388.

Naka, K., Ikeda, K., and Motoyama, N. (2002). Recruitment of NBS1 into PML oncogenic domains via interaction with SP100 protein. *Biochem Biophys Res Commun* **299**, 863-871.

Olins, A. L., and Olins, D. E. (1974). Spheroid chromatin units (v bodies). *Science* **183**, 330-332.

Pederson, T. (2000). Half a century of "the nuclear matrix". *Mol Biol Cell* **11**, 799-805.

Perez, A., Kastner, P., Sethi, S., Lutz, Y., Reibel, C., and Chambon, P. (1993). PMLRAR homodimers: distinct DNA binding properties and heteromeric interactions with RXR. *Embo J* **12**, 3171-3182.

Perrem, K., Bryan, T. M., Englezou, A., Hackl, T., Moy, E. L., and Reddel, R. R. (1999). Repression of an alternative mechanism for lengthening of telomeres in somatic cell hybrids. *Oncogene* **18**, 3383-3390.

Platani, M., Goldberg, I., Lamond, A. I., and Swedlow, J. R. (2002). Cajal body dynamics and association with chromatin are ATP-dependent. *Nat Cell Biol* **4**, 502-508.

Platani, M., Goldberg, I., Swedlow, J. R., and Lamond, A. I. (2000). In vivo analysis of Cajal body movement, separation, and joining in live human cells. *J Cell Biol* **151**, 1561-1574.

Prasher, D. C., Eckenrode, V. K., Ward, W. W., Prendergast, F. G., and Cormier, M. J. (1992). Primary structure of the Aequorea victoria green-fluorescent protein. *Gene* **111**, 229-233.

Reddel, R. R. (2003). Alternative lengthening of telomeres, telomerase, and cancer. *Cancer Lett* **194**, 155-162.

Reddel, R. R., and Bryan, T. M. (2003). Alternative lengthening of telomeres: dangerous road less travelled. *Lancet* **361**, 1840-1841.

Robinett, C. C., Straight, A., Li, G., Willhelm, C., Sudlow, G., Murray, A., and Belmont, A. S. (1996). In vivo localization of DNA sequences and visualization of large-scale chromatin organization using lac operator/repressor recognition. *J Cell Biol* **135**, 1685-1700.

Rosa, A., Maddocks, J. H., Neumann, F. R., Gasser, S. M., and Stasiak, A. (2006). Measuring limits of telomere movement on nuclear envelope. *Biophys J* **90**, L24-26.

Rothbauer, U., Zolghadr, K., Tillib, S., Nowak, D., Schermelleh, L., Gahl, A., Backmann, N., Conrath, K., Muyldermans, S., Cardoso, M. C., and Leonhardt, H. (2006). Targeting and tracing antigens in live cells with fluorescent nanobodies. *Nat Methods* **3**, 887-889.

Sage, D., Neumann, F. R., Hediger, F., Gasser, S. M., and Unser, M. (2005). Automatic tracking of individual fluorescence particles: application to the study of chromosome dynamics. *IEEE transactions on image processing* **14**, 1372-1383.

Salomoni, P., and Pandolfi, P. P. (2002). The role of PML in tumor suppression. *Cell* **108**, 165-170.

Schmiedeberg, L., Weisshart, K., Diekmann, S., Meyer Zu Hoerste, G., and Hemmerich, P. (2004). High- and low-mobility populations of HP1 in heterochromatin of mammalian cells. *Mol Biol Cell* **15**, 2819-2833.

Schwacha, A., and Kleckner, N. (1995). Identification of double Holliday junctions as intermediates in meiotic recombination. *Cell* **83**, 783-791.

Soutoglou, E., Dorn, J. F., Sengupta, K., Jasin, M., Nussenzweig, A., Ried, T., Danuser, G., and Misteli, T. (2007). Positional stability of single double-strand breaks in mammalian cells. *Nat Cell Biol* **9**, 675-682.

Spector, D. L. (2001). Nuclear domains. *J Cell Sci* **114**, 2891-2893.

Sproul, D., Gilbert, N., and Bickmore, W. A. (2005). The role of chromatin structure in regulating the expression of clustered genes. *Nature reviews* **6**, 775-781.

Stoffler, D., Fahrenkrog, B., and Aebi, U. (1999). The nuclear pore complex: from molecular architecture to functional dynamics. *Curr Opin Cell Biol* **11**, 391-401.

Straight, A. F., Belmont, A. S., Robinett, C. C., and Murray, A. W. (1996). GFP tagging of budding yeast chromosomes reveals that protein-protein interactions can mediate sister chromatid cohesion. *Curr Biol* **6**, 1599-1608.

Symington, L. S. (2002). Role of RAD52 epistasis group genes in homologous recombination and double-strand break repair. *Microbiol Mol Biol Rev* **66**, 630-670, table of contents.

Taddei, A., Van Houwe, G., Hediger, F., Kalck, V., Cubizolles, F., Schober, H., and Gasser, S. M. (2006). Nuclear pore association confers optimal expression levels for an inducible yeast gene. *Nature* **441**, 774-778.

Thompson, N. L., Lieto, A. M., and Allen, N. W. (2002). Recent advances in fluorescence correlation spectroscopy. *Curr Opin Struct Biol* **12**, 634-641.

Thomson, I., Gilchrist, S., Bickmore, W. A., and Chubb, J. R. (2004). The radial positioning of chromatin is not inherited through mitosis but is established de novo in early G1. *Curr Biol* **14**, 166-172.

Tseng, Y., Lee, J. S., Kole, T. P., Jiang, I., and Wirtz, D. (2004). Micro-organization and visco-elasticity of the interphase nucleus revealed by particle nanotracking. *J Cell Sci* **117**, 2159-2167.

Tsien, R. Y. (1998). The green fluorescent protein. *Annu Rev Biochem* **67**, 509-544.

Tsukamoto, T., Hashiguchi, N., Janicki, S. M., Tumbar, T., Belmont, A. S., and Spector, D. L. (2000). Visualization of gene activity in living cells. *Nat Cell Biol* **2**, 871-878.

Tumbar, T., Sudlow, G., and Belmont, A. S. (1999). Large-scale chromatin unfolding and remodeling induced by VP16 acidic activation domain. *J Cell Biol* **145**, 1341-1354.

Ulaner, G. A., Hoffman, A. R., Otero, J., Huang, H. Y., Zhao, Z., Mazumdar, M., Gorlick, R., Meyers, P., Healey, J. H., and Ladanyi, M. (2004). Divergent patterns of telomere maintenance mechanisms among human sarcomas: sharply contrasting prevalence of the alternative lengthening of telomeres mechanism in Ewing's sarcomas and osteosarcomas. *Genes Chromosomes Cancer* **41**, 155-162.

Vazquez, J., Belmont, A. S., and Sedat, J. W. (2001). Multiple regimes of constrained chromosome motion are regulated in the interphase Drosophila nucleus. *Curr Biol* **11**, 1227-1239.

von Mikecz, A., Zhang, S., Montminy, M., Tan, E. M., and Hemmerich, P. (2000). CREB-binding protein (CBP)/p300 and RNA polymerase II colocalize in transcriptionally active domains in the nucleus. *J Cell Biol* **150**, 265-273.

Wang, J., Shiels, C., Sasieni, P., Wu, P. J., Islam, S. A., Freemont, P. S., and Sheer, D. (2004). Promyelocytic leukemia nuclear bodies associate with transcriptionally active genomic regions. *J Cell Biol* **164**, 515-526.

Wang, S., and Hazelrigg, T. (1994). Implications for bcd mRNA localization from spatial distribution of exu protein in Drosophila oogenesis. *Nature* **369**, 400-403.

Wang, Z. G., Ruggero, D., Ronchetti, S., Zhong, S., Gaboli, M., Rivi, R., and Pandolfi, P. P. (1998). PML is essential for multiple apoptotic pathways. *Nat Genet* **20**, 266-272.

Weipoltshammer, K., Schofer, C., Almeder, M., Philimonenko, V. V., Frei, K., Wachtler, F., and Hozak, P. (1999). Intranuclear anchoring of repetitive DNA sequences: centromeres, telomeres, and ribosomal DNA. *J Cell Biol* **147**, 1409-1418.

Wu, G., Jiang, X., Lee, W. H., and Chen, P. L. (2003). Assembly of functional ALT-associated promyelocytic leukemia bodies requires Nijmegen Breakage Syndrome 1. *Cancer Res* **63**, 2589-2595.

Wu, G., Lee, W. H., and Chen, P. L. (2000). NBS1 and TRF1 colocalize at promyelocytic leukemia bodies during late S/G2 phases in immortalized telomerase-negative cells. Implication of NBS1 in alternative lengthening of telomeres. *J Biol Chem* **275**, 30618-30622.

Wu, W. S., Vallian, S., Seto, E., Yang, W. M., Edmondson, D., Roth, S., and Chang, K. S. (2001). The growth suppressor PML represses transcription by functionally and physically interacting with histone deacetylases. *Mol Cell Biol* **21**, 2259-2268.

Yeager, T. R., Neumann, A. A., Englezou, A., Huschtscha, L. I., Noble, J. R., and Reddel, R. R. (1999). Telomerase-negative immortalized human cells contain a novel type of promyelocytic leukemia (PML) body. *Cancer Res* **59**, 4175-4179.

Zhong, S., Hu, P., Ye, T. Z., Stan, R., Ellis, N. A., and Pandolfi, P. P. (1999). A role for PML and the nuclear body in genomic stability. *Oncogene* **18**, 7941-7947.

Zhong, S., Muller, S., Ronchetti, S., Freemont, P. S., Dejean, A., and Pandolfi, P. P. (2000). Role of SUMO-1-modified PML in nuclear body formation. *Blood* **95**, 2748-2752.

Zink, D., and Cremer, T. (1998). Cell nucleus: chromosome dynamics in nuclei of living cells. *Curr Biol* **8**, R321-324.

VI. Abbreviations

3D	three dimensional
Acc No.	Accession Number
ALT	Alternative telomere lengthening
APB	ALT associated PML body
ATP	Adenosine-5'triphosphate
BIR	Break-Induced Replication
bp	base pair
BrUTP	5-bromo-uridin-5'-triphosphate
cDNA	Complementary deoxyribonucleic acid
DAPI	4',6-diamidin-2'-phenyllindol-dihydrochloride
DSB	Double Strand Break
DSBR	DSB Repair
dsDNA	double-stranded DNA
D-MEM	Dubeco's modified Eagle Medium
DMSO	Dimethylsulfoxyd
DNA	Deoxyribonucleic acid
DNMTs	DNA Methyltransferases
dNTP	2'-deoxyribonucleotide (5'-triphosphate)
eCFP	enhanced Cyan Fluorescent Protein
E. coli	Escherichia coli
EDTA	Ethylendiaminotetraacetate, exists as sodium salt
eGFP	enhanced Green Fluorescent Protein
ES	Embryonic Stem cell
eXFP	eCFP, eGFP, eYFP or mRFP1
eYFP	enhanced Cyan Yellow Fluorescent Protein
FA	Formamid
FCS	Fetal Calf Serum
FCS	Fluorescence Correlation Spectroscopy
FISH	Fluorescence *in situ* Hybridization
FRAP	Fluorescence Recovery After Photobleaching
GFP	Green Fluorescent Protein

HP1	Heterochromatin Protein 1
hrs	hours
ICF	Centromeric instability and facial dysmorphy
kbp	kilo base pair
LacI	Lac Inhibitor
*lac*O	*lac* Operator
LB	“Luria Bertani”, full medium for bacteria
LSM	Laser Scanning Microscope
mFISH	multicolor FISH
min	minutes
mRFP1	monomeric Red Fluorescent Protein 1
mRNA	messenger RNA
msec	milliseconds
NLS	Nuclear Localization Signal
OD	Optical Density
PBS	“Phosphate Buffered Saline”, buffer
PCR	Polymerase Chain Reaction
PFA	Paraformaldehyde
PML	Promyelocytic Leukemia associated protein/body
PNA	Peptide Nucleic Acid
Q-FISH	Quantitative FISH
RNA	Ribonucleic Acid
RNAse	Ribonuclease
RT	Room Temperature
rRNA	ribosomal RNA
SDS	Sodiumdodecylsulfate
SDSA	Synthesis-Dependant Strand Annealing
sec	seconds
SSC	Sodium chloride/Sodium Citrate buffer
ssDNA	single-stranded DNA
TBE	Tris-HCL Boric acid EDTA, buffer for agarose gel electrophoresis
*tet*O	*tet* Operator
TetR	Tet Repressor
TERP	Telomerase reverse transcriptase subunit

TERC	Telomerase template-RNA subunit
TRF1	Telomere Repeat binding Factor 1
TRF2	Telomere Repeat binding Factor 2
U	Enzymatical Unit
V/V	Volume per Volume
V/W	Volume per Weight

VII. Summary

The higher order chromatin organization and its dynamic properties are directly related to gene expression, replication, DNA repair and recombination. In this thesis the mobility of telomeres was studied with a human U2OS osteosarcoma cell line that had *lac*O operator repeats stably integrated at the telomeres of chromosomes 6, 11 and 12. The mobility of these three telomeres during interphase was monitored by fluorescence microscopy via bound proteins of LacI repressor fused to the autofluorescent GFP or mRFP1 domains. From measurements of the distance change between pairs of two tagged telomeres a confined diffusion model was derived that described the translocation of telomeres in the nucleus on the time scale from milliseconds to hours, using high performance live cell imaging. Three types of movements were identified: (i) Fast local movements on the (milli)second scale with a diffusion constant of $D_{ms} = 2 \cdot 10^{-3}$ μm^2 s^{-1} restricted to a region with radius $r_{ms} \sim 80$ nm, (ii) movement in the second/minute range with $D_{sec} = 4 \cdot 10^{-4}$ μm^2 s^{-1} and $r_{sec} = 150$ nm, and (iii) movements on the minute/hour time scale with $D_{min} = 2 \cdot 10^{-5}$ μm^2 s^{-1}. For the later translocations average confinement radii of $r_{min} = 0.3 \pm 0.1$ µm where determined, while a ~30% fraction of the telomeres showed a highly extended mobility with $r_{min} = 0.8 \pm 0.4$ µm, suggesting that the majority of the telomere are anchored to a stable structure in the nucleus whereas a given fraction can move more freely. We could moreover show a correlation between the proportion of telomere having short repeat length and telomere displaying extended mobility, suggesting that an intact telomere is required for anchoring. In addition, the mobility of promyelocytic leukemia (PML) nuclear bodies relative to the telomeres was analyzed. The PML bodies formed complexes with the telomeres in the telomerase-negative U2OS cell line that have been reported previously to be involved in an alternative lengthening of telomeres (ALT) pathway: the ALT associated PML bodies (APBs). The dynamics of the formation of the APB was monitored. With regards to the differences in telomere mobility, the length of the telomere repeat sequences and their interaction with PML bodies we proposed a model to describe the dynamics of the ALT pathway.

VIII. Zusamenfassung

Die höhere Ordnung der Chromatinorganisation und ihre dynamischen Eigenschaften sind direkt mit Vorgängen wie Genexpression, Replikation, DNA Reparatur und Rekombination verbunden. In dieser Doktorarbeit wurde die Mobilität von Telomeren in einer humanen Osteosarcoma-Zellinie U2OS untersucht, in welche zuvor lacO-Operator Widerholungseinheiten an den Telomeren der Chromosomen 6, 11 und 12 stabil integriert wurden. Die Mobilität dieser drei Telomere wurde während der Interphase mittels Fluoreszenzmikroskopie durch gebundene LacI-Repressoren, welche mit autofluoreszenten GFP oder mRFP1 Domänen fusioniert waren, beobachtet. Durch Messungen der Distanzänderungen zwischen zwei markierten Telomerpaaren mittels Hochgeschwindigkeits-Lebendzellbeobachtung wurde ein begrenztes Diffusionsmodell abgeleitet, welches die Ortsveränderung der Telomere im Zellkern in einer Zeitskala von Millisekunden bis Stunden beschreibt. Drei Arten von Bewegungen wurden identifiziert: (i) Schnelle, lokale Bewegungen im (Milli-)Sekundenbereich mit einer Diffusionskonstante von Dms = $2 \cdot 10^{-3}$ μm^2 s^{-1}, welche auf eine Region mit einem Radius von rms ~ 80 nm begrenzt waren, (ii) Bewegungen im Sekunden/Minutenbereich mir Dsec = $4 \cdot 10^{-4}$ μm^2 s^{-1} und rsec = 150 nm und (iii) Bewegungen im Minuten/Stundenbereich mit Dmin = $2 \cdot 10^{-5}$ μm^2 s^{-1}. Für die letztgenannten Ortsveränderungen wurden mittlere Begrenzungsradien von rmin = 0.3 ± 0.1 µm bestimmt, wobei ein Anteil von ~ 30% der Telomere eine hohe ausgedehnte Mobilität mit rmin = 0.8 ± 0.4 µm zeigte. Dies legt den Schluss nahe, dass die Mehrheit der Telomere an eine stabile Struktur im Zellkern verankert ist , wogegen sich ein gewisser Anteil der Telomere freier bewegen kann. Darüberhinaus konnten wir zeigen, dass eine Korrelation zwischen einem Teil der Telomere mit kurzen Wiederholungssequenzlängen und Telomeren mit ausgeweiteter Mobilität besteht, was darauf hinweist, dass intakte Telomere zur Verankerung notwendig sind. Zudem wurde die Mobilität von Promyelozytische-Leukämie (PML) - Zellkernkörperchen relativ zu den Telomeren analysiert. Die PML Körperchen formten Komplexe mit den Telomeren in der Telomerase-negativen U2OS Zellinie. Diese wurden schon zuvor beschrieben im Weg einer alternativen Verlängerung von Telomeren (alternative lengthening of telomeres, ALT) involviert zu sein und daher ALT assoziierte PML Körperchen (ALT associated PML bodies, APBs) genannt. Die Dynamik der Bildung von APBs wurde beobachtet. Im Hinblick auf die Unterschiede der Telomermobilität, der Länge der Telomersequenzwiederholungen und ihrer Interaktion mit den PML Körperchen erstellten wir ein Modell zur Beschreibung der Dynamik des ALT Wegs.